Technical Report
TR-21-14
February 2022

Buffer homogenisation – status report 5

Ann Dueck
Reza Goudarzi
Viktor Jensen
Lennart Börgesson

SVENSK KÄRNBRÄNSLEHANTERING AB

SWEDISH NUCLEAR FUEL
AND WASTE MANAGEMENT CO

Box 3091, SE-169 03 Solna
Phone +46 8 459 84 00
skb.se

SVENSK KÄRNBRÄNSLEHANTERING

ISSN 1404-0344
SKB TR-21-14
ID 1963211

February 2022

Buffer homogenisation – status report 5

Ann Dueck, Reza Goudarzi, Viktor Jensen, Lennart Börgesson
Clay Technology AB

Keywords: Bentonite, Swelling, Swelling pressure, Homogenisation.

Abstract

The present status report is a compilation of laboratory test results from a project on homogenisation of bentonite. The main purpose of the status report is to account for results derived up to September 2020 that have not been included in previous reports. The results can be used for modelling some well-defined benchmark tests in order to improve the models or determine mechanical parameters for hydro-mechanical modelling of the behaviour of bentonite buffer and backfill.

Results from supplementary fundamental swelling tests with swelling pressure measurement at different positions of specimens, with the height 50–70 mm and the diameter 100 mm, are presented in this status report. In this project homogenisation has also been studied by medium scale tests involving loss of bentonite and the results from sampling of the third and fourth test of this type are presented in this report. Remaining differences in density after long time are studied in a series with long tubes. Initially ten tests of this type were started, three of which have been dismantled and the results of two of the dismantled specimens are reported here.

Sammanfattning

Denna lägesrapport innehåller en sammanställning av laboratorieförsök som utförts för att studera homogeniseringsprocessen i bentonitlera. Huvudsyftet med rapporten är att presentera försöksresultat från försök som utförts fram till och med september 2020 som inte presenterats i tidigare rapporter. Resultaten kan användas för att förbättra modeller eller för att bestämma mekaniska parametrar för den hydro-mekaniska modelleringen av framförallt bentonitbuffertens uppförande.

Resultat från kompletterande svällningsförsök med svälltrycksmätning i olika positioner på prover med höjden 50–70 mm och diametern 100 mm presenteras i denna statusrapport. Homogenisering har i detta projekt också undersökts med så kallade självläkningsförsök där effekten av förlust av bentonitmaterial har studerats. Resultaten från provtagningen av det tredje och fjärde försöket av denna typ presenteras i denna rapport. Skillnader i densitet som kvarstår efter lång tid har studerats i en serie försök med så kallade långa rör. Ursprungligen startades tio försök av denna typ, varav tre har avbrutits, och resultaten från två av de avslutade försöken presenteras här.

Contents

1 Introduction

1.1 Background

Swelling of the buffer blocks and buffer homogenisation are important functions to guarantee that the requirements of the buffer in a deposition hole after full water saturation are fulfilled. It is important to understand and be able to predict the final condition of the buffer after the swelling and homogenisation, which occur both during the initial saturation phase and after possible loss of bentonite caused by for example erosion.

The buffer homogenisation project consists of four parts; theoretical studies, fundamental laboratory tests, laboratory study of the influence of friction and medium scale tests of the scenario involving loss of bentonite. The present status report describes results from three types of laboratory tests.

The tests described were dismantled from March 2016 and until September 2020. This is the fifth status report from the project, and it is a continuation of the previous status reports with laboratory test results (Dueck et al. 2011, 2014, 2016, 2018). Test results from this project were analysed in e.g. Dueck et al. (2019).

1.2 Objective

The objective of the described tests has been to further improve the knowledge of the process of swelling and homogenisation. The main purpose of this status report is to account for results derived up to September 2020 and provide results that can be used for modelling some well-defined benchmark tests in order to improve the models or determine mechanical parameters for hydro-mechanical modelling of the behaviour of the bentonite buffer and backfill.

1.3 Content of the report

The determination of base variables is described in Chapter 2 and the materials used for the tests are mentioned in Chapter 3. In Chapter 4 the test techniques and the results from fundamental swelling tests in the so-called high-resolution series are presented. Chapter 5 contains test description and results from the third and fourth completed and dismantled medium scale test of a scenario involving loss of bentonite. In Chapter 6 the test type with the so-called long tubes is described together with the results from two of the three completed and dismantled specimens, the first one was reported previously. The status of the seven still ongoing long tube tests is also mentioned. Short comments about the test results are given directly after each section with presented results. In addition, detailed results are presented in Appendix 1–3 and in Appendix 4 a tabulated compilation of specimens presented in this and previous reports is shown. Analyses of the test results will be made in a coming report.

Some of the tests run in this project were used as modelling tasks in the SKB project Task Force on Engineered Barriers (TF EBS) and in the EU-project BEACON.

2 Determination of basic variables

2.1 General

The basic variables water content and bulk density are measured in each test and from these variables the dry density and degree of saturation are calculated. The swelling pressure in this project is measured as a stress exerted as a load on a piston with a certain area. In most of the tests the measurement is made in a specified direction, i.e. as an axial or a radial stress.

2.2 Water content and bulk density determination

The basic geotechnical variables water content w (%), void ratio e, degree of saturation S_r (%) and dry density ρ_d (kg/m^3) are determined according to Equations 2-1 to 2-4.

$$w = 100 \cdot \frac{m_{tot} - m_s}{m_s} \tag{2-1}$$

$$e = \frac{\rho_s}{\rho}(1 + w/100) - 1 \tag{2-2}$$

$$S_r = \frac{\rho_s \cdot w}{\rho_w \cdot e} \tag{2-3}$$

$$\rho_d = \frac{m_s}{V} \tag{2-4}$$

where

m_{tot} = total mass of the specimen (kg)

m_s = dry mass of the specimen (kg)

ρ_s = particle density (kg/m^3)

ρ_w = density of water (kg/m^3)

ρ = bulk density of the specimen (kg/m^3)

V = total volume of the specimen (m^3)

The dry mass of a specimen is obtained from drying a wet specimen at 105 °C for 24h. The bulk density is calculated from the total mass of a specimen and the volume determined by weighing the specimen above and submerged into paraffin oil.

3 Materials

3.1 General

Two bentonite materials have been used; the commercial sodium dominated Wyoming bentonite with brand name Volclay MX-80 from American Coll. Co. and the commercial calcium dominated bentonite Calcigel from Clariant (Süd-Chemie AG). Descriptions of the materials and basic variables were presented by e.g. Svensson et al. (2011).

The bentonite powder was delivered with an approximate water content of 10 %. For tests where higher initial water content was used the powder was mixed with de-ionized water. Placed in a mould the powder was compacted to a block in a hydraulic press.

For determination of void ratio and degree of saturation the particle densities ρ_s = 2 780 kg/m^3 and ρ_s = 2 695 kg/m^3 were used for MX-80 and Calcigel, respectively (Svensson et al. 2011) and the water density ρ_w = 1 000 kg/m^3 (see also Dueck et al. 2018).

The majority of the tests were supplied with de-ionized stagnant water if nothing else is specified. However, in many tests the filters were flushed in order to get rid of air bubbles.

4 Fundamental swelling tests

4.1 General

In this chapter results from supplementary tests in the so-called HR series with fundamental swelling tests are presented. The test technique used has been reported in the previous status reports of this project (Dueck et al. 2014, 2016, 2018) and is only briefly described below. In addition to the results presented below, detailed results are given in Appendix 1.

4.2 Fundamental swelling tests – high resolution series

Fundamental swelling tests have been performed in two scales within the project: the basic series and the series with larger specimens (the so-called high resolution, HR, series). In this chapter test results from the latter series are presented.

4.2.1 Test description

In the HR-series three types of swelling were studied; axial swelling (HR-A), radial outward swelling (HR-Ro) and radial inward swelling (HR-Ri). In this report tests involving axial swelling are reported and a set-up of the used equipment is shown in Figure 4-1.With the equipment used the axial stress was measured from both sides of the specimen, i.e. both above and below the specimen. Stresses were also measured radially, at three or four positions, by load cells and movable pistons. Water was added above the specimen into the gap. More information about the equipment used can be found in the previous report (Dueck et al. 2018). In all tests a free swelling surface was present at start, i.e. no counteracting force until the swelling bentonite gel had reached the outer limited surface. In all tests the friction was minimized by use of a mineral-oil based lubricant on relevant surfaces.

In the HR-series the initial degree of saturation was high and for that reason the swelling phase started directly, i.e. the swelling took place at the same time as the small additional water uptake to full saturation. The specimens were in pervious tests sawn and trimmed from larger blocks but were compacted as individual blocks in the later tests, all having high initial water content between 19 % and 24 %. The initial height and diameter of the specimens swelling axially were 40–60 mm and 100 mm, respectively.

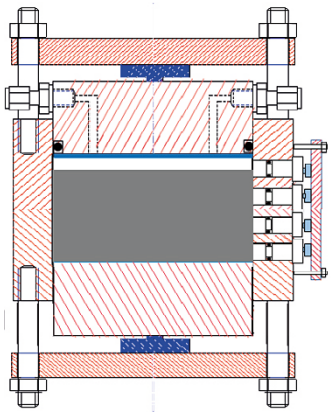

Figure 4-1. *Sketch of the test equipment used for the actual tests in the HR-A-series involving axial swelling. Stresses are measured both axially and radially. Water is added above the specimen into the gap.*

After preparation the specimens were mounted into the actual device, the load cells were fixed at their positions and de-ionized water was applied to the filters after air evacuation of the filters and tubes. In one test water was added by circulation by use of a peristaltic pump instead of adding water after evacuation of air. Water was only added to the upper part of the specimen in the actual tests which only involved axial swelling. The movable pistons and the load cells used for the radially measured swelling pressure were in some tests initially fixed to their positions by applying a small pre-stress, not influencing the final stress as long as the stress increases above the initial value. More details about the assembling of the equipment and mounting of the specimens can be found in the previous report (Dueck et al. 2018).

In the final part of the HR-tests presented in this report water pressure was applied to study the effect on the measured stresses. If a previous comparable test was made without water pressure a comparison of the density gradients after dismantling could also be done. Before dismantling the water pressure was adjusted back to zero, and when no or negligibly small changes were noticed in the measured stresses the homogenisation was considered as completed. Finally, the specimens were dismantled and cut in slices for the determination of water content and density distributions in the direction of swelling.

4.2.2 Results (HR-series)

In the test series with HR-tests the following three tests, all involving axial swelling, were performed and are presented in this report. The resulting water content and dry density are presented with initial and final values as a function of the specimen height, i.e. as distribution in the direction of swelling. The evolution of the swelling pressure, measured as stresses in different directions, is then presented as a function of time and finally the stresses are presented together with some of the previous results from this project.

Table 4-1. Tests run in the high-resolution series and presented in this report.

Specimen/Test	Type of swelling	Material
HR-A9	Axial swelling	Calcigel
HR-A10	Axial swelling	Calcigel
HR-A11	Axial swelling	MX-80

The swelling pressure is determined as an axial stress P_{axial} or a radial stress P_{radial} exerted as loads on a piston with a certain area. In tests with water pressure, P_w, the results are given as an effective stress calculated as the total measured stress minus the water pressure; $P_{axial} - P_w$ or $P_{radial} - P_w$. In some results the stresses are given as an average stress which is then calculated according to Equation 4-1.

$$P_{average} = (P_{axial} + 2 \cdot P_{radial})/3 \quad (4\text{-}1)$$

The measured stresses are shown and compared with models of swelling pressure of MX-80 presented by Börgesson et al. (1995) and by Åkesson et al. (2010) where the latter model was based on results presented by Karnland et al. (2006).

The labels in the diagrams give information about the sample ID, which includes the type of swelling; HR-A (axial swelling). In most of the labels the swelling is given in % but in some of the labels, used for measured stresses, the position of the measurement is given instead and then together with the distance in mm from the bottom of the specimen. The swelling is calculated according to Equation 4-2 where V_i, V_f, ρ_{di} and ρ_{df} are the initial volume, final volume, initial dry density and final dry density, respectively.

$$s = \frac{\Delta V}{V_i} = \frac{V_f}{V_i} - 1 = \frac{\rho_{di}}{\rho_{df}} - 1 \quad (4\text{-}2)$$

Axial swelling

The completed tests of axial swelling are presented in Table 4-2. In Figure 4-2 to Figure 4-7 the distributions of water content w, dry density ρ_d and degree of saturation S_r measured after completed tests, are shown. The evolution of the stresses measured during the tests are shown in Figure 4-8 to

Figure 4-13 where the results from the final weeks of the tests, when water pressure was applied, are shown separately. Water pressure between 100 kPa and 500 kPa was applied for a couple of weeks well before dismantling to check the stability of the measured stresses. In Figure 4-14 the axially and radially measured stresses are plotted as a function of dry density where the results of MX-80 (HR-A11) are shown to the left and of Calcigel (HR-A9, HR-A10) are shown to the right.

Table 4-2. Specimens used in the series with axial swelling, HR-A. The swelling (%) was calculated according to Equation 4-2. The swelling was based on the initial dry density corresponding to the diameter of 100 mm.

Test ID	Material	Initial water content %	Initial compacted dry density[1] kg/m^3	Initial compacted degree of saturation[1] %	Initial dry density[2] kg/m^3	Initial degree of saturation[2] %	Constant diameter mm	Initial height mm	Final height mm	Final swelling %
HR-A9	Calcigel	20	1736	98	1647	85	100	50	70	38
HR-A10	Calcigel	19	1667	85	1581	74	100	58	71	23
HR-A11	MX-80	22	1673	92	1583	81	100	50	70	40

[1] Corresponding to the dry density at compaction with a diameter of 97.4 mm.

[2] Corresponding to the final diameter 100 mm.

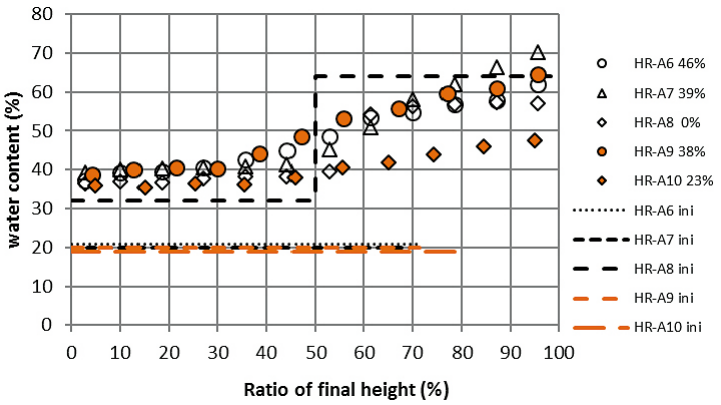

Figure 4-2. *Distribution of water content over the height of specimens HR-A9 and HR-A10 together with the previous results on Calcigel, marked with open symbols. Swelling in % is shown in the legend. HR-A8 started with two different densities and no swelling.*

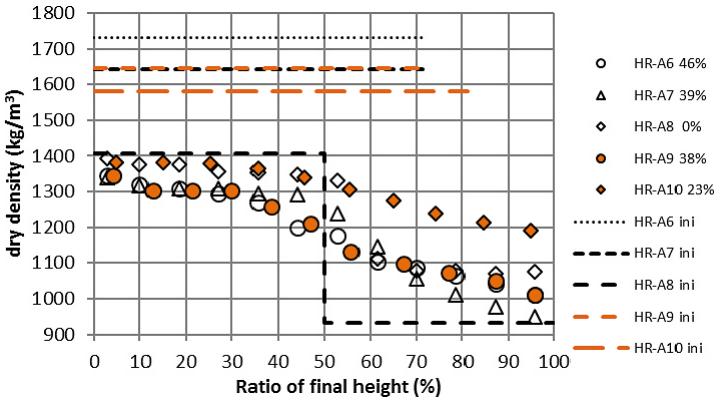

Figure 4-3. *Distribution of dry density over the height of specimens HR-A9 and HR-A10 together with the previous results on Calcigel, marked with open symbols.*

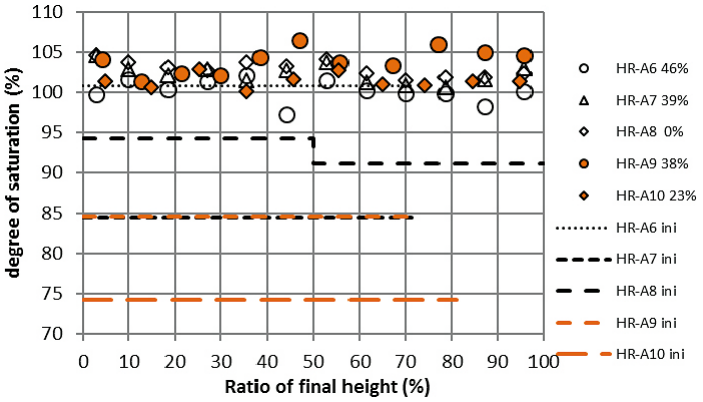

Figure 4-4. *Distribution of degree of saturation over the height of specimens HR-A9 and HR-A10 together with the previous results on Calcigel, marked with open symbols.*

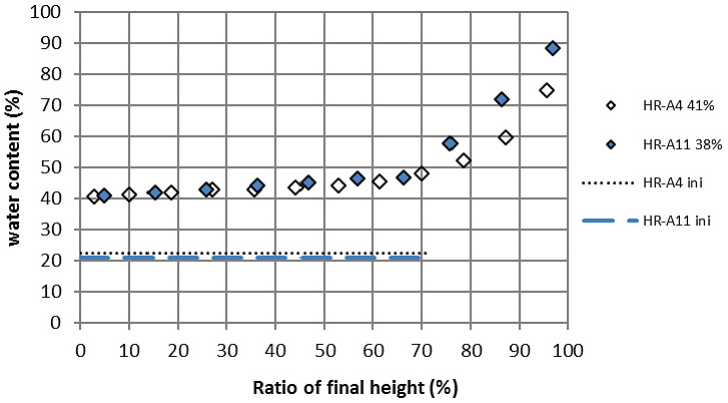

Figure 4-5. *Distribution of water content over the height of specimen HR-A11 of MX-80 together with the similar and previous test on a specimen of MX-80, marked with open symbols.*

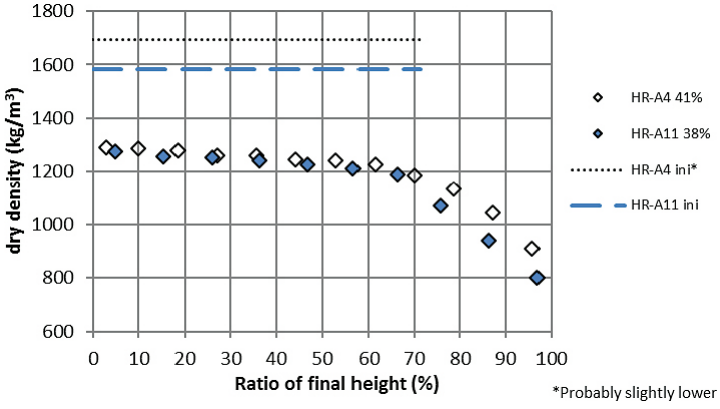

Figure 4-6. *Distribution of dry density over the height of specimen HR-A11 of MX-80 together with the similar and previous test on a specimen of MX-80, marked with open symbols.*

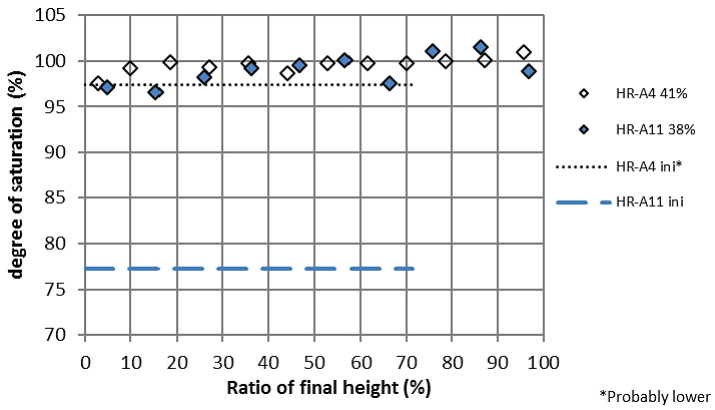

Figure 4-7. *Distribution of degree of saturation over the height of specimen HR-A11 of MX-80 together with the similar and previous test on a specimen of MX-80, marked with open symbols.*

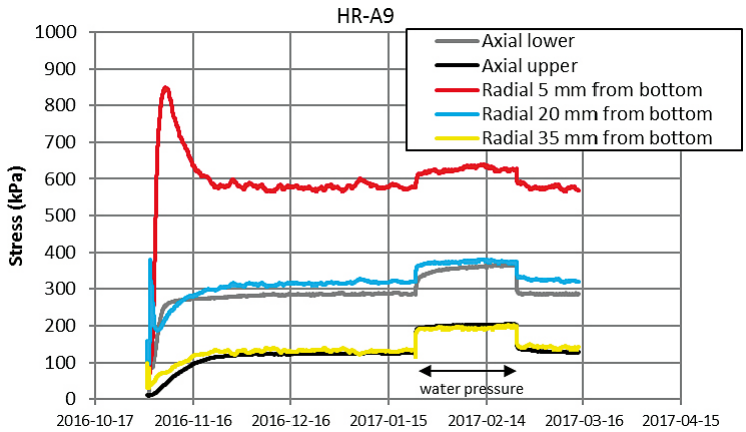

Figure 4-8. *Evolution of total stress with time from HR-A9.*

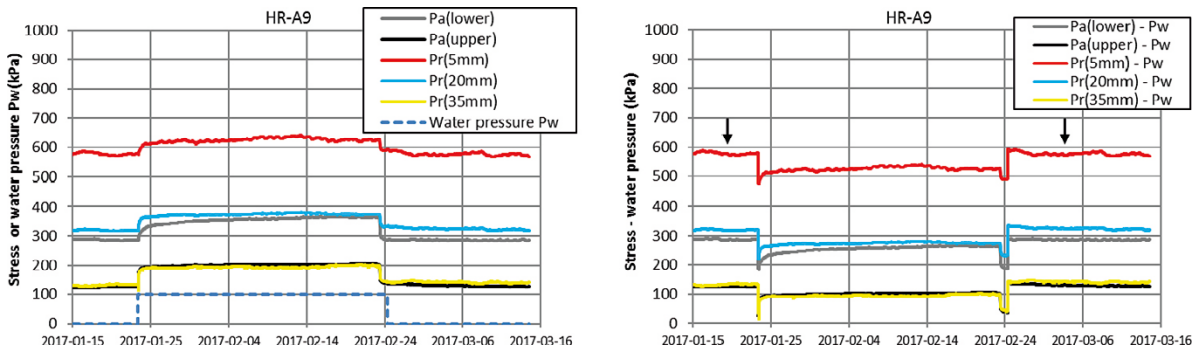

Figure 4-9. *Stress and pressure as a function of time from the last months of HR-A9. The measured stresses are plotted with the applied water pressure (to the left) and the effective stresses calculated as the total stresses minus water pressure (to the right). The arrows mark the stresses measured at zero water pressure.*

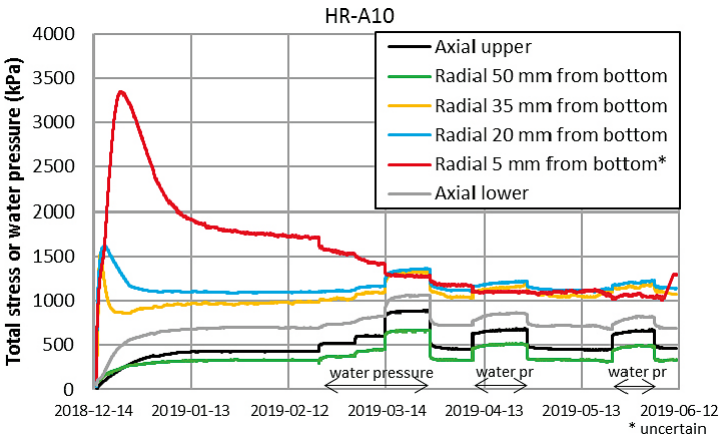

Figure 4-10. *Evolution of total stress with time from HR-A10.*

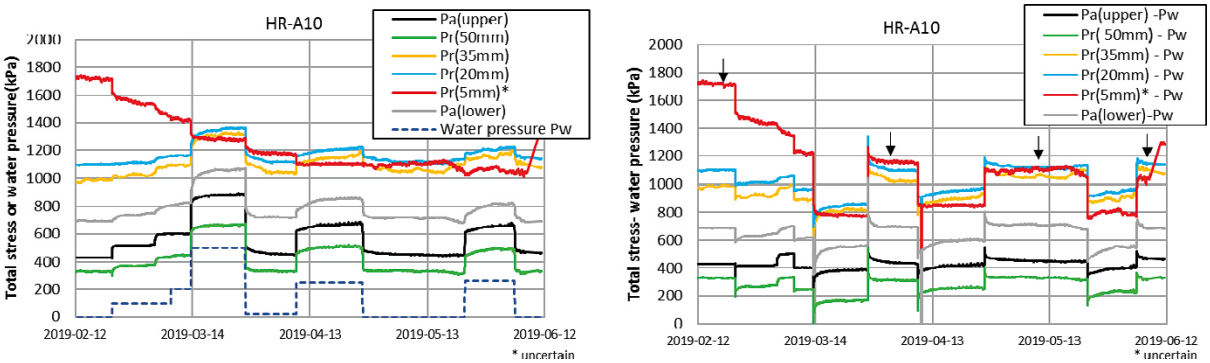

Figure 4-11. *Stress and pressure as a function of time from the four last months of HR-A10. The measured stresses are plotted with the applied water pressure (to the left) and the effective stresses calculated as the total stresses minus water pressure (to the right). The arrows mark the stresses measured at zero water pressure.*

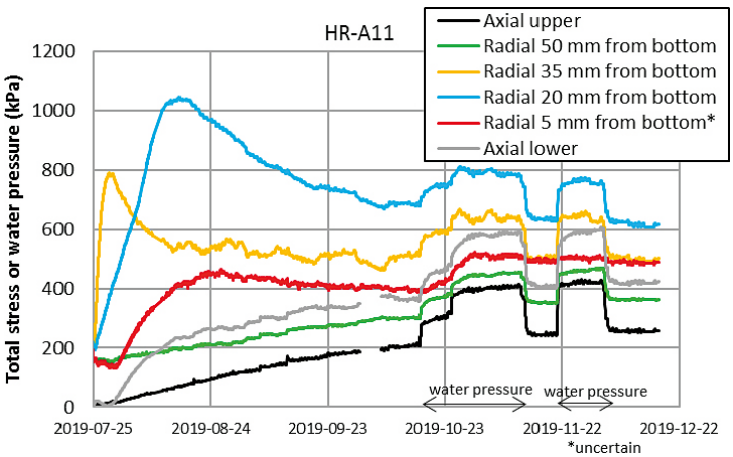

Figure 4-12. *Evolution of total stress with time from HR-A11.*

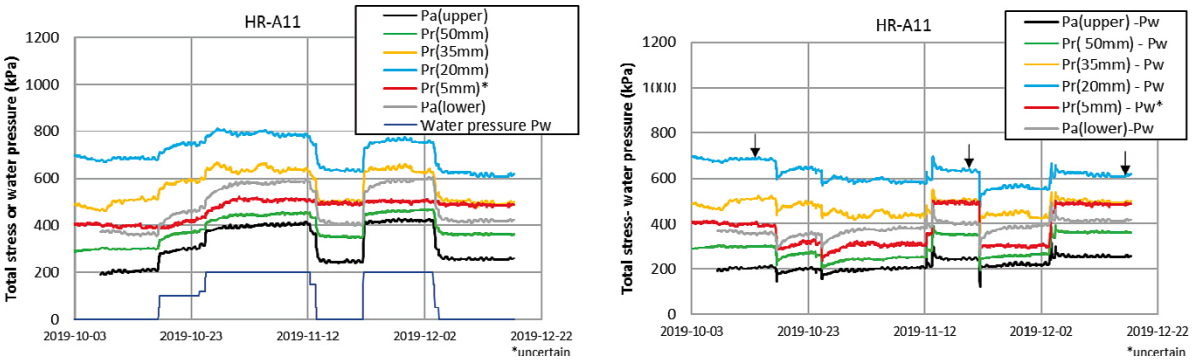

Figure 4-13. *Stress and pressure as a function of time from the three last months of HR-A11. The measured stresses are plotted with the applied water pressure (to the left) and the effective stresses calculated as the total stresses minus water pressure (to the right). The arrows mark the stresses measured at zero water pressure.*

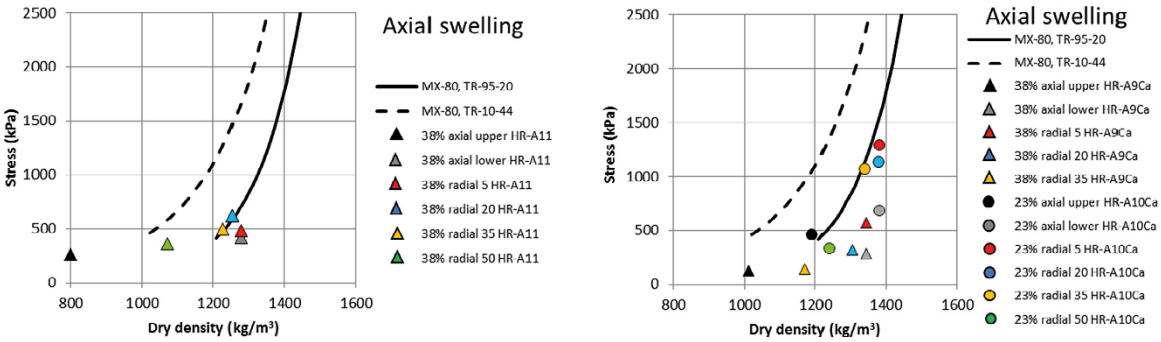

Figure 4-14. *Measured stresses as a function of dry density from specimens of MX-80 (to the left) and Calcigel (to the right). Results of HR-A11 are marked with triangles to the left and results of HR-A9 and HR-A10 are marked with triangles and circles, respectively, to the right. Models of MX-80 presented by Börgesson et al. (1995) and Åkesson et al. (2010) are also shown. The positions of the radially measured stresses are shown in the legends as distances between 5 and 50 mm from the bottom of the specimens.*

4.2.3 Comments

The dry density distributions of the dismantled specimens HR-A9 to HR-A11 are similar to results from previous comparable specimens, cf Figure 4-3 and Figure 4-6. However, there is a difference in behaviour between the two materials in that the density gradient has a maximum in the middle of the specimens of Calcigel while the largest gradient is seen in the very upper part in specimens of MX-80.

Differences in dry density and stress over the specimen height is illustrated in Figure 4-14. The two specimens that swelled 38 % can be compared: HR-A9 of Calcigel and HR-A11 of MX-80. The specimens are considered to be comparable despite that specimen HR-A9 swelled to a final average dry density of 1 190 kg/m^3 after 132 days and specimen HR-A11 swelled to a final average dry density 1 150 kg/m^3 after 145 days. Although the specimen of MX-80 swelled and homogenised for somewhat longer time, larger difference in dry density was seen in HR-A11 compared to HR-A9. Even larger difference in stress is seen over the specimen of Calcigel.

In Figure 4-15 all results from tests involving axial swelling in the HR-series are plotted with the average stress as a function of dry density. Results of MX-80 are shown to the left and results of Calcigel are shown to the right. The bars denote the maximum and minimum of the stresses and dry densities and thus illustrate the remaining inhomogeneity. It can again be observed that larger differences between max and min dry density are seen in specimens of MX-80 while larger differences in stress are seen in the measurements on Calcigel.

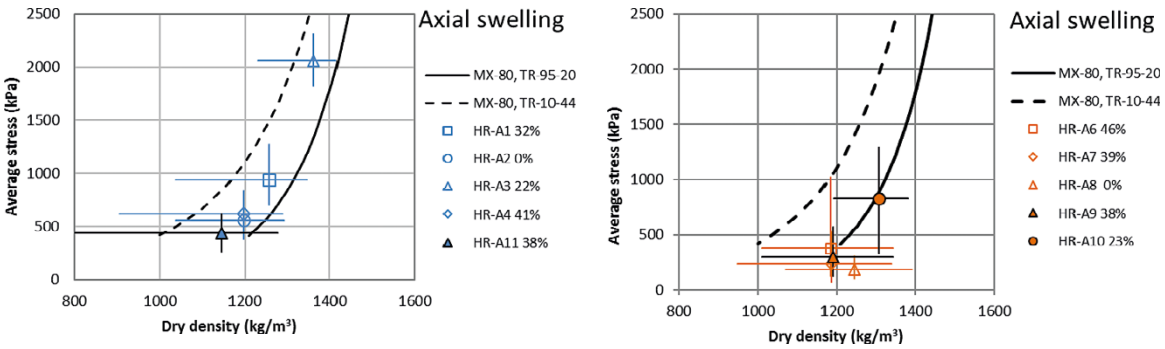

Figure 4-15. *Results from tests on specimens HR-A1–A4 plus HR-A11 of MX-80 (to the left) and HR-A6–A10 of Calcigel (to the right) are presented with average stress as a function of dry density. The open symbols denote results from Dueck et al. (2014, 2016, 2018). The bars show maximum and minimum dry densities and stresses of the specimens and thus illustrate the remaining inhomogeneity.*

In the HR-A tests presented in this report the axial stress was measured above and below the specimens according to Figure 4-1. The difference between the upper and lower values was interpreted as wall friction represented by a friction angle δ in the contact between the cylinder ring and the bentonite calculated according to Equation 4-3. In Equation 4-3 F is the friction force based on the difference in measured axial stress, A_s the radial surface area of the specimen and P_r is the radial stress perpendicular to the ring.

$$F = A_S \cdot P_r \cdot \tan(\delta) \quad (4\text{-}3)$$

In Table 4-3 the friction angle calculated from the equilibrium conditions of HR-A9 to HR-A11 are shown. The difference in axial stress and the average of the radially measured stresses (from three or four positions) used for the calculations are shown. The calculated friction angles fit well into previous results from this project (see e.g. Dueck et al. 2018), both regarding the absolute values and regarding the decrease with the radially measured stress. The results indicate that there is no large difference between the two bentonites.

Table 4-3. Friction angle δ between the cylinder ring and the bentonite specimens based on the difference in upper and lower axially measured stress ΔP_a and the average of the radially measured stresses $P_{r,avr}$.

Test ID	Difference in axial stress ΔP_a kPa	Radial stress $P_{r,avr}$ kPa	Friction angle δ °	Material
HR-A9	160	340	9	Calcigel
HR-A10	230	960	5	Calcigel
HR-A11	160	490	7	MX-80

The overall stability of the measured stresses was studied by comparing measured stresses before and after adding water pressure for a couple of weeks in the later part of the test periods. Stable values or slight increases were seen in the majority of the measured stresses with the exception of the radial stress measured at 20 mm on HR-A11 and the two somewhat uncertain values further mentioned below.

The radial stresses were measured at three or four locations and the radial stress measurement at 5 mm from the bottom has in previous tests of this type been higher than the other measured stresses on the same specimen. However, in HR-A10 and HR-A11 the radial stress measured 5 mm from the bottom was uncertain. In test HR-A10 the lower radial stress suffered from erroneous measurement during a large part of the test period. The final value was probably the most correct value but was only measured during a short time period before dismantling and is therefore marked as uncertain in the test results. In test HR-A11 the lower radial stress did neither increase nor decrease with the applied water pressure, which is not logical, and this measurement is also regarded as somewhat uncertain. These uncertainties are assumed not to influence the trends given above.

The degree of saturation was above 100 % in the samples of Calcigel. In general, the resulting degree of saturation of dismantled specimens of Calcigel in the HR-A series has been between 100 % and 104 %, with an average of 102 %, when based on the particle density ρ_s = 2 695 kg/m^3 (Svensson et al. 2011). Different particle densities of Calcigel have been determined and with the particle density ρ_s = 2 729 kg/m^3 (Dueck et al. 2018) the average degree of saturation is somewhat lower 101 %.

5 Homogenisation after loss of bentonite – the self-healing tests

5.1 General

Buffer homogenisation involving loss of bentonite has been studied by medium scale laboratory tests, called the self-healing tests (SH). Four tests have been started and all of them have been finished and dismantled. The two tests SH1 and SH2, having the same boundary conditions, started in December 2012 and was dismantled after 33 and 17 months, respectively. Test SH3 started in February 2015 and was dismantled in October 2018 after 44 months and test SH4 started in March 2017 and was dismantled in September 2020 after 43 months. Wyoming bentonite MX-80 was used for SH1, SH2 and SH4 while the bentonite Calcigel was used in SH3.

This chapter is focused on tests SH3 and SH4; the preparation, the start condition, the dismantling and the sampling. In addition to the results below, further results can be found in Appendix 2. The set-up used for SH3 was the same as for SH1, SH2 and SH4, however not instrumented as SH1 and SH4. The tests SH1 and SH2 have been reported in SKB Technical Reports (Dueck et al. 2016, 2018).

5.2 Experiment description

The self-sealing ability of large and irregular cavities was studied in this part of the Homogenisation project. Since it was important to be able to determine the final density distribution in detail a suitable combination of block size and cavity size was important to find. The size of the blocks, i.e. cylinder rings, was chosen to be as large as possible, still having a reasonable estimated time to saturation and homogenisation while the size of the cavities was chosen large enough to get good resolution of the sampling after termination of the tests.

5.2.1 Test set-up

The geometry of the set-up used for SH3 and SH4 is shown with photos in Figure 5-1 and a sketch in Figure 5-2. Test SH4 was instrumented and this set-up is further described in Section 5.4. The containment is a very stiff cylinder with the inner diameter 300 mm and the height 100 mm. An inner cylinder with the outer diameter 100 mm is included in the centre mainly to reduce the time for saturation and homogenisation. A stiff filter is mounted to the inside of the outer ring with the purpose to provide water to the bentonite from the radial surface. In the bentonite block two cavities were cut out in two diametrical positions to simulate loss of material.

Figure 5-1. *Photos of the bentonite block used for SH3. The bentonite block with the cavity (left) and installed into the test device (right).*

5.2.2 Test procedure

The preparation of the bentonite rings for SH3 and SH4 was made by compaction of the blocks, which were machined to rings with the correct dimensions and by cutting the cavities. After installation of the bentonite ring and the lids the test SH3 was started by filling the filter and the cavities with de-ionized water and applying a low water pressure (10 kPa). The water was supplied through the filter, which was attached to the inside of the cylinder ring. Circulation of water through the filter was possible by use of the water inlet and outlet, located in two diametrical positions of the steel ring, see Figure 5-2.

Test SH4 differs in that it was instrumented, and it was wetted slowly compared to all other tests in this series. The instruments were installed according to Section 5.4 before the installation of the bentonite ring. At start of SH4 the water inflow rate was set to saturate the block in two years, see Section 5.4.

Test SH3 started in February 2015 (2015-02-23) by opening the water supply and was dismantled after 44 months (2018-10-03). Test SH4 started in March 2017 (2017-03-01) and was dismantled after 43 months (2020-09-07).

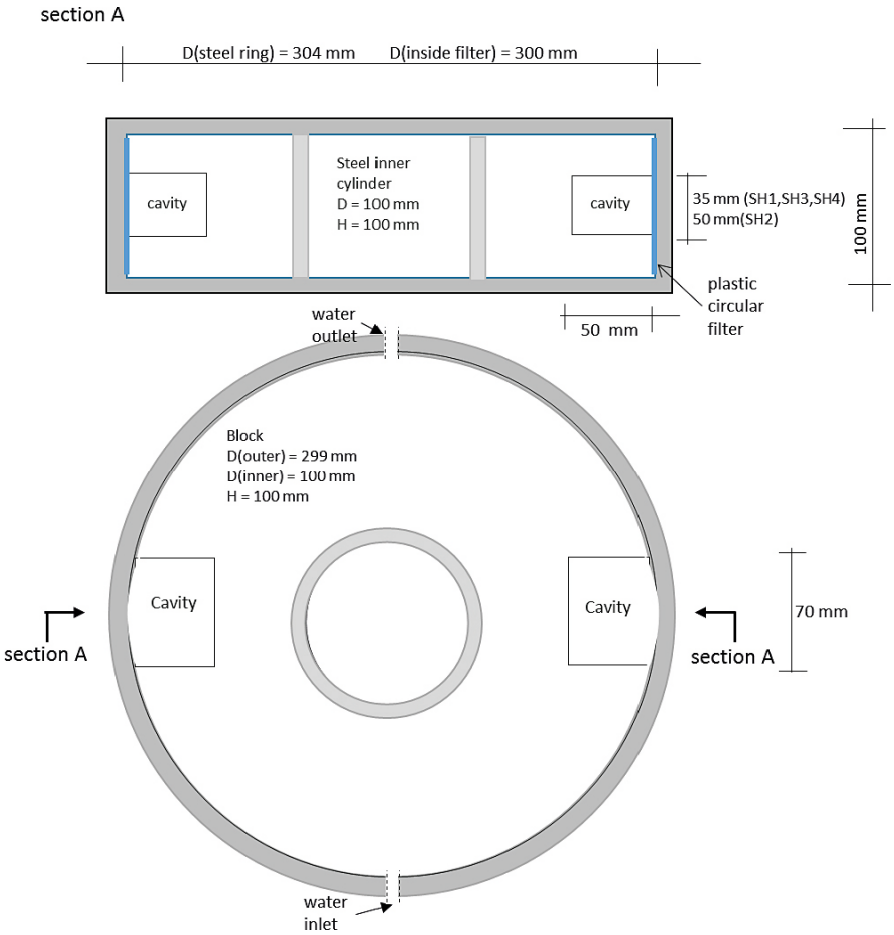

Figure 5-2. *A sketch of the set up used for the tests SH1–SH4. The dimensions of the outer and inner steel cylinder and the bentonite block with the cavities (approximate dimensions) are shown as well as the plastic filters and the locations of the water inlet and outlet.*

5.3 Results from test SH3

The focus of this section is the results from SH3. Additional information can be found in Section A2.1 (Appendix 2) where a timetable for the test, photos from mounting and dismantling, evolution of water pressure and water volume and tabulated values of water content and dry density are shown.

5.3.1 Preparation and installation

The geometry of the test set-up was shown in Figure 5-2. Powder of the Ca-bentonite Calcigel was mixed with de-ionized water to get a water content of 22 % in order to reach a high initial degree of saturation after compaction. Aiming at a dry density of approximately 1 660 kg/m^3 a compaction pressure of approximately 22 MPa was used for the uniaxial compacted cylinder block. The block was machined with a rotating lathe to the following dimensions: height = 100 mm, outer diameter = 298.7 mm and inner diameter = 100.0 mm. There was thus a small gap of 0.65 mm between the block and the outer ring and virtually no gap at the inner ring and at the lids. The dry density was measured on samples from the removed centre cylinder to 1 711 kg/m^3 (cf SH1 1 657 kg/m^3, SH2 1 672 kg/m^3). Cavities were cut in two diametrical positions and the average of the dimensions (height × length × depth) of the cavities in SH3 was 35 × 69 × 47 mm^3, cf Figure 5-2.

In Table 5-1 the initial condition of the installed bentonite block is presented in terms of bulk density ρ, water content w, dry density ρ_d and degree of saturation S_r. The variables are derived in four different ways (Case 1–4);

1. Initial block density calculated from the initial mass and the initial volume of the block.
2. Initial block density measured on a sample of the removed centre cylinder at preparation.
3. Final average density calculated from the initial mass and the final dimensions inside the device without including the cavities.
4. Final average density calculated in the same way as 3 with the filter deformation taken into account without including the cavities.

Table 5-1. Initial conditions of the installed bentonite block in SH3 of Calcigel. The base variables bulk density ρ, water content w, dry density ρ_d, void ratio e and degree of saturation S_r are shown for the initial conditions 1–4.

Case	ρ kg/m^3	w %	ρ_d kg/m^3	e -	S_r %	Remarks
1	2055	21.7	1685	0.60	98	Calculated from the initial mass and the initial volume of the block.
2	2055	20.1	1711	0.57	94	Measured on a centre sample of the block, sampled at preparation.
3	2022	21.7	1662	0.62	98	Calculated from the initial mass and the final dimensions inside the containment with water in the gap.
4	2016	21.7	1657	0.63		Calculated according to Case 3, with the filter deformation taken into account.

5.3.2 Water saturation and water supply

Water was applied through the inlet and let through the filter and out at the opposite side. The volume of the inflow and outflow are plotted with the net-volume as a function of time during the first month in Figure 5-3. The required water volume to fill the available empty space, mainly consisting of filter, gaps and cavities was predicted to 430 ml and the total volume to be filled with water including the saturation of the bentonite was estimated to 560 ml. A leakage was seen from the device and an attempt was made to estimate this leakage but already after one month the estimated net-volume was larger than the calculated required volume, indicating presence of additional evaporation and leakage.

During the first year, attempts were made to increase the water pressure and after one year a water pressure of approximately 100 kPa could be kept during longer periods of days or weeks. After two years (from 2017-02-12) a constant water pressure of 70 kPa was applied and kept and after additional seven months (from 2017-09-11) the water pressure was increased to 100 kPa which was kept until

dismantling. During the last year flushing was made at some limited occasions by opening the drainage and lowering the water pressure to zero at the outflow. At those occasions small amounts of water came through the filter. However, the inflow of water increased when the outlet was closed again, and the water pressure started to build up. This larger inflow after flushing might have been caused by loss of water leaking from the filter during the flushing or by larger parts with air in the filter. After some time with the drainage closed the water inflow stabilized and levelled out, see Section A2.1.

5.3.3 Termination and dismantling

The test was terminated in October 2018 and five days before the termination the applied water pressure of 100 kPa was lowered to zero. Before the opening of the device an attempt was made to evacuate the filter from water but only a small volume of water was possible to remove. The dismantling started with lifting the lid and removing the bottom from the cylinder ring and then marking the planned sampling on the uncovered bentonite surfaces. The dismantling continued by free-drilling, removing the inner steel cylinder and dividing the bentonite cylinder into two half circles by sawing radially. Figure 5-4 shows photos taken during the dismantling. Additional photos can be found in Section A2.1.

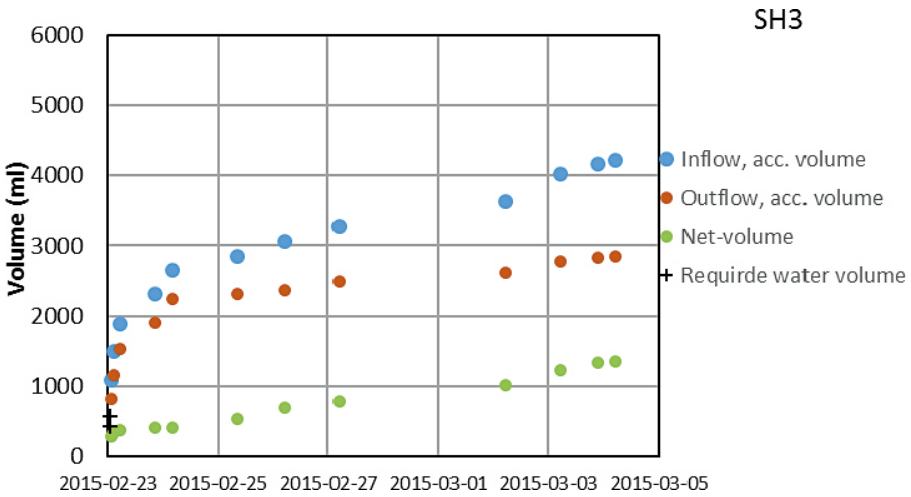

Figure 5-3. *Accumulated in- and outflow of water are shown as a function of time during the first weeks. The difference between the in- and outflow, i.e. the net-volume, is also shown. The estimated required water volume to fill filter, gaps and cavities is shown with black plus signs and the somewhat higher value includes also the saturation of the bentonite.*

Figure 5-4. *Photos from the dismantling of SH3.*

5.3.4 Sampling and denomination of the samples

The bentonite cylinder ring was divided into two half-cylinders during the dismantling. One of the half-cylinders was directly used for the sampling and determination of water content and density distributions while the other one was sealed and stored for later analyses. The two half-cylinders were considered to be equal, with water supply everywhere in the filter from the beginning of the test. The division of the bentonite ring in different parts and the sampling plan are illustrated in Figure 5-5 and Figure 5-6.

The half-cylinder for sampling was further divided axially at the middle height and the determinations of density were made on the upper part while the determinations of water content were made on the lower part, illustrated to the right in Figure 5-5. Extensive sampling was made with two different strategies, i.e. along four lines and continuously within a sector. The lines and the sector are marked red and yellow, respectively, to the left in Figure 5-5. The sampling of SH3 was done in mainly the same way as in the previous tests SH1 and SH2.

The lines were located at the approximate angles 0°, 20°, 65°, and 90° from the middle of the initial cavity and samples taken along these lines were denominated L0, L20, L65, and L90, see Figure 5-6. The sector with continuous sampling was located between 0° and 45° from the middle of the cavity and it included parts both inside and outside of the initial cavity. The sector was divided into the sub-sectors A, B, C and D with the centre angles 6°, 17°, 28° and 39°, respectively, from the centre of the cavity. The sub-sectors A–D were further divided into two parts each, along which the samples were taken. The denominations of all subsectors starting from the centre of the cavity are A, A(2), B, B(2), C, C(2), D, D(2), see Figure 5-6. Both water contents and densities were determined at three different levels axially; 1 – outermost, 2 – second outermost and 3 – innermost, which are illustrated to the right in Figure 5-6. The approximate size of each type of sample is shown in Figure 5-7.

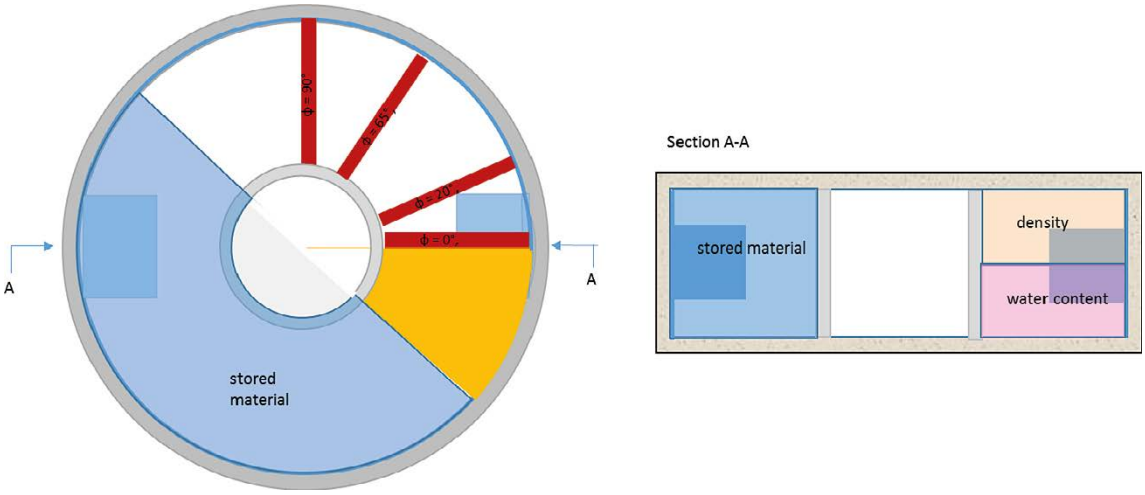

Figure 5-5. *Plan view (to the left) and section (to the right) of the bentonite block at dismantling. The plan view shows the bentonite cylinder ring with the stored material (blue area), the lines of sampling (red lines) and the sector for continuous sampling (yellow area) marked. The section shows the stored part and the parts used for determinations of density and water content.*

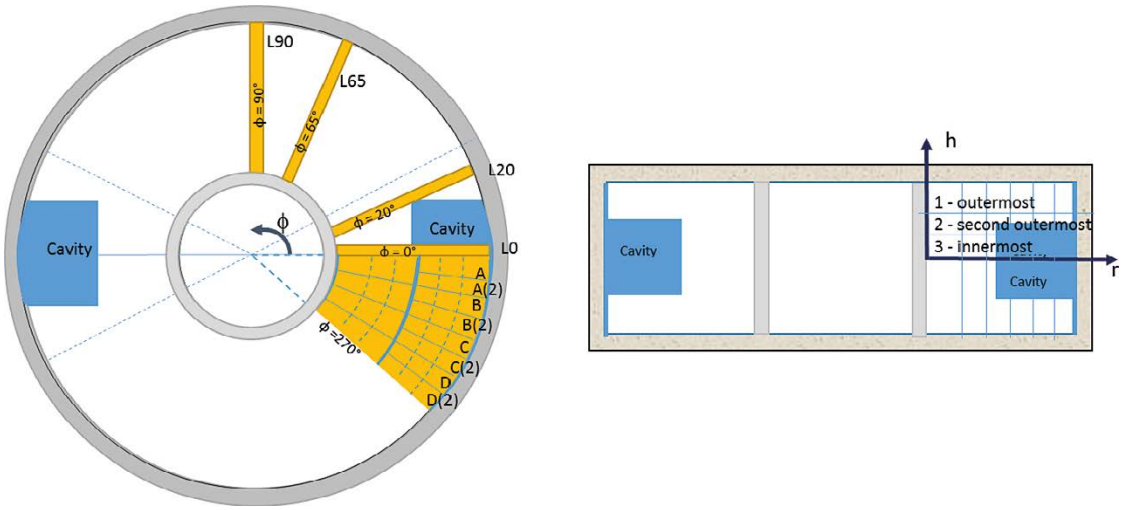

Figure 5-6. *Plan view (to the left) which shows the sampling along lines at different angles from the middle of the cavity; 0°, 20°, 65° and 90° marked L0, L20, L65, L90, respectively, and the continuous sampling within a sector marked A, A(2), B, B(2), C, C(2), D, D(2). The section (to the right) shows the different axial levels for the sampling; outermost, second outermost and innermost.*

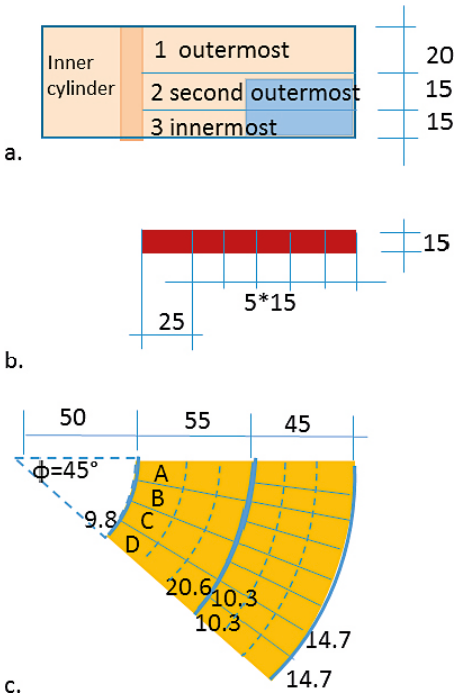

Figure 5-7. *Positions and sizes of the samples. Different parts and views are shown; a. section with different sampling levels, b. plan view of one of the four sampling lines and c. plan view of the sampled sector with subsectors. The numbers show the approximate dimensions of the samples in the unit mm. As shown the centre angle of the sampled sector is 45°.*

5.3.5 Distribution of water content and density of SH3

The measured distributions of dry density determined after dismantling of SH3 at the levels 1, 2, and 3 (outermost, second outermost and innermost) are shown in Figure 5-8, Figure 5-9 and Figure 5-10, respectively. From almost all positions the dry densities were calculated from measured bulk densities and water contents. From line L20 only water contents and no bulk densities were measured but the dry densities were here calculated from an assumed degree of saturation of 100 % which was proven to be valid in adjacent areas. The initial dry density of the block was estimated to 1 685 kg/m^3, see Table 5-1, from the mass and measured dimensions. The average final dry density based on the initial mass and the final volume of the device, i.e. with the cavities taken into account, was calculated to 1 589 kg/m^3. The average final dry density was also calculated from the determinations after dismantling, and a weighted average was estimated to 1 597 kg/m^3.

The distribution of dry density in different directions are shown as a function of the radial distance. The colours (red, brown, orange, yellow) show the results from the sampling lines (L90, L65, L20, L3) at the angles (90°, 65°, 20°, 3°) from the centre of the initial cavity. Within the sector with continuous sampling the colours (green, blue, purple, black) show the sampling lines for the sectors (A, B, C, D). Each subsector was further divided into two parts, marked with dotted and solid lines of each of the colours and from the centre of the cavity the denomination of all sub-sectors are A, A(2), B, B(2), C, C(2), D, D(2) corresponding to the angles (−3°, −8°, −14°, −20°, −25°, −31°, −37°, −42°) from the centre of the cavity. In the diagrams and tables, the positions of two specimens have been corrected and four values are missing which is further mentioned in Section A2.1.

The lowest values (green and yellow) and the highest values (red) were seen in the directions coinciding with and perpendicular to the direction of the centre of the cavity, respectively. Tabulated values of water content and dry density are given in Section A2.1.

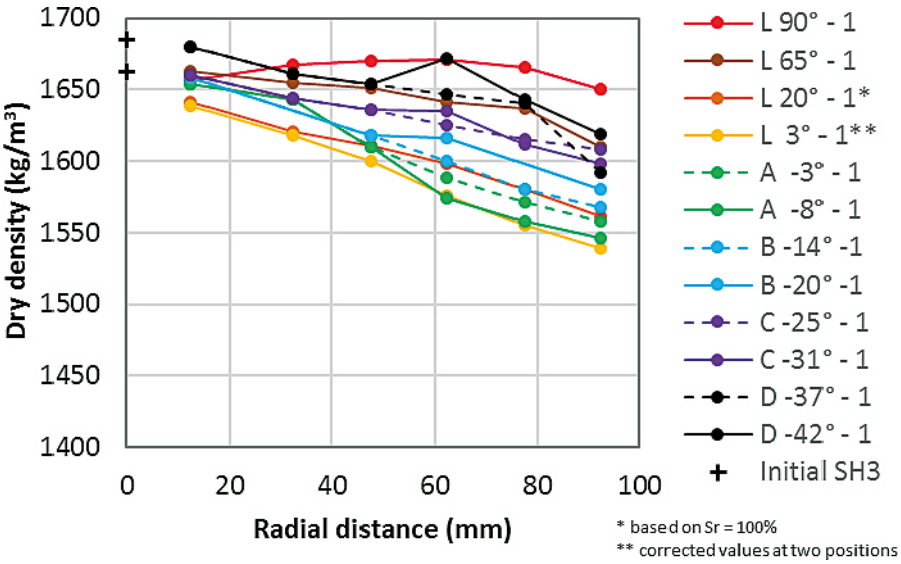

Figure 5-8. *Distribution of dry density at the outermost level 1 in different directions. The colours (red, brown, orange, yellow, green, blue, purple, black) show angles between +90° to −42° from the centre of the initial cavity. The angles are indicated in the labels. The initial conditions (plus signs) correspond to cases 1 and 3 in Table 5-1.*

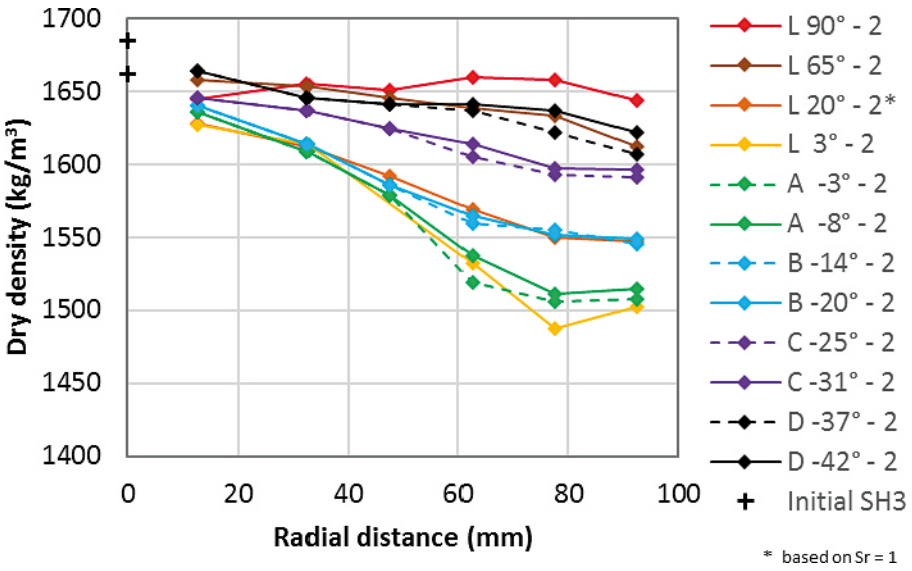

Figure 5-9. *Distribution of dry density at the second outermost level 2 in different directions. The colours are the same as in Figure 5-8. The angles are indicated in the labels. The initial conditions (plus signs) correspond to cases 1 and 3 in Table 5-1.*

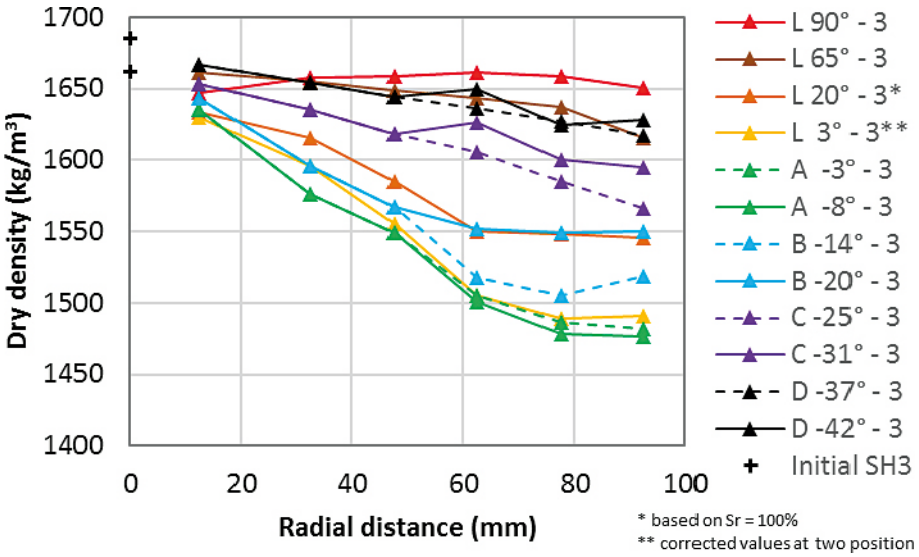

Figure 5-10. *Distribution of dry density at the innermost level 3 in different directions. The colours are the same as in Figure 5-8. The angles are indicated in the labels. The initial conditions (plus signs) correspond to cases 1 and 3 in Table 5-1.*

5.3.6 Comments

The diagrams show that the dry density increases logically from the lines through the centre of the cavity (A-3 and L3, i.e. green and yellow lines) to the lines perpendicular to the centre of the cavity (L90, red line). The relatively low density of the samples at the outermost radial position at all three levels in the direction perpendicular to cavity (red lines) was probably caused by the 0.65 mm gap between the bentonite ring and the outer ring with filter.

In addition to the results presented above samples were taken in order to study the vertical symmetry mirrored by the horizontal symmetry plane, i.e. the correspondence between the results from samples taken from the upper and from the lower half of the bentonite ring. Along line L20 the water content was determined at all levels on both the lower half (levels 1, 2 and 3) and the upper half (levels 1b, 2b, 3b). The results are shown in Figure 5-11 where each colour represents a specific level, i.e. outermost (blue), second outermost (red) and innermost (green). The water contents determined on samples from the lower half (circles) and upper half (triangles) agree fairly well but the results from the upper half are generally a little higher and the largest deviations are located at the outermost level (blue) at the radial distance r = 12.5 mm where the difference was approximately $\Delta w = 0.8$ %.

Both water content and density were determined in all positions, except along L20, so the dry density could be directly calculated as presented above. By use of the particle density ρ_s the degree of saturation could be calculated. The block was saturated at all positions, however, at the innermost positions perpendicular to the direction of the cavity the degree of saturation was about 96 % at all levels. The average of the degree of saturation was 101.8 % with a standard deviation of 1.6 % based on the particle density 2 695 kg/m^3 (Svensson et al. 2011) and water density ρ_w = 1 000 kg/m^3.

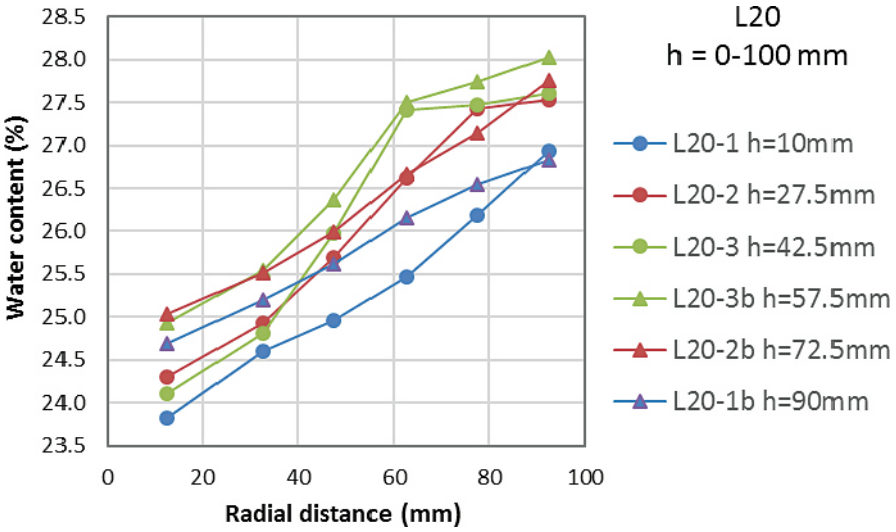

Figure 5-11. *Water contents determined on samples taken along the sampling line L20. Samples were taken from both the lower half (circles) and upper half (triangles) of the bentonite ring. The colours (blue, red, green) show the levels (outermost, second outermost, innermost).*

5.4 Results from test SH4

The focus of this section is the results from SH4. Additional information can be found in Section A2.2 (Appendix 2) where a timetable for the test, photos from mounting and dismantling, evolution of water pressure and water volume and tabulated values of water content and dry density are shown.

5.4.1 Preparation and installation

The geometry of the test set-up was shown in Figure 5-2 and the sensors used in the test SH4 were located similar to the sensors in the previous SH1, i.e. according to Figure 5-12.

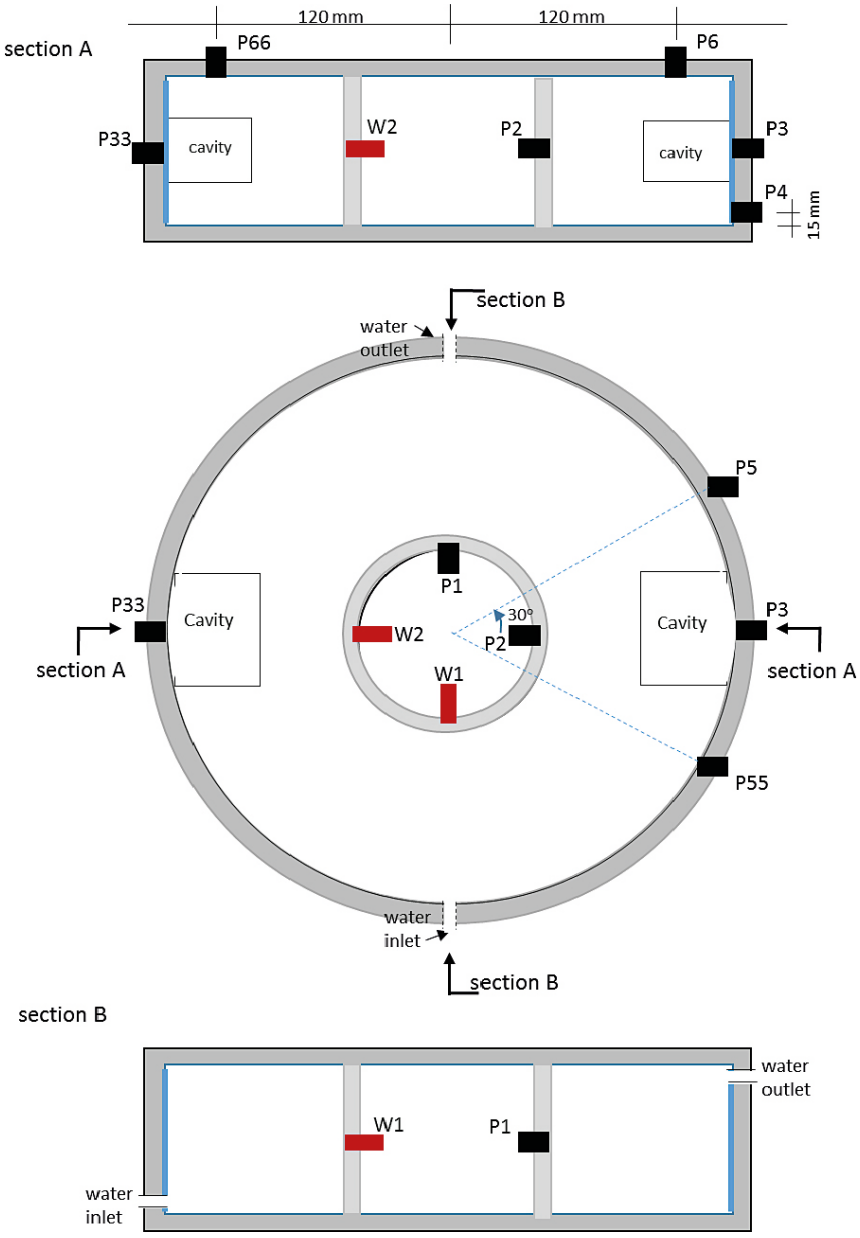

Figure 5-12. *A sketch showing the positions of the sensors used in test SH4, which was also used in SH1. The positions of the cavities and the water inlet/outlet are also shown.*

Powder of the Wyoming bentonite MX-80 was used for the test. The dry density at compaction was calculated to be approximately the same as in the previous SH1 and SH2 and a water content of 15.8 % was chosen to reach a drier condition compared to the previous tests where 24 % was used. The block was machined with a rotating lathe to the following dimensions: height = 100 mm, outer diameter = 298.7 mm and inner diameter = 100.0 mm. There was thus a small gap of 0.65 mm between the block and the outer ring and virtually no gap at the inner ring and at the lids. The dry density measured on samples from the removed centre cylinder was 1 671 kg/m^3 (cf SH1 1 657 kg/m^3, SH2 1 672 kg/m^3).

Cavities were cut in two diametrical positions and the average of the dimensions (height × length × depth) of the cavities in SH4 was 35 × 70 × 50 mm^3.

In Table 5-2 the initial condition of the installed bentonite block is presented in terms of bulk density ρ, water content w, dry density ρ_d and degree of saturation S_r. The variables are derived in four different ways (Case 1–4);

1. Initial block density calculated from the initial mass and the initial volume of the compacted block.
2. Initial block density measured on a sample of the removed centre cylinder at preparation.
3. Final average density calculated from the initial mass and the final dimensions inside the device without including the cavities.
4. Final average density calculated in the same way as 3 with the filter deformation taken into account without including the cavities.

Table 5-2. Initial conditions of the installed bentonite block in SH4. The base variables bulk density ρ, water content w, dry density ρ_d, void ratio e and degree of saturation S_r are shown for the initial conditions 1–4.

Case	ρ kg/m³	w %	ρ_d kg/m³	e -	S_r %	Remarks
1	1 916	15.8	1 655	0.68	65	Calculated from the initial mass and the initial volume of the block.
2	1 936	15.8	1 671	0.66	66	Measured on a centre sample of the block, sampled at preparation.
3	1 895	16.5	1 636	0.70	66	Calculated from the initial mass and the final dimensions inside the containment with water in the gap.
4	1 889	16.5	1 631	0.70		Calculated according to Case 3, with the filter deformation taken into account.

5.4.2 Water saturation and water supply

Water was supplied through the inlet at an inflow rate of 0.072 ml/h. The required water volume to fill the available empty space of SH4, mainly consisting of filter, gaps and cavities was predicted to 380 ml and the total volume to be filled with water including the saturation of the bentonite was estimated to 1 230 ml. The water inflow rate was set to saturate the block in two years. The controlled water inflow differs from previous tests in the series where water was added unlimited, filling filter and cavities from the beginning.

The controlled water inflow started on 2017-03-01. In Figure 5-13 the water pressure at the inlet is shown. After half a year the water pressure was approximately 50 kPa and after two years above 100 kPa. In January 2020 the water pressure at the inlet started to increase and the water flow control was exchanged to a controlled water pressure set to 400 kPa at the inflow (marked with a plus-sign in Figure 5-13).

The volume of the water inflow was larger than the predicted 1 230 ml. The inflow was approximately 2 000 ml. An observation of salt accumulation was made at a specific point between the steel ring and lid and the conclusion was drawn that leakage and evaporation took place from this point. A month after the observation of leakage, water was for the first time observed at the outflow during flushing and after additional month the water pressure started to increase which gave that the water pressure was controlled and set to 400 kPa (2020-01-16).

To remove air from the system, the outflow valve was opened occasionally during the first two years and during the last year it was opened more often and regularly. During the last months air was no longer visible during drainage. The controlled water pressure during the last part of the test period (from January 2020 until termination) was applied to the inlet side and to check the pressure at the outflow side the water pressure was measured during the last weeks of the test. Although the controlled pressure was set to 400 kPa at the inflow the measured pressure at the outflow, on the opposite side, was as a maximum 55 kPa. More details can be found in Section A2.2.

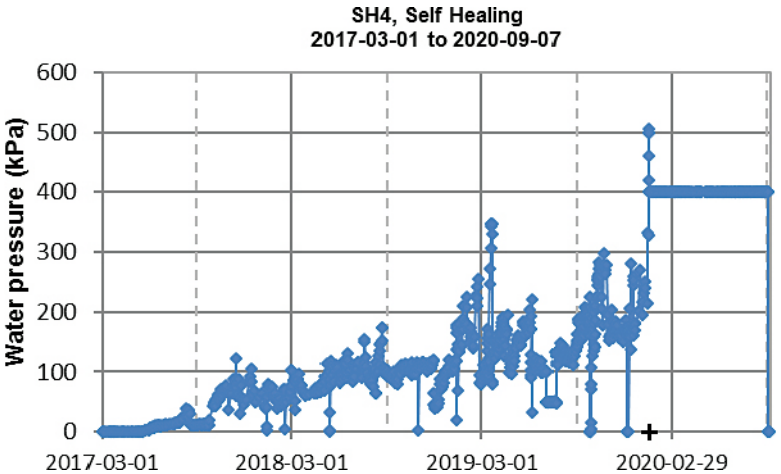

Figure 5-13. *Water pressure build-up at the water inflow in test SH4. Water was added with a water-flow control of 0.072 ml/h from the beginning until 2020-01-16 (marked with a black plus-sign) when the water pressure was set to a controlled value of 400 kPa.*

5.4.3 Swelling pressure measurements

The results from the swelling pressure measurements in test SH4 are presented in Figure 5-14. The measured stresses include the effect of water pressure and are thus measured as a total pressure. The minimum values (green lines) and maximum value (light blue line) were measured at the outside and at the middle height of the cylinder ring and while the minimum values were measured at the centre of one of the cavities the maximum value was measured well outside the cavity. The results from the last part of the test period are magnified and shown again in Figure 5-15. In the diagrams the number of the sensors are shown in the legend and they are also indicated at each measured stress. The positions of the sensors are shown in Figure 5-12. The control of the sensors after the test showed an error less than 3 % in all sensors but P55. This sensor may have shown 8 % too high value at the end of the test. This gives that the difference between P5 and P55, positioned on either side of a cavity, was even larger than shown in Figure 5-14.

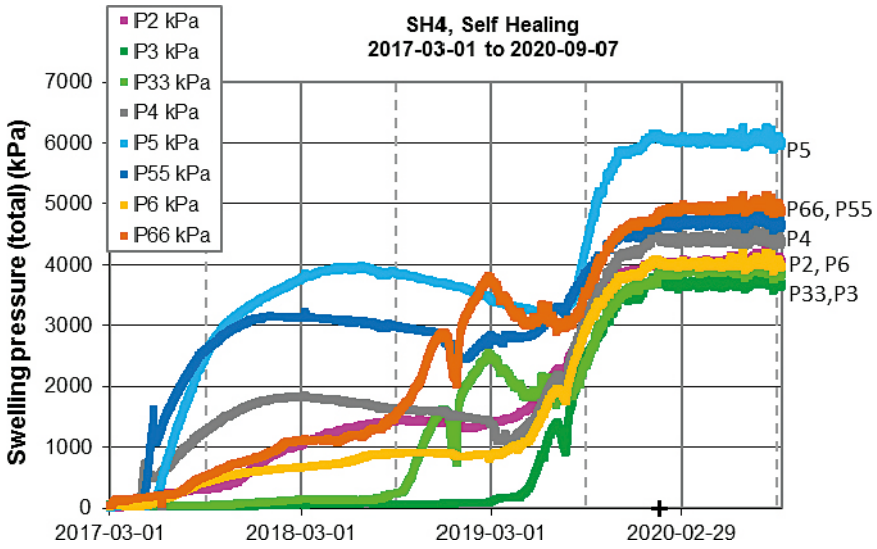

Figure 5-14. *Evolution of swelling pressure (total pressure) from the load cells installed in test SH4. The number of the sensors are shown to the right. The black plus-sign marks the change from flow control to water pressure control. The positions of the sensors are shown in Figure 5-12.*

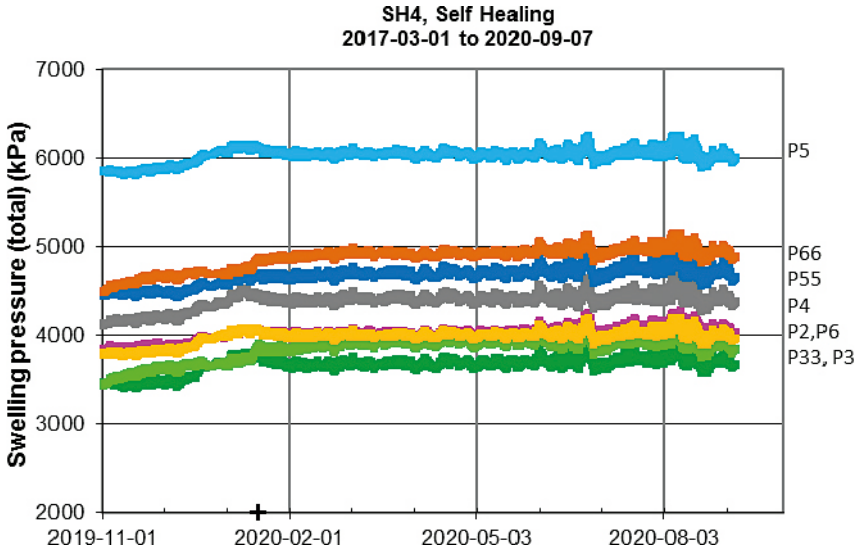

Figure 5-15. *Evolution of swelling pressure (total pressure) from the last ten months of the test. The number of the sensors are shown to the right. See also Figure 5-14.*

The results show somewhat non-symmetric results at the end of the test. The sensors P5 and P55 (light and dark blue, respectively) show different results although they are positioned at middle height at the same distance from one of the cavities. Lower swelling pressure is measured closer to the water inlet (P55) compared to the higher value measured on the other side of the cavity, towards the water outlet (P5). This indicates that the results are not symmetric on different sides of the cavities.

Different results are also measured by the sensors P6 and P66 which are located at similar positions on the lid. Since they are positioned at different sides of the device (P66 to the left and P6 to right) this indicates non-symmetric results between the left and right side of the device. Thus, there are indications that there are no vertical symmetry planes. However, the same swelling pressure (total stress) are measured in the centre of the two cavities (P3 and P33).

The evolution with time was different at the different positions. For example, the longest delay in the response was seen in the response from the sensors positioned in the centre of the cavities (green lines, P3 and P33), which is logical. Another difference between different positions are the peaks after approximately two years which are seen in the results from the only two sensors positioned on the left side of the device (P33 and P66). The peaks are not observed in the results from any other sensor. The cause of the peak is discussed in Section A2.2.

An attempt was made to measure the water potential with thermocouple psychrometers from Wescor®. However, the sensors did not give any response during the testing period. Problem was also noted in the results from the sensor P1, the results from this sensor was regarded as unreliable and are not shown in the diagrams above, see also Section A2.2.

5.4.4 Termination and dismantling

The test was terminated in September 2020, after 43 months. Five days before the termination the applied water pressure of 400 kPa was lowered to zero. The dismantling started with removing the sensors. In Figure 5-16 photos from the dismantling are shown. After that the lid and bottom were removed, marks were made on the upper surface to facilitate the sampling. The block was then forced upwards through the ring by a hydraulic jack. The method used was more rapid and saved the bentonite block compared to the method used for the dismantling of the previous blocks in the series. The previous method was based on free-drilling of the inner steel-cylinder.

Figure 5-16. *Photos from the dismantling of SH4. The device before opening the device to the left and the dismantled block to the right.*

5.4.5 Sampling and denomination of the samples

The sampling after the previous tests in the series were all made according to Section 5.3. The sampling along lines and within a sector were made with an assumption of a horizontal symmetry plane along the centre of the block. With this symmetry, density determinations were made on samples in the upper part and the corresponding water content determinations were made on samples at the same positions in the lower part.

The same type of sampling was made on the right side of the dismantled block SH4. On the left side of the block, however, the sampling was made by determination of both water content and density at the same level and at all levels. The sampling is indicated in Figure 5-17 where a horizontal symmetry was used in the sampling along the so called L-lines and within the sectors A–D to the right. No symmetry was used in the sampling along the so-called M-lines to the left.

The samples on the right side were taken along the L-lines at different angles from the centre of the initial cavity (−90°, −65°, 0°, 20°, 65°, 90°) and within the sectors A to D at angles between 0° and −45°. Dry density distributions were determined from a density in the upper part and a water content at the corresponding position in the lower part.

The samples on the left side were taken along the M-lines at different angles from the centre of the initial cavity at that side (−65°, 0°, 20°, 65°, 90°) where M90 is located adjacent to L90, i.e. at the water outlet.

The denomination of the lines and the subsectors are shown in Figure 5-17. The approximate size of each type of sample is shown in Figure 5-18 and Figure 5-19 (compare Figure 5-7).

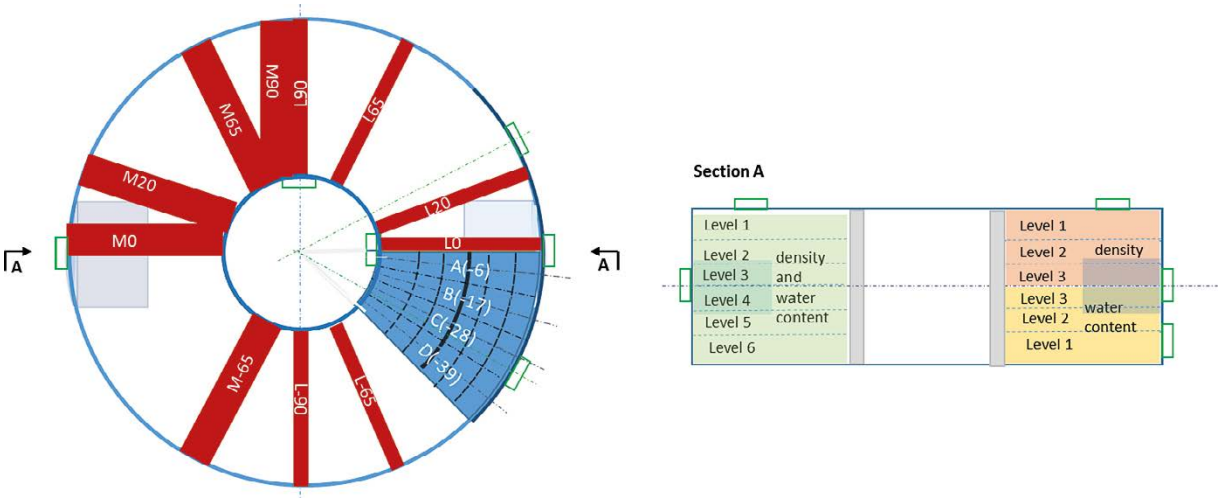

Figure 5-17. *Plan view (to the left) and section (to the right) of the bentonite block at dismantling. The plan view shows the bentonite cylinder ring with sampling lines M-lines to the left and L-lines to the right of the block. To the right of the block sampling was also done within a sector. The section shows the sampling for density and water content determinations along M-lines to the left and L-lines and within the sector to the right.*

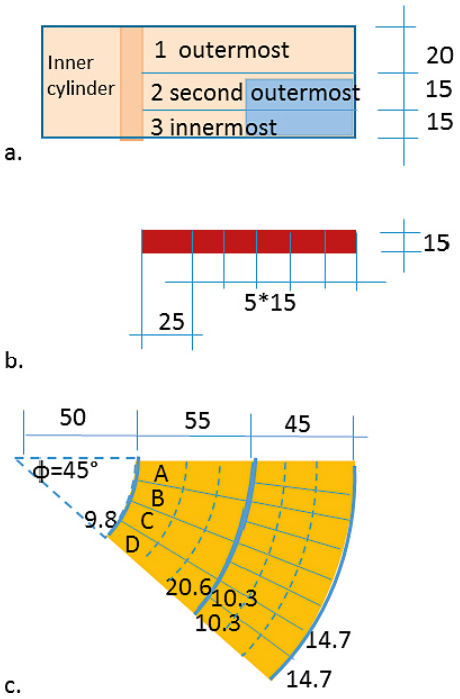

Figure 5-18. *Positions and sizes of the samples from the right side of the dismantled block. Different parts and views are shown; a) Section with sampling levels 1 to 3 on the upper half, b) Plan view of one of the sampling L-lines and c). Plan view of the sampled sector with the centre angle 45° and subsectors A to D. The dimensions are given in mm.*

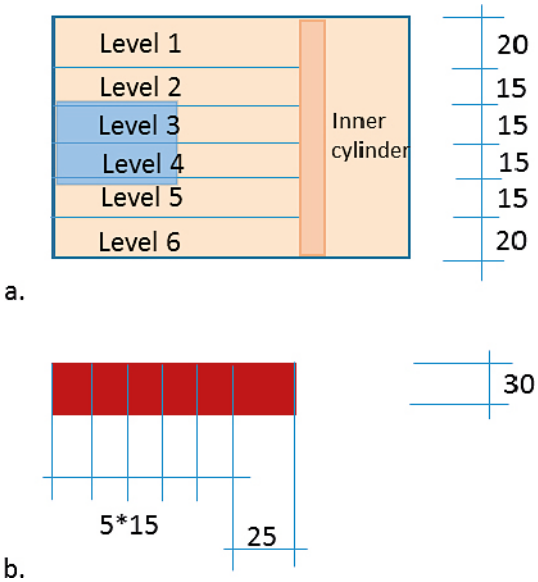

Figure 5-19. *Positions and sizes of the samples from the left side of the dismantled block. Different parts and views are shown; a) Section with sampling levels 1 to 6 over the full height, b) Plan view of one of the sampling M-lines. Results from some of the M-lines were only determined at 5 levels. The dimensions are given in mm.*

5.4.6 Distribution of water content and density of SH4

In this section the results refer to the right side of the block where the sampling was made according to previous tests in this series. The measured distributions of dry density determined after dismantling of SH4 at the levels 1, 2, and 3 (outermost, second outermost and innermost) are shown in Figure 5-20, Figure 5-21 and Figure 5-22, respectively. The diagrams represent the over-all behaviour but show only the results from the right side, i.e. from L-lines and the sector. The results from the left side, from M-lines, are presented below. The sampling plan along L-lines and M-lines was described in Figure 5-17. The block was saturated at dismantling with an average degree of saturation of 99.3 %. All results are tabulated in Section A2.2.

The dry density shown in Figure 5-20, Figure 5-21 and Figure 5-22 is calculated from density measurements in the upper half and water content measurements in the lower half, see Figure 5-17. The initial dry density of the block was estimated to 1 655 kg/m^3, see Table 5-2, from the mass and measured dimensions. The average final dry density based on the initial mass and the final volume of the device, i.e. with the cavities taken into account, was calculated to approximately 1 560 kg/m^3. The average final dry density was also calculated from the determinations after dismantling, and a weighted average was estimated to 1 530 kg/m^3.

The distribution of dry density in different directions are shown as a function of the radial distance. The colours (red, brown, orange, yellow, dark blue and dark green) show the results from the sampling lines (L90, L65, L20, L0, L-65, L-90) at the angles (90°, 65°, 20°, 0°,−65°, −90°) from the centre of the initial cavity. Within the sector with continuous sampling the colours (light green, light blue, purple, grey) show the sampling lines for the sectors (A, B, C, D) corresponding to angles decreasing from the centre of the initial cavity (−6°, −17°, −28°, −39°). Each subsector was further divided into two parts, marked with dotted and solid lines of each of the colours corresponding to approximately ±1.4° from the centre of the sub-sectors (i.e. −3°, −8°, −14°, −20°, −25°, −31°, −37°, −42°).

The lowest values (light green and yellow) and the highest values (red) were seen in the directions coinciding with and perpendicular to the direction of the centre of the cavity, respectively, which is logical. However, the dry density along the lines L(-65) and L(-90) are lower than expected and indicate a non-symmetric result towards the water inlet compared to towards the outlet. Comparing with the initial condition, marked with plus signs in the diagrams below, the dry density after dismantling is lower at all positions.

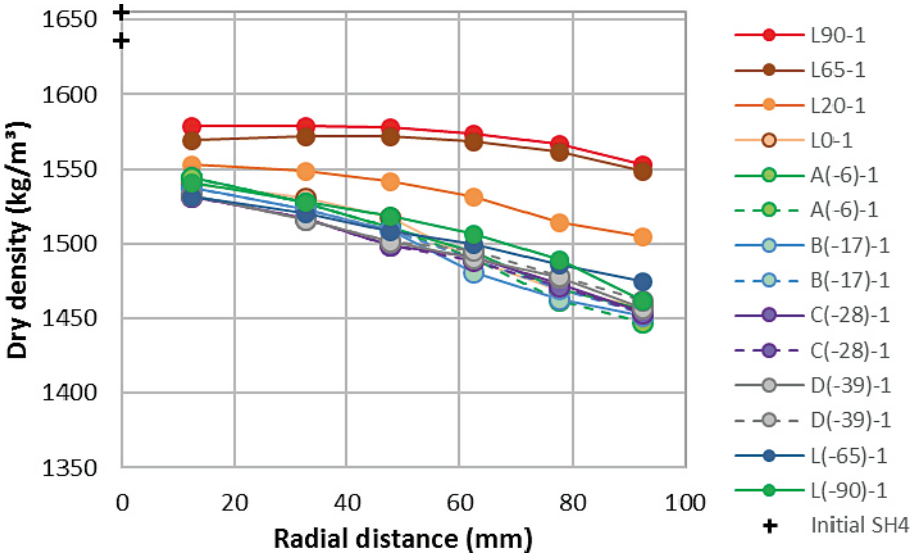

Figure 5-20. *Distribution of dry density at the outermost level 1 in different directions. The colours (red, brown, orange, yellow, light green, light blue, purple, grey, dark blue, dark green) show angles between +90° to −90° from the centre of the initial cavity. The angles are indicated in the labels. The initial conditions (plus signs) correspond to cases 1 and 3 in Table 5-2.*

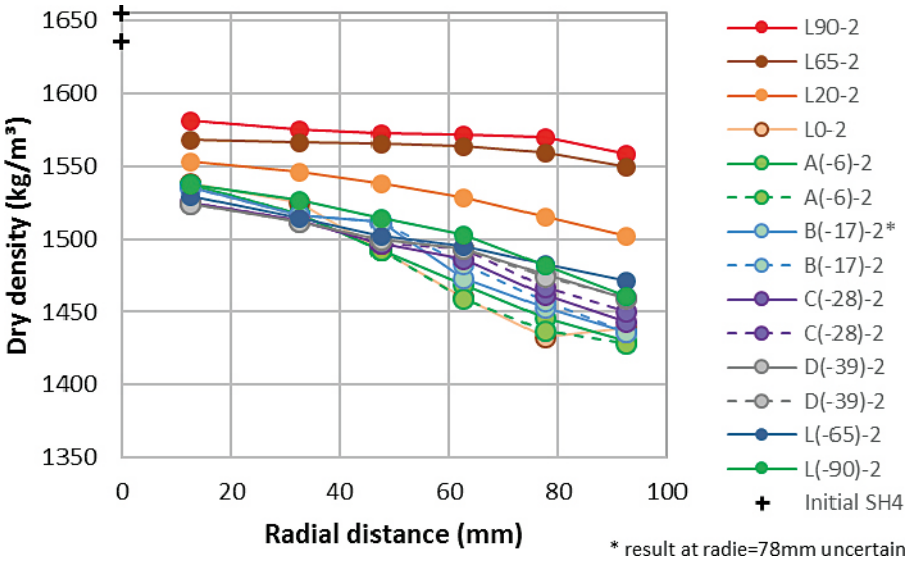

Figure 5-21. *Distribution of dry density at the second outermost level 2 in different directions. The colours are the same as in Figure 5-20. The angles are indicated in the labels. The initial conditions (plus signs) correspond to cases 1 and 3 in Table 5-2. One uncertain value in sub-sector B is marked.*

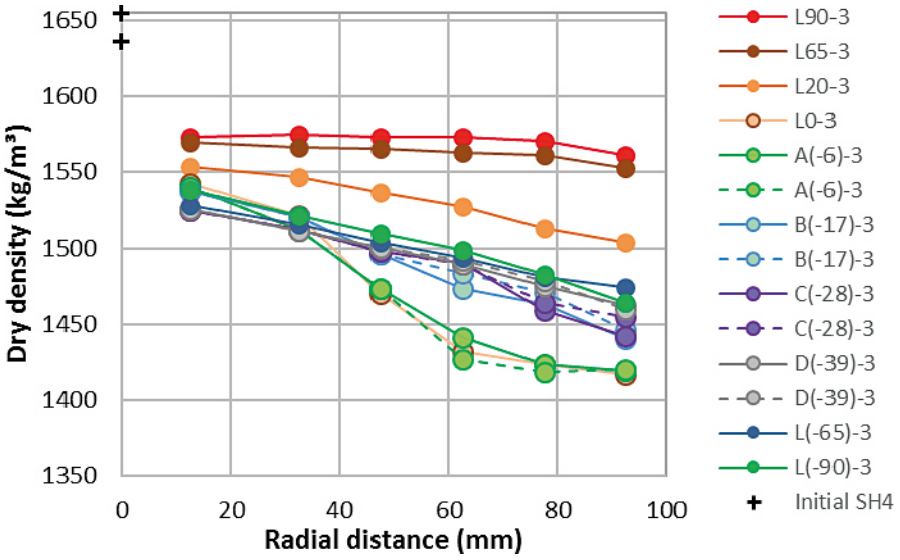

Figure 5-22. *Distribution of dry density at the innermost level 3 in different directions. The colours are the same as in Figure 5-20. The angles are indicated in the labels. The initial conditions (plus sign) correspond to cases 1 and 3 in Table 5-2.*

5.4.7 Additional results

The slightly different sampling along M-lines was made on the left side of the block to get more information about any symmetry plane. In Figure 5-23, Figure 5-24 and Figure 5-25 corresponding results from both L-lines and M-lines are shown together at the different levels; outermost, second outermost and innermost. The colours used, denote the same angles as above.

In the results from the M-lines (to the left) dry density profiles of the upper and lower half at comparable distances from the middle-hight are shown with diamonds and triangles, respectively. It seems as horizontal symmetry, between the upper and lower part, is present in the innermost positions while less symmetry is seen at the outermost level. The largest difference between the upper and the lower half of the block is seen at the outermost level at the radial position 92 mm, i.e. close to the steel ring and lid, where the difference is approximately 50 kg/m^3. The corresponding difference in water content at the same position is $\Delta w = 2.7$ %.

However, no large differences could be seen between the dry density at comparable positions on either side of the vertical plane through 90°/−90°, i.e. by comparing results from the left side (M-lines) with corresponding results from the right side (L-lines).

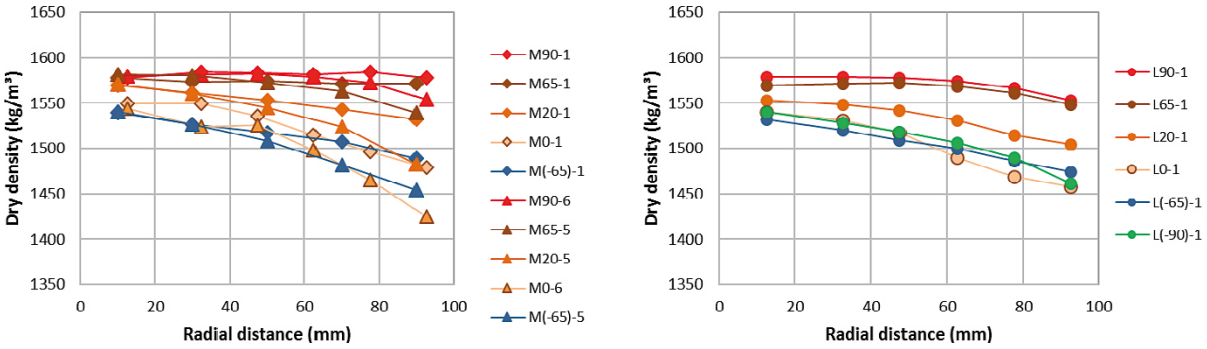

Figure 5-23. *Distribution of dry density at the outermost level 1 in different directions. The colours (red, brown, orange, yellow, blue and green) denote different angles to the centre of the initial cavity. While the results from M-lines (to the left) were determined on both the upper half (diamonds) and lower half (triangles) the results from the L-lines (to the right) are based on horizontal symmetry. The results to the right were also shown in Figure 5-20.*

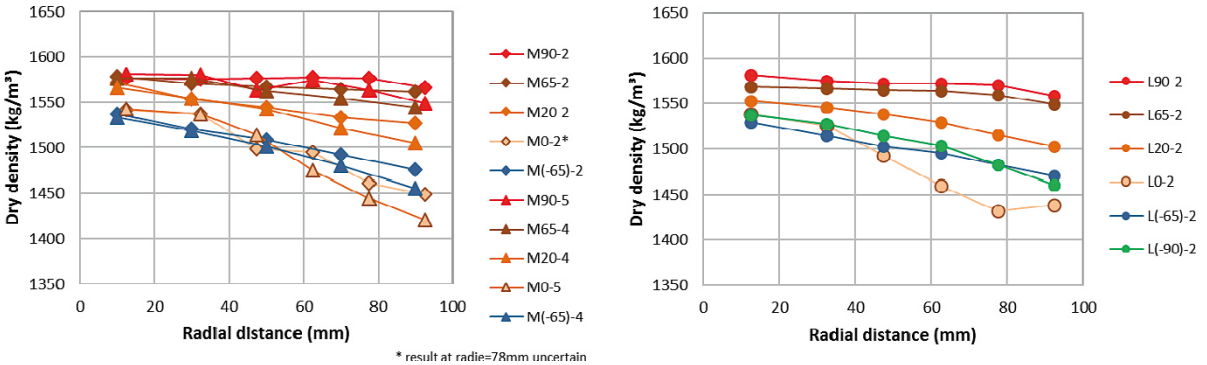

Figure 5-24. *Distribution of dry density at the second outermost level 2 in different directions. The same design and markers as in Figure 5-23 are used. The results to the right were also shown in Figure 5-21. One uncertain value in line M0 is marked.*

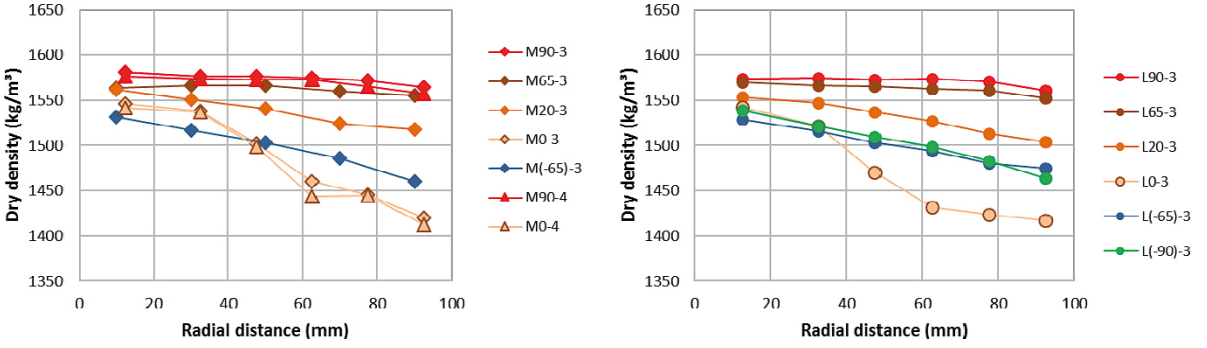

Figure 5-25. *Distribution of dry density at the innermost levels 3 and 4 in different directions. The same design and markers as in Figure 5-23 are used. The results to the right were also shown in Figure 5-22.*

5.4.8 Comments

The block was water saturated, and the average degree of saturation was 99.3 %. The degree of saturation varied mainly between 98 and 101 % but single values of 97 % and 103 % were also present. At the water outlet (at the angle 90°) the sampling, for determination of water content and bulk density, was made both by taking two adjacent samples (M90) and by considering horizontal symmetry and determining bulk density on the upper part and water content on the lower part (L90). The profiles of degree of saturation at the water outlet based on the two sampling techniques are shown in Figure 5-26. No large variations over the radius is seen in the results to the left (M-lines) while a trend of increasing degree of saturation with radius is seen in the results to the right (L-lines). The trend seen to the right is probably an effect of the differences in the outer positions between the upper and lower part of the block, shown in Figure 5-23 to Figure 5-25 above. The trend is thus only an artefact since the two specimens used for the determinations of water content and density, which are used for the calculation of degree of saturation, do not represent the same condition.

To illustrate the different behaviour towards the water inlet and outlet, respectively, contour plots of the calculated dry density were made using an interpolation program. Contour plots of the outermost and innermost levels are illustrated in Figure 5-27 and Figure 5-28, respectively. In Figure 5-29 and Figure 5-30 vertical sections through the cavities (0°/180°) and perpendicular to the cavities (90°/−90°) are shown. The diagrams illustrate the non-symmetry between the water inlet and outlet, and the difference between the right and left side of the block can also be seen. However, due to the interpolation and the chosen scale the differences between the upper and lower part of the block, discussed above, cannot be observed.

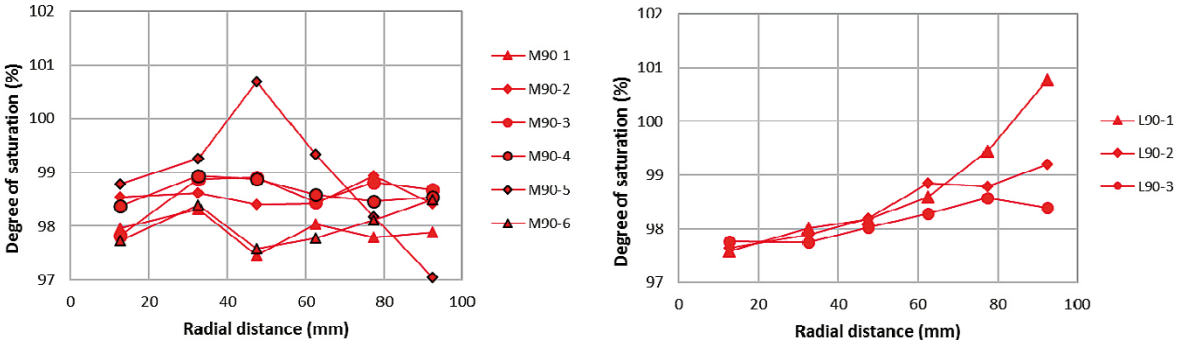

Figure 5-26. *Calculated degree of saturation from sampling along M90 (to the left) and L90 (to the right).*

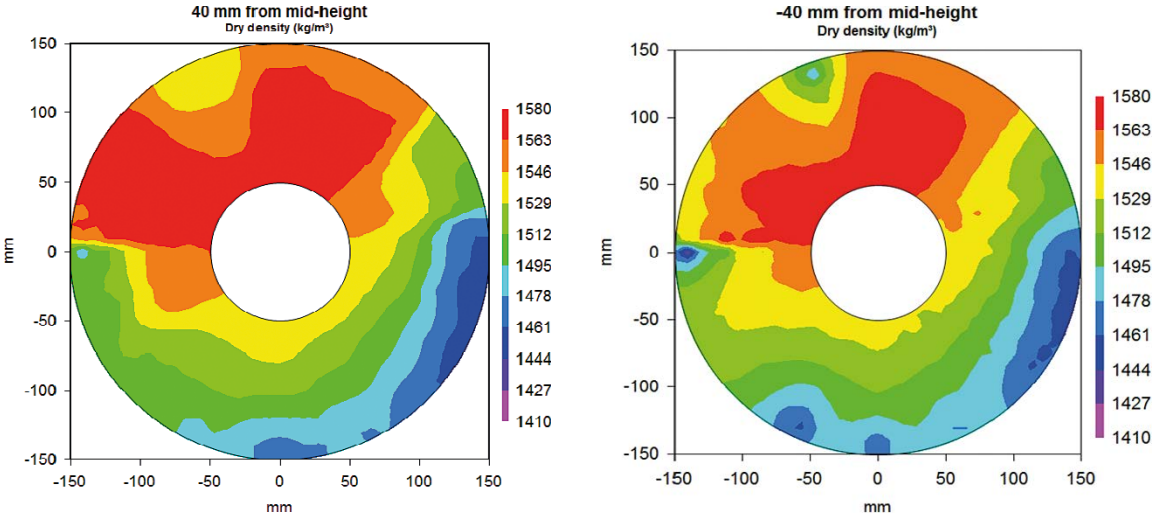

Figure 5-27. *Contour plots showing dry density distribution at the outermost level 1 of SH4.*

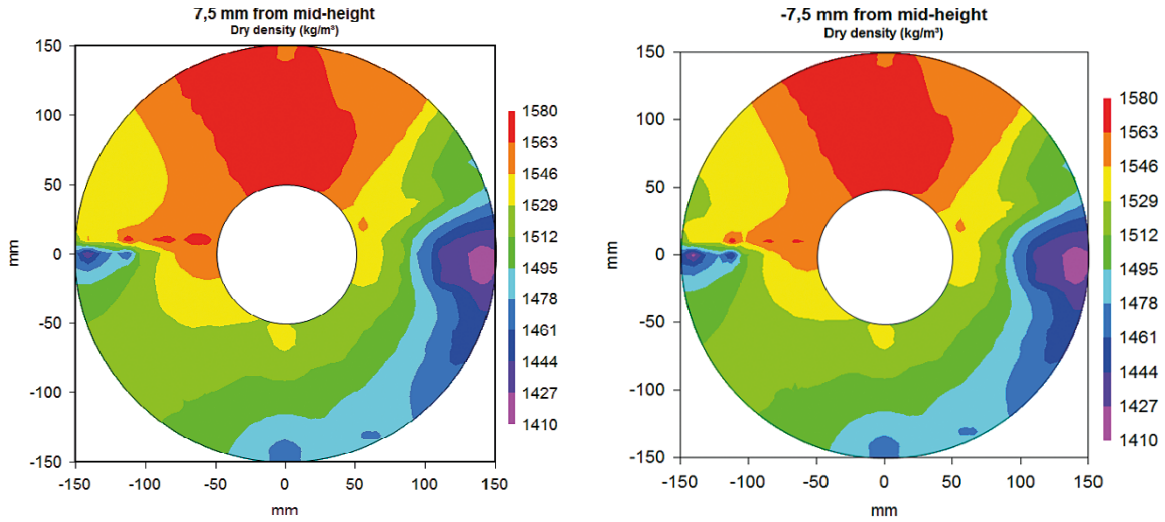

Figure 5-28. *Contour plots showing dry density distribution at the innermost level 3 of SH4.*

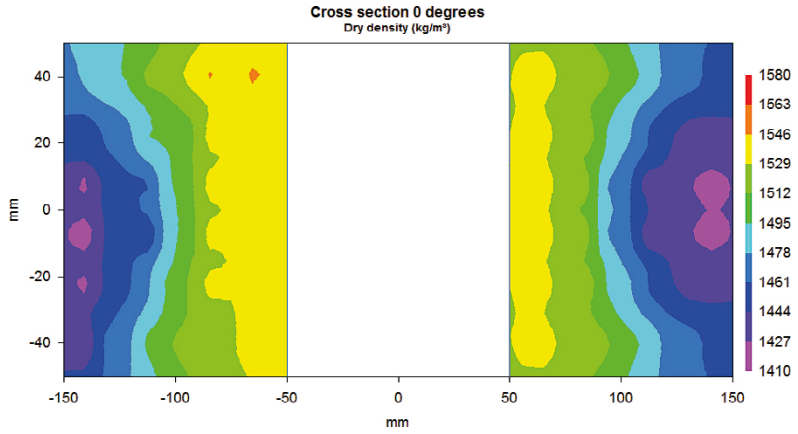

Figure 5-29. *Contour plot showing dry density distribution at a vertical section through the initial cavities (0°/180°).*

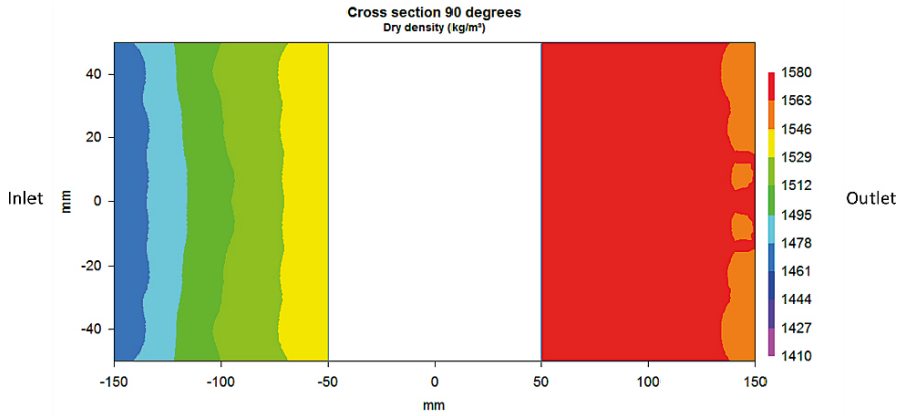

Figure 5-30. *Contour plot showing dry density distribution at a vertical section perpendicular to the initial cavities (90°/−90°) with the inlet to the left and outlet to the right.*

6 Homogenisation in long tubes

6.1 General

Swelling and homogenisation in long tubes are studied with this test type where ten tubes having similar design and content are used. The height of the tubes is 250 or 350 mm and the diameter is 25 or 35 mm. While the lower half of each tube is filled with highly compacted bentonite the upper half is filled with bentonite pellets. Water is added from the upper end, i.e. above the pellets. Swelling pressure is determined from some of the tubes by measuring radial and axial stresses exerted on pistons with certain areas. By different test durations of the tubes the distribution of density and the evolution of swelling pressure can both be studied as a function of time. Three tests have been finished; after 2, 4 and 6 years, while seven are still ongoing.

The purpose of this test type is to study:

- the effect of friction for limiting homogenisation,
- the influence of time on the remaining density gradients after completed swelling and compression.

In addition to study the ability of the bentonite to homogenise the result can also be applied to evaluate to what extent the so called “transition zones” in tunnels can be used to downshift the swelling pressure against e.g. a plug.

6.2 Experimental description

6.2.1 Test set-up

A general sketch of the set-up used in this series is shown in Figure 6-1. The height of the tubes is ten times the diameter and the tubes were placed in an upright position during the tests. The lower half of the tubes was filled with highly compacted bentonite and the upper half was filled with bentonite pellets. The material used in this test type was MX-80. The tube walls contained grooves to increase the friction between the bentonite and the tube.

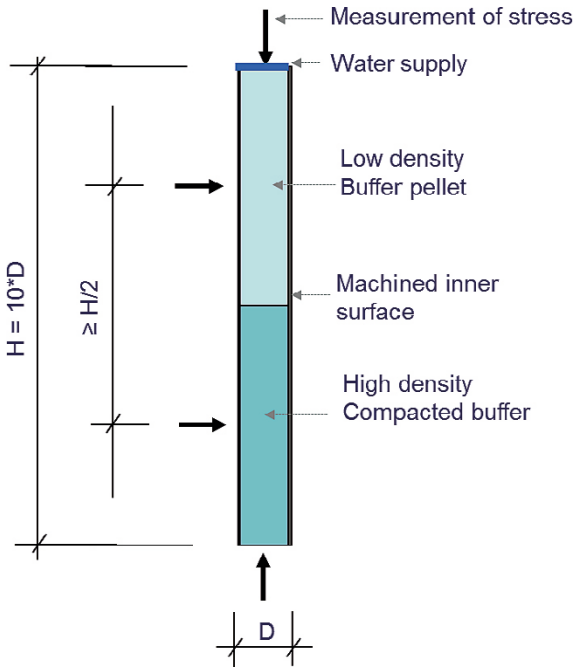

Figure 6-1. *Sketch of the set-up used for the series with long tubes. Axial and radial stress measurements are made in some of the tubes (marked with arrows).*

Four different varieties of the tube were manufactured with the main difference being the features of the inner wall and the dimensions of the tubes, Figure 6-2. The features of the inner walls are marked with different lines in Figure 6-2; rectangular shaped grooves (grey lines), triangular shaped grooves (black lines) and smooth inner wall (no lines). The different types of grooves are shown with greater details in Figure 6-3. Two different dimensions of tubes were used and while nine had the diameter 25 mm (and height 250 mm) one had the diameter 35 mm (and height 350 mm). The tests FLR1 to FRL4 were run according to Figure 6-2 while tests FLR5–FLR10 were run with similar conditions as FLR2 but without any measurements of swelling pressure. Details about each specimen used in tests FLR1 to FLR10 including the initial dry density are shown in Table 6-1.

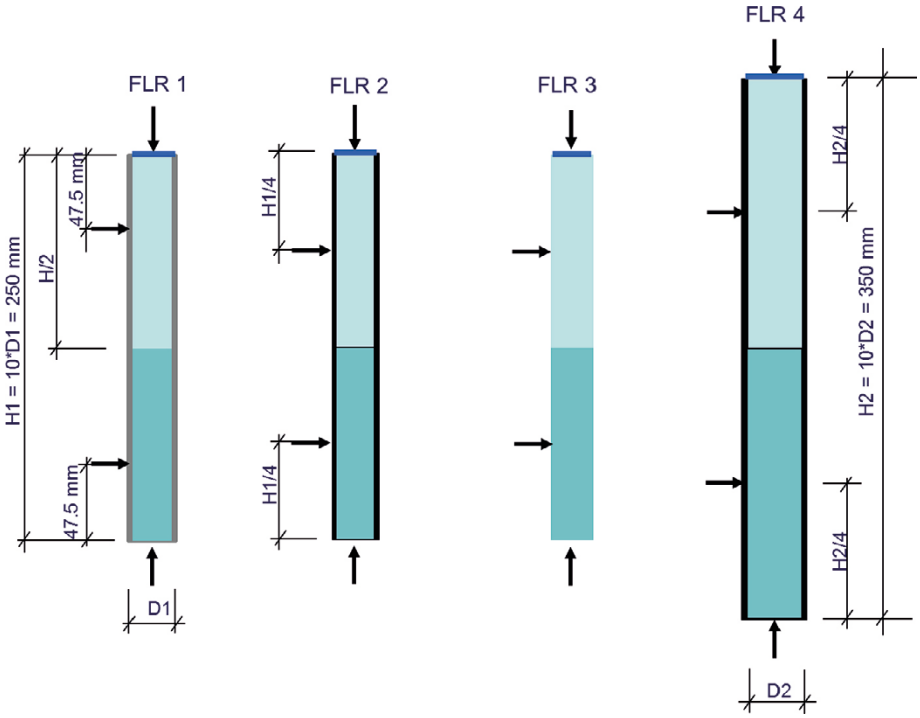

Figure 6-2. *Sketches of the tubes used in the test series and the boundary conditions of tests FLR1 to FLR4. The different lines surrounding the specimens denote the different features of the inner surface of the tubes (grey line = rectangular grooves, black line = triangular grooves, no line = polished smooth surface). The tests FLR5–FLR10 were run in tubes similar to the one used for test FLR2 but without swelling pressure measurements.*

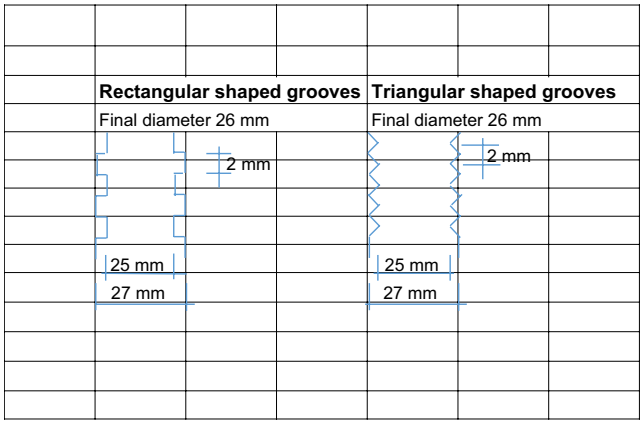

Figure 6-3. *Sketch of the rectangular and triangular shaped grooves inside the tubes.*

Table 6-1. Test conditions and target initial densities for all specimens in the series with long tubes.

Labels	FLR1	FLR2	FLR3	FLR4	FLR5–FLR10
Start date	March 2012	May 2013	May 2013	May 2013	May 2013
Set-up					
Total height (mm)	250	250	250	350	250
Final average diameter (mm)	26	26	25	36	26
Inside friction (grooves)	rectangular	triangular	smooth	triangular	triangular
Stress measurements	yes	yes	yes	yes	no
Material upper half	MX-80 extruded pellet				
Material lower half	MX-80 high density blocks				
Water supply	From the upper drainage only				
Type of water	2–50 mM NaCl				
Initial target dry density					
Upper part ρ_d,upper (kg/m^3)	772	882	882	882	882
Lower part ρ_d,lower (kg/m^3)	1 566	1 561	1 561	1 561	1 561

6.2.2 Test procedure

The compacted material in the lower part of each tube was prepared by compression of powder to 5 samples with the height and diameter 25 mm and 24.9 mm, respectively (or in case of FLR4 the height 35 mm and the diameter 34.5 mm) which, were placed on top of each other. The upper part with pellets was prepared by dividing each pellet into two pieces and putting them in place by hand to achieve the predetermined density. After closing the tubes with pistons in both ends load cells were attached to the instrumented tubes.

The test started by adding a solution of 2 mM NaCl to the upper drainage. The water was initially added by use of vacuum but after the initial phase a peristaltic pump was attached to the system to be used for the regular water circulation. After the planned testing period the tubes are dismantled, and the distribution of water content and density are determined with as good resolution as possible.

To be able to study the time effect on the density gradient, different testing periods were planned for the ten tubes. The date of the dismantling of the last tube has not yet been decided but the non-instrumented tubes are planned to be dismantled before the instrumented ones. The first dismantling was done already after 2 years and the second and third dismantling were done after 4 and 6 years.

6.3 Results (FLR-series)

The focus of this chapter is the results of the dismantled FLR6 and FLR7. In Appendix 3 additional information is given.

6.3.1 Installation and water supply

The initial target dry density is given in Table 6-1. More details of the preparation and installation are given in Appendix 3 (see also Dueck et al. 2018). At start a solution of 2 mM NaCl was added by evacuation of filters, tubes and devices. This increased the average degree of saturation to about 100 % in all tubes (see Appendix 3). From the initial 2 mM NaCl the salt content of the solutions was increased to 50 mM NaCl in all tubes in April/May 2014, i.e. after two years for FLR1 and after one year for FLR2–FLR10.

A constant water pressure of 70 kPa was introduced on 2015-10-05 in all devices, except FLR1 and FLR5 (already in September 2015 different water pressures between 0 and 100 kPa was used during shorter or longer time intervals). Regarding FLR1 a constant water pressure of 70 kPa was not introduced until 2016-01-15 and regarding FLR5 no water pressure was introduced before the dismantling.

6.3.2 Swelling pressure measurements

The swelling pressure is measured in four (FLR1–FLR4) of the ten set-ups. In this chapter the swelling pressure, in tables and diagrams, is shown as total pressure, with the water pressure included. The evolution of swelling pressure during the first six years, measured in the set-up similar to the one used for FLR5–FLR10, is shown in Figure 6-4 and the time for the dismantling of FLR5–FLR7 are marked. Stresses at the time of dismantling of FLR6 and FLR7 i.e. after 4 and 6 years are tabulated in Table 6-2. The evolution of the swelling pressure from all four set-ups from start to October 2019 are shown in Appendix 3. Further comments on the evolution of the swelling pressure is given in Section 6.3.5 below.

Table 6-2. Swelling pressure, total stress, from set-up FLR2 with similar set-up as FLR6 and FLR7 at the time corresponding to the dismantling of FLR6 and FLR7, i.e. after 4 and 6 years, respectively.

Type	Distance[2] mm	Swelling pressure 4 years (FLR6) kPa	Swelling pressure 6 years (FLR7) kPa	Direction[1]	Label
pellet	250	309	408	axial	FLR2 pellet (axial)
pellet	187.5	232	242	radial	FLR2 pellet (radial)
block	62.5	3066	2235	radial	FLR2 block (radial)
block	0	5981	5440	axial	FLR2 block (axial)

[1] The swelling pressure is measured as the total radial and axial stresses.

[2] Distance from the bottom.

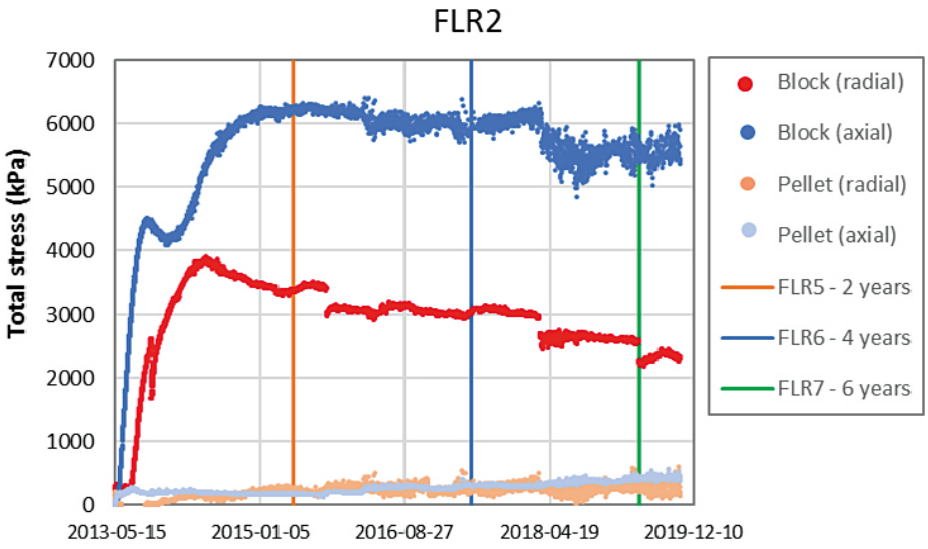

Figure 6-4. *Evolution of swelling pressure as total stress from the start to 2019-10-22 with the time for the dismantling of FLR5, FLR6 and FLR7 marked. The stresses were not measured on the dismantled set-up but on the equivalent set-up of FLR2.*

For comparison, the corresponding values measured with the set-up FLR1 after 4 and 6 years differed 10–44 % from the values measured with the set up FLR2 (given in Table 6-2). The measured stresses from FLR1 are given in Table 6-3. Comparing these results, it is important to notice that rectangular shaped grooves were used in FLR1 while triangular ones were used in FLR2, and that the positions of the radially measured stresses were slightly different in the two tests (in the set-up FLR1 the radially measurements were done 47.5 mm and 202.5 mm from the bottom but 62.5 mm and 187.5 mm in the set-up FLR2).

Table 6-3. Swelling pressure, total stress, from set-up FLR1 after 4 and 6 years, respectively.

Type	Distance[2] mm	Swelling pressure 4 years kPa	Swelling pressure 6 years kPa	Direction[1]	Label
pellet	250	177	228	axial	FLR1 Pellet (axial)
pellet	202.5	276	314	radial	FLR1 Pellet (radial)
block	47.5	2798	2832	radial	FLR1 Block (radial)
block	0	4942	4838	axial	FLR1 Block (axial)

[1] The swelling pressure is measured as total radial and axial stresses.

[2] Distance from the bottom.

6.3.3 Termination, dismantling and sampling

The tests FLR6 and FLR7 were terminated on 2017-05-29 and 2019-05-02, respectively. The filters at the upper pistons and the plastic tubes were emptied from fluid by a peristaltic pump and the samples were forced upwards through the steel tube. Samples with a thickness of 5–10 mm were taken continuously, see Figure 6-5.

The sampling was made to provide information regarding

- if the buffer and pellet sections were saturated,
- the dry densities at the positions of the swelling pressure measurements,
- the distribution of dry density over the 250 mm specimen, with good resolution.

The degree of saturation, the first bullet point, was determined from three samples of each of FLR6 and FLR7, from the middle and from the lower part, where both water content and density were determined. Determination of dry density, the lower two bullet points, were made by continuous sampling and measurements of water content only.

Figure 6-5. *Continuous sampling of FLR6.*

6.3.4 Distribution of water content and density of FLR6 and FLR7

Both water content and density were determined on three samples from each of FLR6 and FLR7 presented in Table 6-4 and Table 6-5, respectively. The specimens were considered to be fully saturated.

Table 6-4. Results from three samples from FLR6. The distances from the bottom to the centre of each sample are given with the thickness, water content, bulk density, dry density and the evaluated degree of saturation.

Sample ID	Distance[1] mm	Thickness mm	Water content %	Bulk density kg/m^3	Dry density kg/m^3	Degree of saturation %
FLR6-16	165	10	56.3	1713	1095	102
FLR6-39	45	10	31.9	1957	1483	101
FLR6-46	5	10	27.9	2022	1581	102

[1] Distance from the bottom.

Table 6-5. Results from three samples from FLR7. The distances from the bottom to the centre of each sample are given with the thickness, water content, bulk density, dry density and the evaluated degree of saturation.

Sample ID	Distance[1] mm	Thickness mm	Water content %	Bulk density kg/m^3	Dry density kg/m^3	Degree of saturation %
FLR7-16	173	10	57.9	1679	1063	100
FLR7-39	55	9	35.0	1906	1412	100
FLR7-47	7	11	28.4	1986	1547	99

[1] Distance from the bottom.

The distributions of water content and dry density over the height of the specimens are shown in Figure 6-6. In the diagram to the right circles mark the values from the samples where both water content and density were measured, cf the positions given in Table 6-4 and Table 6-5. The main part of the dry densities used in the diagram to the right was evaluated from the measured water contents and a degree of saturation of 100 %. In the diagram to the right the initial distribution of dry density is also shown which is based on the condition after radial swelling. All values are tabulated in Appendix 3.

No large differences can be seen between the resulting density distributions after 4 and 6 years. However, due to some problems during the dismantling there are some uncertainties regarding the water content and thereby also the dry density at the very upper positions of FLR7. In addition, the water content at one position of FLR6 was uncertain and is marked with * in Figure 6-6.

6.3.5 Comments

In Figure 6-7 the results from Figure 6-6 are shown again together with the results from the first dismantled specimen FLR5 (Dueck et al. 2018). All densities given are calculated from measured water contents and the degree of saturation 100 % since the specimens were considered to be saturated. When comparing the results, it can be seen that the transition zone seems to have approximately the same distribution. However, the height of the transition zone after 4 and 6 years is approximately 195 mm (from 15 mm to 210 mm in the results from FLR6 and FLR7) which is somewhat larger compared to 193 mm after 2 years (from 27 mm to 220 mm in the results from FLR5).

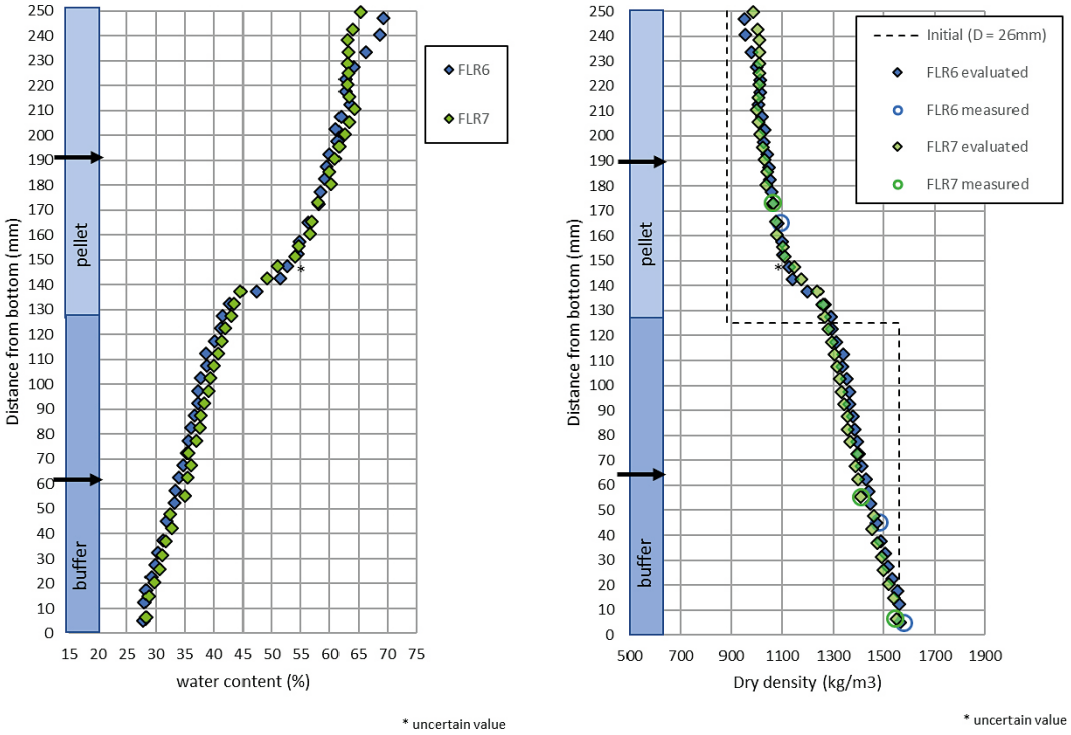

Figure 6-6. *Distribution of water content (to the left) and dry density (to the right) after dismantling of FLR6 and FLR7. To the right the initial distribution of dry density, calculated with the final volume, i.e. final diameter, is also shown. The dry density was determined from the water content and an assumption of Sr = 100 % (labelled evaluated) and from measured water content and bulk density (labelled measured).*

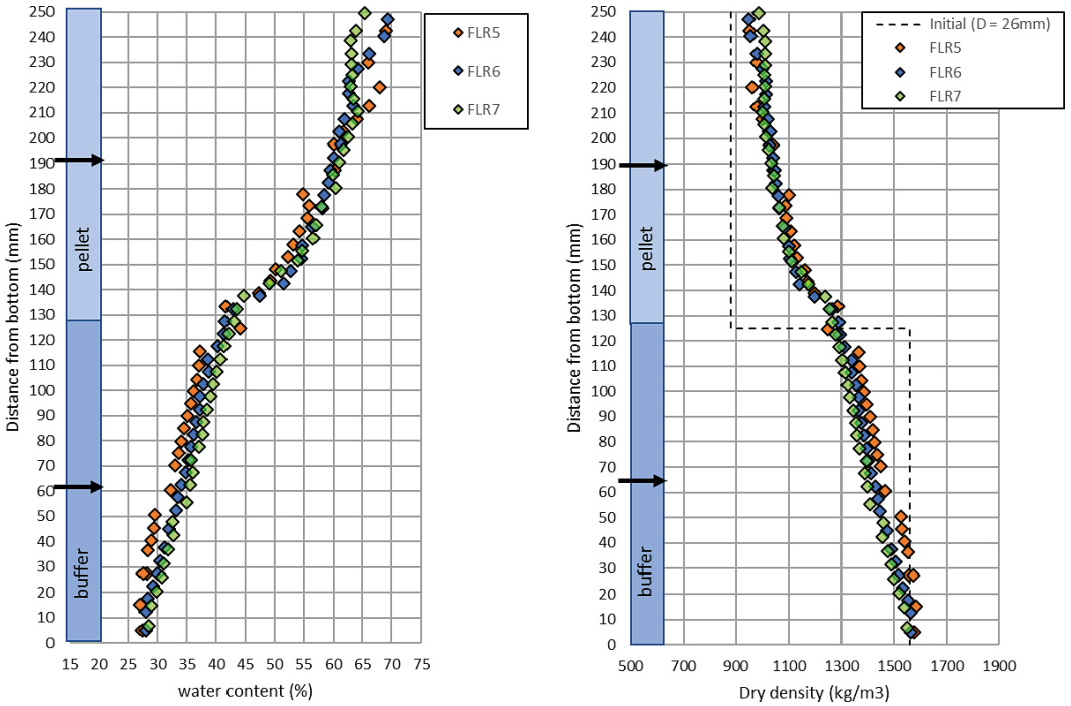

Figure 6-7. *Distribution of dry density of FLR6 and FLR7 (from Figure 6-6) together with FLR5 (Dueck et al. 2018). The dry densities were determined from the water content and S_r = 100 %.*

After dismantling the average dry density was evaluated according to Table 6-6 where the corresponding initial values are also given. From the table it can be seen that the average dry density of FLR5 (dismantled after 2 years) were somewhat higher than that of FLR6 and FLR7. In Figure 6-8 the dry density ρ_d are therefore normalized with the ratio of the weighted actual average density $\rho_{d,FLRn}$ to the average dry density $\rho_{d,avr}$ of all three tests, according to Equations 6-1 to 6-4. The average density $\rho_{d,avr}$ was calculated to be 1 255 kg/m^3.

$$\rho_{d,normalized} = r_{FLRn} * \rho_d \tag{6-1}$$

$$r_{FLRn} = \frac{\rho_{d,FLRn}}{\rho_{d,avr}} \tag{6-2}$$

$$\rho_{d,FLRn} = \frac{\sum(\rho_d * \Delta h)}{\sum \Delta h} \tag{6-3}$$

$$\rho_{d,avr} = (\rho_{d,FLR5} + \rho_{d,FLR6} + \rho_{d,FLR7})/3 \tag{6-4}$$

Table 6-6. Results from FLR5–FLR7. The total time are given together with values of average dry density.

Sample ID	FLR5	FLR6	FLR7
Start date	2013-05-15	2013-05-16	2013-05-16
End of test	2015-05-20	2017-05-29	2019-05-02
Total time	2 years	4 years	6 years
Initial target dry density			
Upper part $\rho_{d,upper}$ (kg/m^3)	882	882	882
Lower part $\rho_{d,lower}$ (kg/m^3)	1 561	1 561	1 561
Final average dry density			
Upper part $\rho_{d,upper}$ (kg/m^3)	1 067	1 066	1 070
Lower part $\rho_{d,lower}$ (kg/m^3)	1 472	1 438	1 414
Average $\rho_{d,FLRn}$ (kg/m^3)	1 270	1 252	1 243

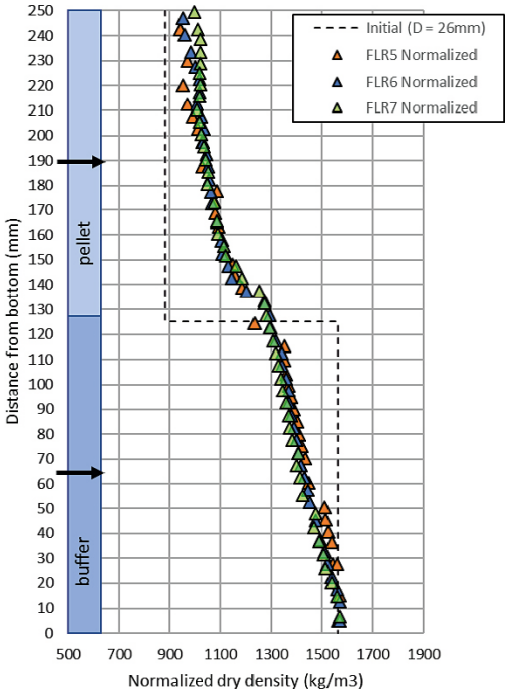

Figure 6-8. *Distribution of normalized dry density where the dry density in Figure 6-7 are normalized with the ratio of the actual average density to the average dry density over all three specimens (i.e. 1 255 kg/m^3).*

A small change with time is indicated in Figure 6-8 which agrees with the stress measurements in FLR2 in Figure 6-4. Future dismantling of the still running tests will give further information if this is a trend or not.

In Figure 6-9 and Table 6-7 the swelling pressure and the corresponding dry density after 2, 4 and 6 years are shown. The swelling pressure was measured as the total stress on the set-up FLR2, cf Figure 6-4 and Table 6-2, and the dry densities were measured after dismantling of FLR5, FLR6 and FLR7 at the positions of the actual sensors, cf Figure 6-7.

Table 6-7 Dry density after 2, 4 and 6 years determined after dismantling of FLR5, FLR6 and FLR7, respectively, and the corresponding swelling pressure, total stress, measured on FLR2 with similar set-up. (Data from FLR5, see Dueck et al. 2018.)

Time		2 years	4 years	6 years	2 years	4 years	6 years	
Sample ID		FLR5	FLR6	FLR7	FLR2	FLR2	FLR2	
Distance[1] mm	Block/Pellet[2]	Dry density kg/m³	kg/m³	kg/m³	Swelling pressure[3] kPa	kPa	kPa	Direction[4]
250	Pellet	946	950	987	179	309	408	axial
187.5	Pellet	1046	1047	1042	247	232	242	radial
62.5	Block	1476	1429	1399	3381	3066	2235	radial
0	Block	1588	1581	1553	6231	5981	5440	axial

[1] Measured from the bottom of the device.

[2] Initially pellet or high-density block.

[3] FLR2 has similar set-up as FLR5, FLR6 and FLR7.

[4] Measured axially or radially as load on a piston.

In the diagram of the stress evolution with time in Figure 6-4 a decrease is observed in the axial stress measured at the bottom of the set-up (dark blue markers). In March 2018 the devices with on-going tests in the FLR-series were moved to another location and the average temperature increased approximately one degree. At that time FLR5 and FLR6 were already dismantled. The decrease observed in the axial stress is probably related to the expansion of the steel tube, however small. Similar stress decrease in the lower part of the set-up was also observed in the other instrumented tests, see Appendix 3 where the measured swelling pressures are shown together with the temperature.

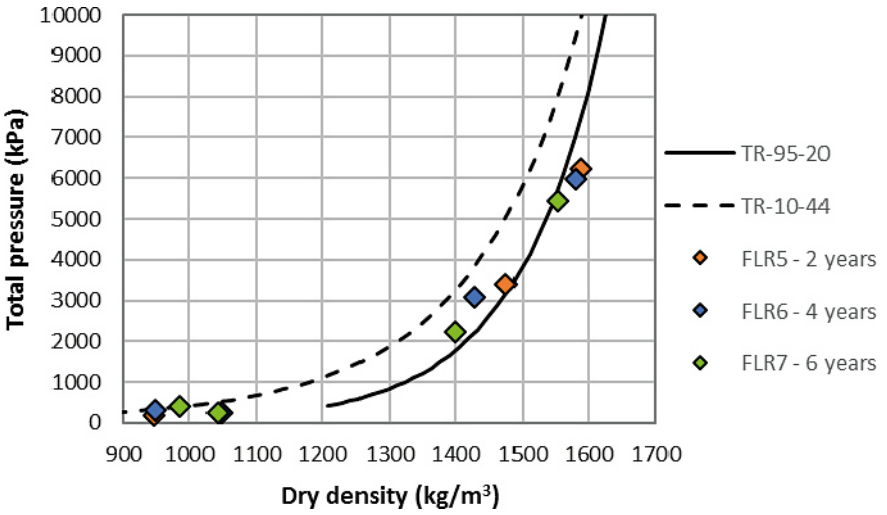

Figure 6-9. *Swelling pressure as a function of dry density. Results after dismantling of FLR5, FLR6 and FLR7 plotted with swelling pressure measured on the similar set up FLR2. Models presented by Börgesson et al. (1995) and Åkesson et al. (2010) are also shown.*

A fluctuation of the stresses over a shorter time period was also observed. The fluctuation corresponded well to the fluctuation of the temperature but in this case an increase in temperature resulted in an increase in the measured stresses. The probable explanation for this is that an increase in temperature causes volume expansion of the water in the bentonite and with the geometry used, i.e. long tubes with drainage at one end only, it takes time for the excess water pressure to disappear. In Appendix 3 two diagrams show the fluctuation of the stresses of FLR1 and temperature for one month.

7 Summary

The present status report is a compilation of laboratory test results from a project on homogenisation tests of bentonite. The main purpose of the status report is to account for results derived up to September 2020 and not included in previous reports. The results can be used for modelling some well-defined benchmark tests in order to improve the models or determine mechanical parameters for hydro-mechanical modelling of the behaviour of the bentonite buffer and backfill. The tests and results presented in this report are briefly summarised below.

Three tests have been made on axial swelling of specimens with the height 50–70 mm and the diameter 100 mm, two tests on the calcium dominated Calcigel and one on the sodium dominated MX-80. The density distributions and the stresses measured at different positions have been presented. In all three tests the axial stress was measured both above and below the specimens and the difference between the upper and lower values has been interpreted as wall friction, represented by a friction angle δ in the contact between the cylinder ring and the bentonite.

Homogenisation has also been studied by medium scale tests involving loss of bentonite and the results from the third and fourth such test have been presented in this report. Both tests consisted of a bentonite block with the diameter 300 mm and the height 100 mm. In each block two cavities with dimensions (height × length × depth) $35 \times 70 \times 50$ mm^3 were cut out in two diametrical positions to simulate loss of material. One test was done on MX-80 with slow water access and instrumented with load cells. The other test was done with Calcigel and not instrumented. After 43–44 months the specimens were dismantled, and the density and water content distributions have been shown.

Remaining differences of density after long time is studied in a series with long tubes. Initially ten tests of this type were started, and MX-80 was used for all specimens. Three of the specimens have been dismantled and the results of two of the dismantled specimens, dismantled after 4 and 6 years, have been reported here. The results have been presented as the density and stress distributions.

References

SKB's (Svensk Kärnbränslehantering AB) publications can be found at www.skb.com/publications.

Börgesson L, Johannesson L-E, Sandén T, Hernelind J, 1995. Modelling of the physical behaviour of water saturated clay barriers. Laboratory tests, material models and finite element application. SKB TR 95-20, Svensk Kärnbränslehantering AB.

Dueck A, Goudarzi R, Börgesson L, 2011. Buffer homogenisation, status report. SKB TR-12-02, Svensk Kärnbränslehantering AB.

Dueck A, Goudarzi R, Börgesson L, 2014. Buffer homogenisation, status report 2. SKB TR-14-25, Svensk Kärnbränslehantering AB.

Dueck A, Goudarzi R, Börgesson L, 2016. Buffer homogenisation. Status report 3. SKB TR-16-04, Svensk Kärnbränslehantering AB.

Dueck A, Goudarzi R, Börgesson L, 2018. Buffer homogenisation – status report 4. SKB TR-17-04, Svensk Kärnbränslehantering AB.

Dueck A, Börgesson L, Kristensson O, Malmberg D, Åkesson M, Hernelind J, 2019. Bentonite homogenisation. Laboratory study, model development and modelling of homogenisation processes. SKB TR-19-11, Svensk Kärnbränslehantering AB.

Karnland O, Olsson S, Nilsson U, 2006. Mineralogy and sealing properties of various bentonites and smectite-rich clay materials. SKB TR-06-30, Svensk Kärnbränslehantering AB.

Svensson D, Dueck A, Nilsson U, Olsson S, Sandén T, Lydmark S, Jägerwall S, Pedersen K, Hansen S, 2011. Alternative buffer material. Status of the ongoing laboratory investigation of reference materials and test package 1. SKB TR-11-06, Svensk Kärnbränslehantering AB.

Åkesson M, Börgesson L, Kristensson O, 2010. SR-site Data report, THM modelling of buffer, backfill and other system components. SKB TR-10-44, Svensk Kärnbränslehantering AB.

Appendix 1

Basic variables and swelling pressure from the HR-series

The main part of the results is given in Chapter 4. In the tables the final values of the basic variables (water content w, dry density ρ_d, degree of saturation S_r) and the swelling pressure (axial stress P_a, radial stress P_r) are given. The last column contains the total time for the swelling and homogenisation. In the table the axial stresses are given both as an upper and lower value together with corresponding base variables and the radial stresses are given at the positions 5, 20, 35 and 50 mm, respectively from the bottom surface of the specimens, together with corresponding base variables. The abbreviation avr. means average over the specimen. The degree of saturation has been calculated with a particle density of ρ_s = 2 695 kg/m^3 for Calcigel and ρ_s = 2 780 kg/m^3 for MX-80.

Table A1-1. Axial swelling. Results from test series HR-A.

		Initial values[1]		Swelling		Final average values			Swelling pressure		Total time
Sample ID	Material	w %	ρ_d kg/m^3	$\rho_{d0}/\rho_{df} - 1$ %	pos. mm	w %	ρ_{df} kg/m^3	S_r %	Axial P_a kPa	Radial P_r kPa	Days
HR-A9	Calcigel	20	1 647	38	avr.	49.7	1 190	104	206	343	133
					upper	64.6	1 011	105	127		
					lower	38.8	1 344	104	285		
					5	38.8	1 344	104		570	
					20	40.4	1 304	102		319	
					35	50.9	1 170	105		141	
HR-A10	Calcigel	19.4	1 581	23	avr.	40.2	1 307	101	573	958	179
					upper	47.5	1 192	101	462		
					lower	35.8	1 381	101	685		
					5	35.8	1 381	101		1 294[2]	
					20	36.4	1 379	103		1 136	
					35	38.1	1 340	102		1 072	
					50	44.0	1 239	101		331	
HR-A11	MX-80	21.9	1 583	38	avr.	52.7	1 147	99	340	492	145
					upper	88.3	799	99	261		
					lower	41.1	1 277	97	420		
					5	41.1	1 277	97		486[3]	
					20	43.0	1 254	98		619	
					35	45.3	1 228	99		499	
					50	57.7	1 071	101		362	

[1] Based on final diameter D = 100 mm.

[2] Uncertain value due to erroneous measurement.

[3] Somewhat uncertain value.

The resulting dry density distribution after the HR-tests can be plotted as a function of radius due to detailed sampling after dismantling of HR-A10 and HR-A11, Figure A1-1 and A1-2. No large difference over the radius of the specimens were observed. In addition, the initial distribution was determined on a duplicate specimen of HR-A11, Figure A1-3, where the difference between the highest and lowest value was 35 kg/m^3 (4 % of the average dry density).

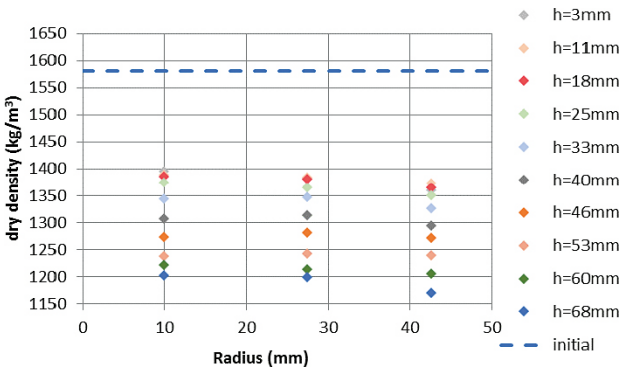

Figure A1-1. *Final dry density after dismantling at different radius of HR-A10. The labels show the different heights 3–68 mm.*

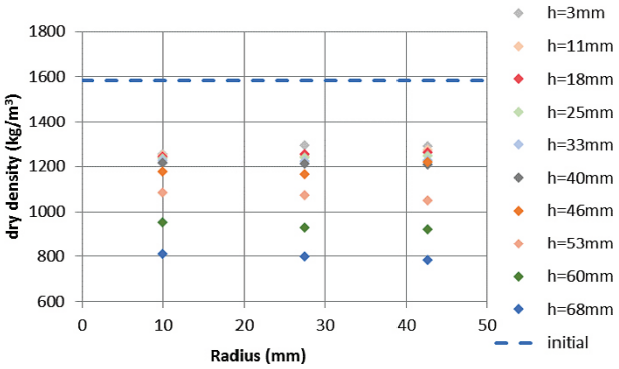

Figure A1-2. *Final dry density after dismantling at different radius of HR-A11. The labels show the different heights 3–68 mm.*

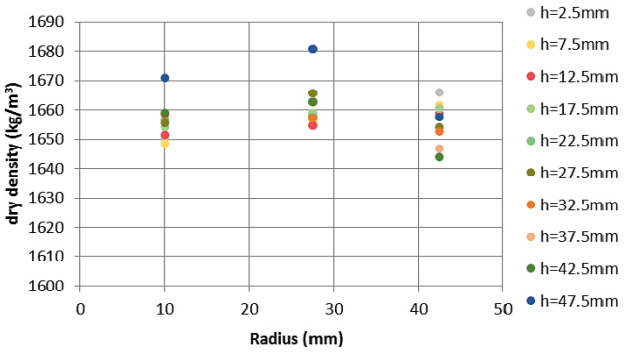

Figure A1-3. *Initial dry density of a duplicate of HR-A11 at different radius. The labels show the different heights 0–50 mm.*

Appendix 2

Results from the dismantled SH3 and SH4

A2.1 Results from the dismantled SH3

A2.1.1 Photos from start and dismantling

Below photos of the bentonite block, the test device, the dismantling and the sampling of the self-healing test SH3 are shown.

Figure A2-1. *Photo of cylinder ring with cavity and the device used for test SH3 (left) also shown in Figure 5-1 and the confined cylinder at start (right).*

Figure A2-2. *The confined cylinder at dismantling.*

Figure A2-3. *The bentonite cylinder ring at dismantling with the upper side (left) and the lower side (right) with the rubber sealings left. The centre cylinder is located in the centre of the device, the photos are somewhat misleading.*

Figure A2-4. *The bentonite ring still inside the steel device with the cavities marked on the upper surface (left) and the free-drilling to be able to remove the inner steel cylinder (right).*

Figure A2-5. *The inner steel cylinder is almost (left) and completely (right) removed.*

Figure A2-6. *The bentonite cylinder is sawn (left) into two half cylinders (right).*

Figure A2-7. *Photos of each of the two cavities after removal of the radial filter.*

Figure A2-8. *Sampling was made within a sector and along lines. The sector was divided into four wedges A to D and one of these is shown (left). Sampling was made at the angles 0, 20, 65 and 90 degrees from the centre of the cavity and the lines L0, L20, L65 and L90 are marked (right).*

A2.1.2 Timetable, from start to end of test (SH3)

Project	**Buffer homogenisation SH**
Sample ID	SH3
Material	Calcigel #2014
Sensors	No sensors
Type of water	De-ionized pressurized water
Dimension	
Diameter	D(outer) = 300 mm, D(inner) = 100 mm
Height	H = 100 mm

Cavities	Length = 69 mm (circumferential) Height = 35 mm Depth = 47 mm

Estimated required volume of water	
Cavities, gaps, filter and bevels	4.3 dl
including saturation	5.6 dl

Date	**Activity**
2014-12-16	Compaction of blocks
2015-01-15	Block preparation with turning lathe
2015-02-20	Preparation of cavities Mounted into device
2015-02-23	**Start of test**
	Filter, gaps and tubes were filled with de-ionized water, no vacuum Water pressure Pw = 0–10 kPa
2015-03-03	Water pressure Pw = 10–30 kPa
2015-04-14	Water pressure Pw = 10–100 kPa
2015-12-28	Water pressure Pw = 70–140 kPa
2016-03-11	Water pressure Pw = 135 kPa and water is coming through the filter
2016-03-12	Water pressure Pw = 70–135 kPa
2017-02-14	A constant water pressure of 70 kPa applied
2017-09-11	A constant water pressure of 100 kPa applied
	End of test
2018-09-28	Water pressure lowered to almost zero
2018-10-03	The test was terminated Dismantling started after attempts to evacuate the filter The upper lid and the bottom plate were removed The block was divided into two half circles. One was stored for later studies The sampling for determinations of water content was completed
2018-10-04	The sampling for determinations of density was completed

A2.1.3 Evolution of water pressure and water volume (SH3)

The volume of the water inflow and the water pressure, registered manually, are shown in Figure A2-9 and Figure A2-10 where the total time period is shown to the left and the last months are shown to the right. At start and during the first year leakage from the device was observed. Small leakage was probably present during the whole test period but from 2017-01-31 a constant pressure was possible to keep. The filter was flushed periodically and to the right in Figure A2-9 and Figure A2-10 the registered net volume could be correlated to the flushing of the filter, marked at zero pressure.

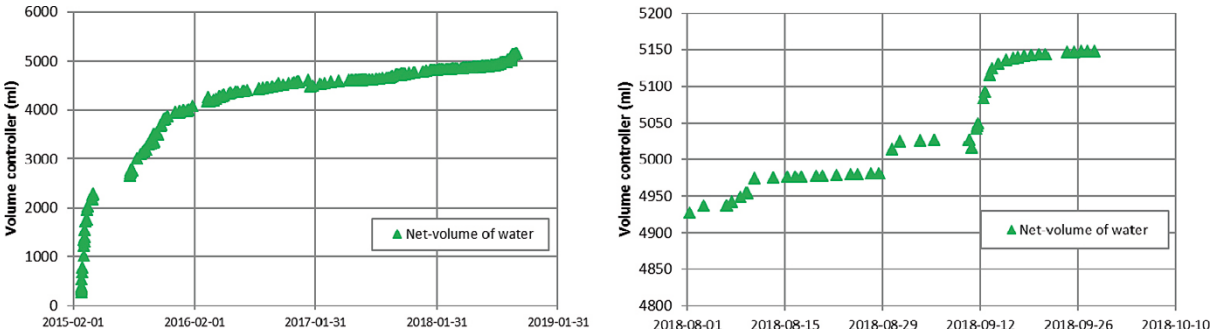

Figure A2-9. *Evolution of the accumulated net-volume of water going into the device as a function of time. The results from two different time periods are shown; the total test period (left) and the two last months (right).*

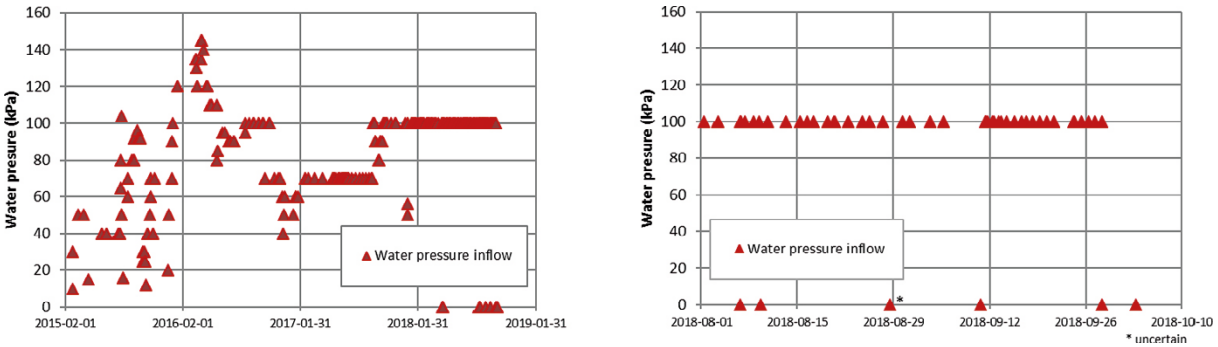

Figure A2-10. *The registered water pressure at the inlet as a function of time. The results from two different time periods are shown; the total test period (left) and the two last months (right). The time scales are the same as in Figure A2-9.*

A2.1.4 Tabulated values of water content and density (SH3)

Table A2-1, Table A2-2 and Table A2-3 contain tabulated values of water content and dry density after dismantling of SH3 at different levels; outermost, second outermost and innermost (denoted 1, 2 and 3). The Sample ID in the first column indicates the direction of the sampling and the level of the specimen (1, 2 or 3) and the letter indicates how the specimen was sampled (L – along a line or A to D – continuously within a sector). The direction of the specimen is given as a horizontal angle from the centre of the cavity (−42° to +90°). The radial distance in the second column is calculated from the inner steel cylinder (having a diameter of 100 mm). In the diagrams and tables the positions of two specimens have been corrected (from L3°-1 and L3°-3) and four values are missing from L3°-2 (r = 47.5 mm), B14°-1 (r = 32.5 mm) and B20°-1 (r = 32.5 mm and r = 77.5 mm). In the tables the water content and dry density are given with the degree of saturation calculated from a particle density of ρ_s = 2 695 kg/m^3.

Table A2-1. Distribution of water content, dry density and degree of saturation at level 1, i.e. outermost and towards the lid. The sample ID indicates if the specimens were taken along a line (L) or as a continuous sample within a sector (A–D), the angle from the centre of the cavity and the final figure shows the level. The radial distance is given from the inner steel cylinder. The degree of saturation was calculated from a particle density of ρ_s = 2 695 kg/m^3. The dry density of some specimens was calculated from the assumptions of S_r = 100 %, marked *, and the position of some specimens was corrected, marked **.

Sample ID	Radial distance mm	Water content %	Dry density kg/m^3	Degree of saturation %
L3°-1	12.5	24.3	1 640	101
L3°-1	32.5	24.9	1 620	101
L3°-1	47.5	25.6	1 600	101
L3°-1	62.5	26.6	1 580	101
L3°-1**	77.5	27.5	1 560	101
L3°-1**	92.5	28.2	1 540	101
L20°-1*	12.5	23.8	1 640	100
L20°-1*	32.5	24.6	1 620	100
L20°-1*	47.5	25	1 610	100
L20°-1*	62.5	25.5	1 600	100
L20°-1*	77.5	26.2	1 580	100
L20°-1*	92.5	26.9	1 560	100
L65°-1	12.5	23.2	1 660	101
L65°-1	32.5	23.5	1 660	101
L65°-1	47.5	23.7	1 650	101
L65°-1	62.5	23.8	1 640	100
L65°-1	77.5	24	1 640	100
L65°-1	92.5	25.5	1 610	102
L90°-1	12.5	22.4	1 660	96
L90°-1	32.5	22.7	1 670	99
L90°-1	47.5	22.9	1 670	100
L90°-1	62.5	23.1	1 670	101
L90°-1	77.5	23.6	1 670	103
L90°-1	92.5	25.3	1 650	108
A−3°-1	12.5	24.1	1 650	103
A−3°-1	32.5	24.8	1 640	104
A−3°-1	47.5	25.7	1 610	103
A−3°-1	62.5	26.2	1 590	102
A−3°-1	77.5	26.8	1 570	101
A−3°-1	92.5	27.6	1 560	102
A−8°-1	12.5	24.1	1 650	103
A−8°-1	32.5	24.8	1 640	104
A−8°-1	47.5	25.7	1 610	103
A−8°-1	62.5	26.5	1 570	100
A−8°-1	77.5	27.7	1 560	102

Sample ID	Radial distance mm	Water content %	Dry density kg/m^3	Degree of saturation %
A−8°-1	92.5	28.4	1 550	103
B−14°-1	12.5	23.9	1 660	103
B−14°-1	32.5	40.2		
B−14°-1	47.5	25.4	1 620	103
B−14°-1	62.5	25.8	1 600	102
B−14°-1	77.5	26.9	1 580	103
B−14°-1	92.5	27.8	1 570	104
B−20°-1	12.5	23.9	1 660	103
B−20°-1	32.5	40.2		
B−20°-1	47.5	25.4	1 620	103
B−20°-1	62.5	25.1	1 620	101
B−20°-1	77.5	40.3		
B−20°-1	92.5	27.4	1 580	105
C−25°-1	12.5	23.5	1 660	101
C−25°-1	32.5	24.2	1 640	102
C−25°-1	47.5	24.3	1 640	101
C−25°-1	62.5	24.8	1 630	102
C−25°-1	77.5	25.2	1 620	102
C−25°-1	92.5	26.4	1 610	105
C−31°-1	12.5	23.5	1 660	101
C−31°-1	32.5	24.2	1 640	102
C−31°-1	47.5	24.3	1 640	101
C−31°-1	62.5	24.3	1 640	101
C−31°-1	77.5	25	1 610	100
C−31°-1	92.5	26.4	1 600	104
D−37°-1	12.5	22.8	1 680	102
D−37°-1	32.5	23.5	1 660	102
D−37°-1	47.5	23.9	1 650	102
D−37°-1	62.5	24.4	1 650	103
D−37°-1	77.5	24.2	1 640	102
D−37°-1	92.5	26.2	1 590	102
D−42°-1	12.5	22.8	1 680	102
D−42°-1	32.5	23.5	1 660	102
D−42°-1	47.5	23.9	1 650	102
D−42°-1	62.5	23.7	1 670	104
D−42°-1	77.5	24	1 640	101
D−42°-1	92.5	25.6	1 620	104

Table A2-2. Distribution of water content, dry density and degree of saturation at level 2, i.e. the second outermost level. The sample ID indicates if the specimens were taken along a line (L) or as a continuous sample within a sector (A–D), the angle from the centre of the cavity and the final figure shows the level. The radial distance is given from the inner steel cylinder. The degree of saturation was calculated from a particle density of ρ_s = 2 695 kg/m^3. The dry density of some specimens was calculated from the assumptions of S_r = 100 %, marked *, and the position of some specimens was corrected, marked **.

Sample ID	Radial distance mm	Water content %	Dry density kg/m^3	Degree of saturation %
L3°-2	12.5	24.9	1 630	102
L3°-2	32.5	25.7	1 610	103
L3°-2	47.5	27		
L3°-2	62.5	28.6	1 530	102
L3°-2	77.5	29.3	1 490	97
L3°-2	92.5	29.5	1 500	100
L20°-2*	12.5	24.3	1 630	100
L20°-2*	32.5	24.9	1 610	100
L20°-2*	47.5	25.7	1 590	100
L20°-2*	62.5	26.6	1 570	100
L20°-2*	77.5	27.4	1 550	100
L20°-2*	92.5	27.5	1 550	100
L65°-2	12.5	23.5	1 660	101
L65°-2	32.5	23.7	1 650	101
L65°-2	47.5	23.9	1 650	101
L65°-2	62.5	24.4	1 640	102
L65°-2	77.5	24.4	1 630	101
L65°-2	92.5	25.5	1 610	102
L90°-2	12.5	22.8	1 650	96
L90°-2	32.5	23.4	1 660	100
L90°-2	47.5	23.5	1 650	100
L90°-2	62.5	23.6	1 660	102
L90°-2	77.5	24	1 660	103
L90°-2	92.5	25.4	1 640	107
A−3°-2	12.5	24.9	1 640	104
A−3°-2	32.5	25.9	1 610	103
A−3°-2	47.5	27.1	1 580	103
A−3°-2	62.5	28.7	1 520	100
A−3°-2	77.5	28.8	1 510	98
A−3°-2	92.5	29.3	1 510	100
A−8°-2	12.5	24.9	1 640	104
A−8°-2	32.5	25.9	1 610	103
A−8°-2	47.5	27.1	1 580	103
A−8°-2	62.5	28.7	1 540	103
A−8°-2	77.5	29.5	1 510	101
A−8°-2	92.5	29.6	1 510	102
B−14°-2	12.5	24.4	1 640	102
B−14°-2	32.5	25.6	1 610	103
B−14°-2	47.5	26.4	1 590	102
B−14°-2	62.5	27.8	1 560	103
B−14°-2	77.5	28.1	1 550	103
B−14°-2	92.5	28.7	1 550	104
B−20°-2	12.5	24.4	1 640	102
B−20°-2	32.5	25.6	1 610	103
B−20°-2	47.5	26.4	1 590	102
B−20°-2	62.5	27	1 570	101
B−20°-2	77.5	27.5	1 550	101
B−20°-2	92.5	28.2	1 550	103

Sample ID	Radial distance mm	Water content %	Dry density kg/m^3	Degree of saturation %
C−25°-2	12.5	24.3	1650	103
C−25°-2	32.5	24.3	1640	101
C−25°-2	47.5	24.8	1620	102
C−25°-2	62.5	24.2	1610	96
C−25°-2	77.5	26.1	1590	102
C−25°-2	92.5	27	1590	105
C−31°-2	12.5	24.3	1650	103
C−31°-2	32.5	24.3	1640	101
C−31°-2	47.5	24.8	1620	102
C−31°-2	62.5	25.4	1610	102
C−31°-2	77.5	25.7	1600	101
C−31°-2	92.5	26.2	1600	103
D−37°-2	12.5	23.5	1660	102
D−37°-2	32.5	24.4	1650	103
D−37°-2	47.5	24.5	1640	103
D−37°-2	62.5	24.7	1640	103
D−37°-2	77.5	25.2	1620	103
D−37°-2	92.5	25.9	1610	103
D−42°-2	12.5	23.5	1660	102
D−42°-2	32.5	24.4	1650	103
D−42°-2	47.5	24.5	1640	103
D−42°-2	62.5	24.4	1640	103
D−42°-2	77.5	24.7	1640	103
D−42°-2	92.5	25.3	1620	103

Table A2-3. Distribution of water content, dry density and degree of saturation at level 3, i.e. the innermost and through the cavity centre. The sample ID indicates if the specimens were taken along a line (L) or as a continuous sample within a sector (A–D), the angle from the centre of the cavity and the final figure shows the level. The radial distance is given from the inner steel cylinder. The degree of saturation was calculated from a particle density of ρ_s = 2 695 kg/m^3. The dry density of some specimens was calculated from the assumptions of S_r = 100 %, marked *, and the position of some specimens was corrected, marked **.

Sample ID	Radial distance mm	Water content %	Dry density kg/m^3	Degree of saturation %
L3°-3	12.5	24.7	1 630	102
L3°-3	32.5	25.7	1 600	100
L3°-3	47.5	27.7	1 560	102
L3°-3	62.5	30.1	1 510	103
L3°-3**	77.5	30.9	1 490	103
L3°-3**	92.5	30.9	1 490	103
L20°-3*	12.5	24.1	1 630	100
L20°-3*	32.5	24.8	1 620	100
L20°-3*	47.5	26	1 590	100
L20°-3*	62.5	27.4	1 550	100
L20°-3*	77.5	27.5	1 550	100
L20°-3*	92.5	27.6	1 550	100
L65°-3	12.5	23.3	1 660	101
L65°-3	32.5	23.6	1 650	101
L65°-3	47.5	23.8	1 650	101
L65°-3	62.5	24	1 640	101
L65°-3	77.5	24.3	1 640	101
L65°-3	92.5	25.4	1 620	102
L90°-3	12.5	22.7	1 650	96
L90°-3	32.5	23.2	1 660	100
L90°-3	47.5	23.3	1 660	101
L90°-3	62.5	23.3	1 660	101
L90°-3	77.5	23.8	1 660	102
L90°-3	92.5	25	1 650	107
A−3°-3	12.5	24.7	1 640	103
A−3°-3	32.5	26.1	1 580	99
A−3°-3	47.5	28.1	1 550	102
A−3°-3	62.5	29.8	1 510	102
A−3°-3	77.5	30.6	1 490	101
A−3°-3	92.5	30.6	1 480	101
A−8°-3	12.5	24.7	1 640	103
A−8°-3	32.5	26.1	1 580	99
A−8°-3	47.5	28.1	1 550	102
A−8°-3	62.5	30.1	1 500	102
A−8°-3	77.5	30.9	1 480	101
A−8°-3	92.5	31.1	1 480	101
B−14°-3	12.5	24.5	1 640	103
B−14°-3	32.5	25.6	1 600	100
B−14°-3	47.5	26.8	1 570	101
B−14°-3	62.5	29.3	1 520	102
B−14°-3	77.5	29.6	1 510	101
B−14°-3	92.5	29.4	1 520	102
B−20°-3	12.5	24.5	1 640	103
B−20°-3	32.5	25.6	1 600	100
B−20°-3	47.5	26.8	1 570	101
B−20°-3	62.5	27.5	1 550	101
B−20°-3	77.5	27.8	1 550	101
B−20°-3	92.5	28.1	1 550	102

Sample ID	Radial distance mm	Water content %	Dry density kg/m^3	Degree of saturation %
C−25°-3	12.5	23.8	1650	102
C−25°-3	32.5	24.4	1630	101
C−25°-3	47.5	24.9	1620	101
C−25°-3	62.5	25.5	1610	101
C−25°-3	77.5	25.2	1580	97
C−25°-3	92.5	26.5	1570	99
C−31°-3	12.5	23.8	1650	102
C−31°-3	32.5	24.4	1630	101
C−31°-3	47.5	24.9	1620	101
C−31°-3	62.5	24.7	1630	101
C−31°-3	77.5	26.1	1600	103
C−31°-3	92.5	26	1600	102
D−37°-3	12.5	23.2	1670	101
D−37°-3	32.5	23.7	1650	102
D−37°-3	47.5	24.1	1640	102
D−37°-3	62.5	24.5	1640	102
D−37°-3	77.5	24.9	1630	102
D−37°-3	92.5	25.1	1620	102
D−42°-3	12.5	23.2	1670	101
D−42°-3	32.5	23.7	1650	102
D−42°-3	47.5	24.1	1640	102
D−42°-3	62.5	23.7	1650	101
D−42°-3	77.5	24.2	1620	99
D−42°-3	92.5	24.7	1630	101

A2.2 Results from the dismantled SH4

A2.2.1 Photos from start and dismantling

Below photos of the bentonite block, the test device and the dismantling of the self-healing test SH4 are shown.

Figure A2-11. *Cavity in the block used for test SH4. A second cavity was cut out on the other side of the block.*

Figure A2-12. *The device with filter and sensors used for the test (to the left) with the installed block (to the right).*

Figure A2-13. *The device before dismantling.*

Figure A2-14. *A hydraulic jack was used for the dismantling of the block (to the left) and the dismantled block with the inner steel cylinder left (to the right).*

Figure A2-15. *The block was divided in two parts before the sampling for determination of water content and bulk density.*

A2.2.2 Timetable, from start to end of test (SH4)

Project	**Buffer homogenisation SH**
Sample ID	SH4
Material	MX-80 #2012
Sensors	Nine load cells
Type of water	De-ionized water
Dimension	
Diameter	D(outer) = 300 mm, D(inner) = 100 mm
Height	H = 100 mm

Cavities	Length ≈ 70 mm (circumferential) Height ≈ 35 mm Depth ≈ 50 mm

Estimated required volume of water	
Cavities, gaps, filter and bevels	4 dl
including saturation	12 dl

Date	**Activity**
2016-10-26	Compaction of blocks Block preparation with turning lathe and drilling
2016-11-30	Preparation of cavities
2016-12-01	Mounted into device
2017-03-01	**Start of test**
	Water inflow of 0.072 ml/h
2018-11-29	Longer power outage, approximately 6 h
2019-06-23	Water pressure set to 50 kPa for 1 month
2019-07-22	Water inflow again set to 0.072 ml/h
2019-11-07	Salt accumulation observed just above the water outlet
2019-12-16	Outflow of water observed at flushing, for the first time
2020-01-16	Water pressure at inflow set to 400 kPa
2020-08-25	Start measurement of water pressure, 0–50 kPa
	End of test
2020-09-02	Water pressure lowered to zero
2020-08-07	The test was terminated Sensors were dismantled and the device was moved The upper lid and the bottom plate were removed Observation that the upper o-ring was not in place The block was forced uppwards through the steel ring Removed filter after less than 5 minutes Block sawn in four pieces, start sampling
2020-09-09	The sampling was completed
2020-09-10	Remaining material in sealed aluminium bags
2020-09-11	Sensors controlled, error mainly less than 8 %

A2.2.3 Evolution of swelling pressure, water pressure and water volume (SH4)

In Figure A2-16 and Figure A2-17 the evolutions of swelling pressure, water pressure and water volume are shown, see also Figure 5-13 and Figure 5-14 in Section 5.4. In the diagrams below the specific occasions 1 to 8 are marked according to the following:

1. Test start, water inflow of 0.072 ml/h.
2. Longer power outage.
3. Water pressure set to 50 kPa for 1 month.
4. Water flow control set back to 0.072 ml/h.
5. Salt accumulation observed.
6. Outflow of water observed at flushing.
7. Water pressure at the inflow set to 400 kPa.
8. End of test, dismantling.

The flow rate used in the test was set to saturate the block in 2 years. The total volume needed for the saturation was calculated to 1 200 ml which is marked in Figure A2-17 on the right axis (plus sign). However, the water inflow continued and after the total testing time an additional inflow of 800 ml was measured. Accumulated salt was observed at one specific position, above one of the drainage points between the steel ring and the lid of the test device. The first observation of this was made after 2 years and 8 months (mark 5). It is thus assumed that at least from this date leakage and evaporation took place. After additional month (mark 6) water outflow was seen in the outgoing tube at flushing. After another month the water pressure started to increase and was maximized to 400 kPa (mark 7).

Approximately two years after start (mark 2) a longer power outage occurred and for at least 6 hours no water was supplied. This caused a rapid decrease in the water pressure, see Figure A2-17, and it probably also caused the decrease in swelling pressure clearly seen in the measurements by two of the sensors, P33 and P66, in Figure A2-16. These two sensors were the only sensors located on the left side of the block and the measurements indicate a non-symmetric behaviour between the left and right side of the block.

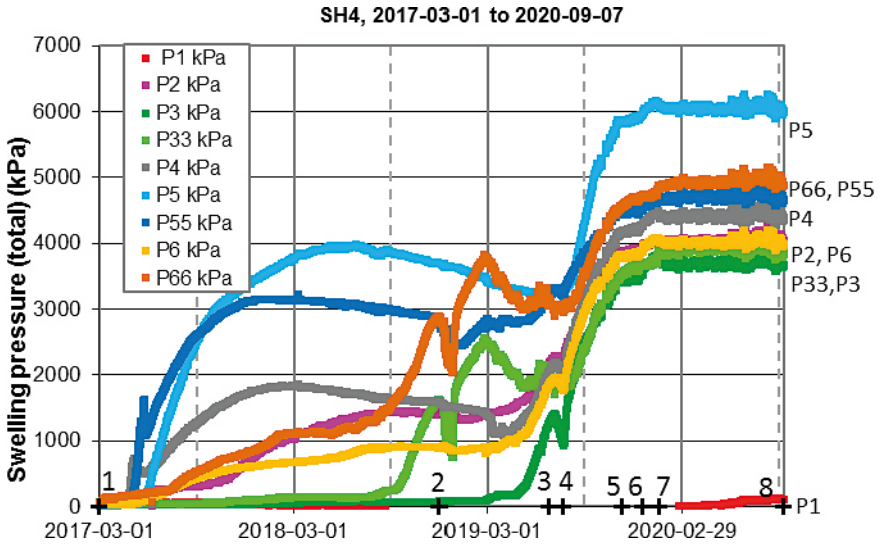

Figure A2-16. *Evolution of swelling pressure (total pressure) during test SH4. The numbers between P1 and P66 denote the different load cells see Figure 5-12. The marks 1 to 8 are described in the text. The only registered values by sensors P1 are also shown.*

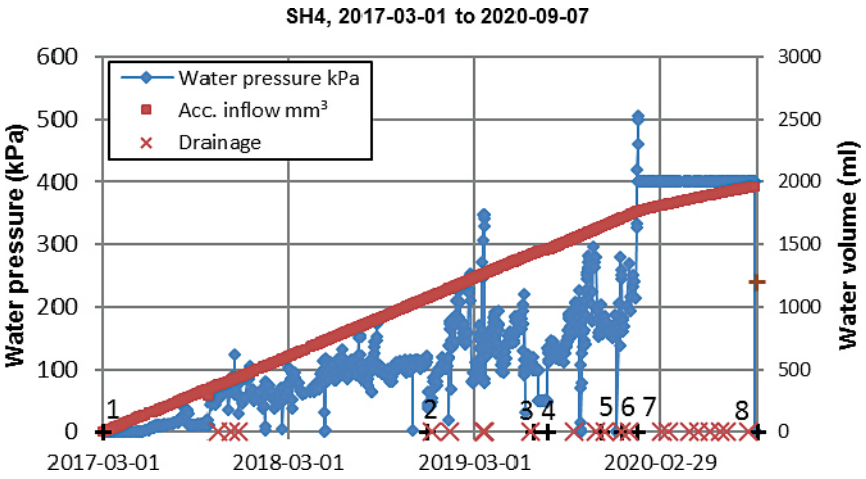

Figure A2-17. *Measured water pressure at the inflow (blue points, see Figure 5-13) together with the accumulated volume of inflowing water (solid brown line). The predicted volume to saturate the block is marked to the right (brown plus sign). Drainage or flushing was done at short time periods (crosses). The marks 1 to 8 are described in the text.*

A2.2.4 Tabulated values of water content and density (SH4)

Table A2-4, Table A2-5 and Table A2-6 contain tabulated values of water content and dry density after dismantling of SH4 and sampling along M-lines, L-lines and within sub-sectors, respectively. The different sampling techniques are described in Figure 5-17. The Sample ID in the second column indicates the direction (angle −90° to +90°) of the sampling line, the level of the specimen (1–6) and position number from the inner ring (1–9). In columns three to five the position is given more generally with a global angle 0° to 360°, a distance from mid-height and upwards (−40 mm to +40 mm) and the radial distance from the inner ring (0 mm – 100 mm). In the tables the water content of two specimens were corrected (B-2-5 and M0-2-5). The degree of saturation was calculated from a particle density of ρ_s = 2 780 kg/m^3.

Table A2-4. Distribution of water content, dry density and degree of saturation determined along M-lines based on bulk density and water content from all levels over the full height. The table contains the position of each specimen with a global angle from the centre of the cavity, level from mid-height and distance from the inner cylinder.

Line	Sample ID	Global angle (from main cavity) 0° – 360°	Level (from mid-height) mm	Distance (from inner ring) mm	Dry density kg/m^3	Water content %	Deg. of Saturation %
M0	M0-1-1	180	40	12.5	1 550	28.3	99
	M0-1-2	180	40	32.5	1 550	28.3	99
	M0-1-3	180	40	47.5	1 540	28.9	99
	M0-1-4	180	40	62.5	1 510	29.8	99
	M0-1-5	180	40	77.5	1 500	30.7	99
	M0-1-6	180	40	92.5	1 480	31.3	99
	M0-2-1	180	22.5	12.5	1 540	28.7	99
	M0-2-2	180	22.5	32.5	1 540	28.8	99
	M0-2-3	180	22.5	47.5	1 500	31.0	101
	M0-2-4	180	22.5	62.5	1 490	30.8	100
	M0-2-5	180	22.5	77.5	1 460	32.1[1]	99
	M0-2-6	180	22.5	92.5	1 450	32.4	98
	M0-3-1	180	7.5	12.5	1 550	28.3	99
	M0-3-2	180	7.5	32.5	1 540	29.0	100
	M0-3-3	180	7.5	47.5	1 500	30.8	101
	M0-3-4	180	7.5	62.5	1 460	32.0	98
	M0-3-5	180	7.5	77.5	1 450	33.3	100
	M0-3-6	180	7.5	92.5	1 420	34.7	101
	M0-4-1	180	−7.5	12.5	1 540	28.5	99
	M0-4-2	180	−7.5	32.5	1 540	29.1	100
	M0-4-3	180	−7.5	47.5	1 500	29.9	97
	M0-4-4	180	−7.5	62.5	1 440	32.2	97
	M0-4-5	180	−7.5	77.5	1 440	33.4	100
	M0-4-6	180	−7.5	92.5	1 410	34.4	99
	M0-5-1	180	−22.5	12.5	1 540	28.3	98
	M0-5-2	180	−22.5	32.5	1 540	28.7	99
	M0-5-3	180	−22.5	47.5	1 510	30.2	100
	M0-5-4	180	−22.5	62.5	1 480	31.9	100
	M0-5-5	180	−22.5	77.5	1 440	32.6	98
	M0-5-6	180	−22.5	92.5	1 420	34.6	100
	M0-6-1	180	−40	12.5	1 540	28.2	98
	M0-6-2	180	−40	32.5	1 520	28.9	97
	M0-6-3	180	−40	47.5	1 530	29.0	98
	M0-6-4	180	−40	62.5	1 500	30.3	98
	M0-6-5	180	−40	77.5	1 470	32.2	100
	M0-6-6	180	−40	92.5	1 430	34.0	99
M90	M90-1-1	90	40	12.5	1 580	26.8	98
	M90-1-2	90	40	32.5	1 580	26.7	98
	M90-1-3	90	40	47.5	1 580	26.5	97
	M90-1-4	90	40	62.5	1 580	26.7	98
	M90-1-5	90	40	77.5	1 580	26.6	98
	M90-1-6	90	40	92.5	1 580	26.8	98
	M90-2-1	90	22.5	12.5	1 580	27.1	99
	M90-2-2	90	22.5	32.5	1 580	27.1	99
	M90-2-3	90	22.5	47.5	1 580	27.0	98
	M90-2-4	90	22.5	62.5	1 580	27.0	98
	M90-2-5	90	22.5	77.5	1 580	27.2	99
	M90-2-6	90	22.5	92.5	1 570	27.4	98
	M90-3-1	90	7.5	12.5	1 580	26.7	98
	M90-3-2	90	7.5	32.5	1 580	27.2	99
	M90-3-3	90	7.5	47.5	1 580	27.2	99

Table A2-4. Continued.

Line	Sample ID	Global angle (from main cavity) 0°–360°	Level (from mid-height) mm	Distance (from inner ring) mm	Dry density kg/m^3	Water content %	Deg. of Saturation %
	M90-3-4	90	7.5	62.5	1570	27.1	98
	M90-3-5	90	7.5	77.5	1570	27.3	99
	M90-3-6	90	7.5	92.5	1560	27.6	99
	M90-4-1	90	−7.5	12.5	1580	27.0	98
	M90-4-2	90	−7.5	32.5	1570	27.3	99
	M90-4-3	90	−7.5	47.5	1570	27.3	99
	M90-4-4	90	−7.5	62.5	1570	27.2	99
	M90-4-5	90	−7.5	77.5	1570	27.5	98
	M90-4-6	90	−7.5	92.5	1560	27.8	99
	M90-5-1	90	−22.5	12.5	1580	27.0	99
	M90-5-2	90	−22.5	32.5	1580	27.1	99
	M90-5-3	90	−22.5	47.5	1560	28.2	101
	M90-5-4	90	−22.5	62.5	1570	27.4	99
	M90-5-5	90	−22.5	77.5	1560	27.5	98
	M90-5-6	90	−22.5	92.5	1550	27.7	97
	M90-6-1	90	−40	12.5	1580	26.7	98
	M90-6-2	90	−40	32.5	1580	26.8	98
	M90-6-3	90	−40	47.5	1580	26.6	98
	M90-6-4	90	−40	62.5	1580	26.7	98
	M90-6-5	90	−40	77.5	1570	27.1	98
	M90-6-6	90	−40	92.5	1550	27.9	98
M65	M65-1-1	115	40	10	1580	27.2	99
	M65-1-2	115	40	30	1570	27.4	99
	M65-1-3	115	40	50	1570	27.0	98
	M65-1-4	115	40	70	1570	27.3	98
	M65-1-5	115	40	90	1570	27.3	99
	M65-2-1	115	20	10	1580	26.9	98
	M65-2-2	115	20	30	1570	27.5	99
	M65-2-3	115	20	50	1570	27.6	99
	M65-2-4	115	20	70	1560	27.5	98
	M65-2-5	115	20	90	1560	27.7	99
	M65-3-1	115	0	10	1560	27.4	98
	M65-3-2	115	0	30	1570	27.6	99
	M65-3-3	115	0	50	1570	27.6	99
	M65-3-4	115	0	70	1560	28.0	99
	M65-3-5	115	0	90	1560	27.9	99
	M65-4-1	115	−20	10	1580	26.9	98
	M65-4-2	115	−20	30	1580	27.0	98
	M65-4-3	115	−20	50	1560	27.8	99
	M65-4-4	115	−20	70	1550	28.1	99
	M65-4-5	115	−20	90	1540	28.5	99
	M65-5-1	115	−40	10	1580	26.6	98
	M65-5-2	115	−40	30	1580	26.9	98
	M65-5-3	115	−40	50	1570	27.3	99
	M65-5-4	115	−40	70	1560	27.7	99
	M65-5-5	115	−40	90	1540	28.5	98
M20	M20-1-1	160	40	10	1570	27.3	99
	M20-1-2	160	40	30	1560	27.6	98
	M20-1-3	160	40	50	1550	28.1	99
	M20-1-4	160	40	70	1540	28.6	99
	M20-1-5	160	40	90	1530	29.1	99
	M20-2-1	160	20	10	1570	27.5	99
	M20-2-2	160	20	30	1550	28.1	99
	M20-2-3	160	20	50	1540	28.5	99

Table A2-4. Continued.

Line	Sample ID	Global angle (from main cavity) 0°–360°	Level (from mid-height) mm	Distance (from inner ring) mm	Dry density kg/m^3	Water content %	Deg. of Saturation %
	M20-2-4	160	20	70	1530	29.1	99
	M20-2-5	160	20	90	1530	29.0	98
	M20-3-1	160	0	10	1560	27.7	99
	M20-3-2	160	0	30	1550	28.3	99
	M20-3-3	160	0	50	1540	28.7	99
	M20-3-4	160	0	70	1520	29.4	99
	M20-3-5	160	0	90	1520	29.8	100
	M20-4-1	160	−20	10	1570	27.6	99
	M20-4-2	160	−20	30	1550	28.1	99
	M20-4-3	160	−20	50	1540	28.6	99
	M20-4-4	160	−20	70	1520	29.6	100
	M20-4-5	160	−20	90	1500	30.3	99
	M20-5-1	160	−40	10	1570	27.4	99
	M20-5-2	160	−40	30	1560	27.7	99
	M20-5-3	160	−40	50	1540	28.4	99
	M20-5-4	160	−40	70	1520	29.1	98
	M20-5-5	160	−40	90	1480	31.5	100
M(−65)	M(−65)-1-1	245	40	10	1540	28.7	99
	M(−65)-1-2	245	40	30	1530	29.3	99
	M(−65)-1-3	245	40	50	1520	29.7	99
	M(−65)-1-4	245	40	70	1510	30.0	99
	M(−65)-1-5	245	40	90	1490	30.8	99
	M(−65)-2-1	245	20	10	1540	28.9	99
	M(−65)-2-2	245	20	30	1520	29.7	100
	M(−65)-2-3	245	20	50	1510	30.2	99
	M(−65)-2-4	245	20	70	1490	30.8	99
	M(−65)-2-5	245	20	90	1480	31.4	99
	M(−65)-3-1	245	0	10	1530	29.1	99
	M(−65)-3-2	245	0	30	1520	29.8	100
	M(−65)-3-3	245	0	50	1500	30.4	99
	M(−65)-3-4	245	0	70	1490	31.2	99
	M(−65)-3-5	245	0	90	1460	32.2	99
	M(−65)-4-1	245	−20	10	1530	29.1	99
	M(−65)-4-2	245	−20	30	1520	29.7	99
	M(−65)-4-3	245	−20	50	1500	30.4	99
	M(−65)-4-4	245	−20	70	1480	31.3	99
	M(−65)-4-5	245	−20	90	1460	32.4	99
	M(−65)-5-1	245	−40	10	1540	28.6	99
	M(−65)-5-2	245	−40	30	1530	29.2	99
	M(−65)-5-3	245	−40	50	1510	30.0	99
	M(−65)-5-4	245	−40	70	1480	31.1	99
	M(−65)-5-5	245	−40	90	1450	32.6	99

[1] The water content of M0-2-5 is corrected.

Table A2-5. Distribution of water content, dry density and degree of saturation determined along L-lines based on bulk density determined on the upper half and water content determined on the lower half. The table contains the position of each specimen (at the upper half) with a global angle from the centre of the cavity, level from mid-height and distance from the inner cylinder.

Line	Sample ID	Global angle (from main cavity) 0°–360°	Level (from mid-height) mm	Distance (from inner ring) mm	Dry density kg/m^3	Water content %	Deg. of Saturation %
L0	L0-1-1	0	40	12.5	1540	28.6	99
	L0-1-2	0	40	32.5	1530	29.2	99
	L0-1-3	0	40	47.5	1520	29.8	100
	L0-1-4	0	40	62.5	1490	31.4	101
	L0-1-5	0	40	77.5	1470	32.3	101
	L0-1-6	0	40	92.5	1460	32.9	101
	L0-2-1	0	22.5	12.5	1540	28.7	99
	L0-2-2	0	22.5	32.5	1530	29.4	99
	L0-2-3	0	22.5	47.5	1490	30.9	100
	L0-2-4	0	22.5	62.5	1460	32.5	100
	L0-2-5	0	22.5	77.5	1430	34.2	101
	L0-2-6	0	22.5	92.5	1440	33.6	100
	L0-3-1	0	7.5	12.5	1540	28.6	99
	L0-3-2	0	7.5	32.5	1520	29.6	99
	L0-3-3	0	7.5	47.5	1470	31.8	99
	L0-3-4	0	7.5	62.5	1430	33.8	100
	L0-3-5	0	7.5	77.5	1420	34.1	99
	L0-3-6	0	7.5	92.5	1420	34.5	100
L20	L20-1-1	20	40	12.5	1550	27.9	98
	L20-1-2	20	40	32.5	1550	28.3	99
	L20-1-3	20	40	47.5	1540	28.6	99
	L20-1-4	20	40	62.5	1530	29.2	100
	L20-1-5	20	40	77.5	1510	30.1	100
	L20-1-6	20	40	92.5	1500	30.9	101
	L20-2-1	20	22.5	12.5	1550	28.1	99
	L20-2-2	20	22.5	32.5	1550	28.5	99
	L20-2-3	20	22.5	47.5	1540	28.9	100
	L20-2-4	20	22.5	62.5	1530	29.4	100
	L20-2-5	20	22.5	77.5	1520	30.0	100
	L20-2-6	20	22.5	92.5	1500	30.7	100
	L20-3-1	20	7.5	12.5	1550	28.1	99
	L20-3-2	20	7.5	32.5	1550	28.4	99
	L20-3-3	20	7.5	47.5	1540	28.9	99
	L20-3-4	20	7.5	62.5	1530	29.2	99
	L20-3-5	20	7.5	77.5	1510	29.9	99
	L20-3-6	20	7.5	92.5	1500	30.5	100
L65	L65-1-1	65	40	12.5	1570	27.1	98
	L65-1-2	65	40	32.5	1570	27.2	98
	L65-1-3	65	40	47.5	1570	27.3	99
	L65-1-4	65	40	62.5	1570	27.4	99
	L65-1-5	65	40	77.5	1560	28.0	100
	L65-1-6	65	40	92.5	1550	29.1	102
	L65-2-1	65	22.5	12.5	1570	27.3	98
	L65-2-2	65	22.5	32.5	1570	27.5	99
	L65-2-3	65	22.5	47.5	1570	27.6	99
	L65-2-4	65	22.5	62.5	1560	27.8	99
	L65-2-5	65	22.5	77.5	1560	28.1	100
	L65-2-6	65	22.5	92.5	1550	28.6	100
	L65-3-1	65	7.5	12.5	1570	27.4	99
	L65-3-2	65	7.5	32.5	1570	27.6	99
	L65-3-3	65	7.5	47.5	1570	27.6	99
	L65-3-4	65	7.5	62.5	1560	27.7	99
	L65-3-5	65	7.5	77.5	1560	27.9	99
	L65-3-6	65	7.5	92.5	1550	28.3	99

Table A2-5. Continued.

Line	Sample ID	Global angle (from main cavity) 0°–360°	Level (from mid-height) mm	Distance (from inner ring) mm	Dry density kg/m^3	Water content %	Deg. of Saturation %
L90	L90-1-1	90	40	12.5	1580	26.7	98
	L90-1-2	90	40	32.5	1580	26.8	98
	L90-1-3	90	40	47.5	1580	26.9	98
	L90-1-4	90	40	62.5	1570	27.2	99
	L90-1-5	90	40	77.5	1570	27.7	99
	L90-1-6	90	40	92.5	1550	28.6	101
	L90-2-1	90	22.5	12.5	1580	26.6	98
	L90-2-2	90	22.5	32.5	1570	26.9	98
	L90-2-3	90	22.5	47.5	1570	27.1	98
	L90-2-4	90	22.5	62.5	1570	27.3	99
	L90-2-5	90	22.5	77.5	1570	27.4	99
	L90-2-6	90	22.5	92.5	1560	28.0	99
	L90-3-1	90	7.5	12.5	1570	27.0	98
	L90-3-2	90	7.5	32.5	1570	26.9	98
	L90-3-3	90	7.5	47.5	1570	27.1	98
	L90-3-4	90	7.5	62.5	1570	27.1	98
	L90-3-5	90	7.5	77.5	1570	27.3	99
	L90-3-6	90	7.5	92.5	1560	27.6	98
L(−65)	L−65-1-1	295	40	12.5	1530	29.2	100
	L−65-1-2	295	40	32.5	1520	29.8	100
	L−65-1-3	295	40	47.5	1510	30.3	100
	L−65-1-4	295	40	62.5	1500	30.8	100
	L−65-1-5	295	40	77.5	1490	31.6	101
	L−65-1-6	295	40	92.5	1470	32.1	101
	L−65-2-1	295	22.5	12.5	1530	29.1	99
	L−65-2-2	295	22.5	32.5	1510	29.8	99
	L−65-2-3	295	22.5	47.5	1500	30.4	99
	L−65-2-4	295	22.5	62.5	1500	30.8	99
	L−65-2-5	295	22.5	77.5	1480	31.5	100
	L−65-2-6	295	22.5	92.5	1470	31.9	100
	L−65-3-1	295	7.5	12.5	1530	29.2	99
	L−65-3-2	295	7.5	32.5	1520	30.0	100
	L−65-3-3	295	7.5	47.5	1500	30.4	99
	L−65-3-4	295	7.5	62.5	1490	31.0	100
	L−65-3-5	295	7.5	77.5	1480	31.4	100
	L−65-3-6	295	7.5	92.5	1470	31.9	100
L(−90)	L−90-1-1	270	40	12.5	1540	28.6	99
	L−90-1-2	270	40	32.5	1530	29.3	99
	L−90-1-3	270	40	47.5	1520	29.9	100
	L−90-1-4	270	40	62.5	1510	30.6	101
	L−90-1-5	270	40	77.5	1490	31.5	101
	L−90-1-6	270	40	92.5	1460	33.6	104
	L−90-2-1	270	22.5	12.5	1540	28.8	99
	L−90-2-2	270	22.5	32.5	1530	29.3	99
	L−90-2-3	270	22.5	47.5	1510	29.9	99
	L−90-2-4	270	22.5	62.5	1500	30.5	100
	L−90-2-5	270	22.5	77.5	1480	31.6	100
	L−90-2-6	270	22.5	92.5	1460	32.9	101
	L−90-3-1	270	7.5	12.5	1540	28.8	99
	L−90-3-2	270	7.5	32.5	1520	29.5	99
	L−90-3-3	270	7.5	47.5	1510	30.0	99
	L−90-3-4	270	7.5	62.5	1500	30.5	99
	L−90-3-5	270	7.5	77.5	1480	31.2	99
	L−90-3-6	270	7.5	92.5	1460	32.3	100

Table A2-6. Distribution of water content, dry density and degree of saturation determined continuously within a sector divided into the sub-sectors A–D based on bulk density determined on the upper half and water content determined on the lower half. The table contains the position of each specimen (at the upper half) with a global angle from the centre of the cavity, level from mid-height and distance from the inner cylinder.

Sector	Sample ID	Global angle (from main cavity) 0° – 360°	Level (from mid-height) mm	Distance (from inner ring) mm	Dry density kg/m^3	Water content %	Deg. of Saturation %
Sector A	A-1-1	357	40	12.5	1540	28.5	99
	A-1-2	357	40	32.5	1530	29.4	100
	A-1-3	357	40	47.5	1510	30.3	100
	A-1-4	357	40	62.5	1490	31.2	101
	A-1-5	357	40	77.5	1470	32.2	101
	A-1-6	357	40	92.5	1460	32.7	100
	A-1-1	352	40	12.5	1540	28.5	99
	A-1-2	352	40	32.5	1530	29.4	100
	A-1-3	352	40	47.5	1510	30.3	100
	A-1-7	352	40	62.5	1490	31.2	100
	A-1-8	352	40	77.5	1460	32.4	100
	A-1-9	352	40	92.5	1450	33.2	100
	A-2-1	357	22.5	12.5	1540	28.8	99
	A-2-2	357	22.5	32.5	1520	29.7	99
	A-2-3	357	22.5	47.5	1490	30.8	99
	A-2-4	357	22.5	62.5	1470	32.1	100
	A-2-5	357	22.5	77.5	1450	33.3	100
	A-2-6	357	22.5	92.5	1430	34.0	100
	A-2-1	352	22.5	12.5	1540	28.8	99
	A-2-2	352	22.5	32.5	1520	29.7	99
	A-2-3	352	22.5	47.5	1490	30.8	99
	A-2-7	352	22.5	62.5	1460	32.4	100
	A-2-8	352	22.5	77.5	1440	33.3	99
	A-2-9	352	22.5	92.5	1430	33.9	100
	A-3-1	357	7.5	12.5	1540	28.7	99
	A-3-2	357	7.5	32.5	1510	29.9	99
	A-3-3	357	7.5	47.5	1470	31.5	99
	A-3-4	357	7.5	62.5	1440	32.7	98
	A-3-5	357	7.5	77.5	1420	33.7	98
	A-3-6	357	7.5	92.5	1420	34.3	99
	A-3-1	352	7.5	12.5	1540	28.7	99
	A-3-2	352	7.5	32.5	1510	29.9	99
	A-3-3	352	7.5	47.5	1470	31.5	99
	A-3-7	352	7.5	62.5	1430	33.2	97
	A-3-8	352	7.5	77.5	1420	33.7	98
	A-3-9	352	7.5	92.5	1420	34.2	99
Sector B	B-1-1	346	40	12.5	1540	28.8	99
	B-1-2	346	40	32.5	1520	29.6	100
	B-1-3	346	40	47.5	1510	30.3	100
	B-1-4	346	40	62.5	1480	32.4	103
	B-1-5	346	40	77.5	1460	33.1	102
	B-1-6	346	40	92.5	1450	33.4	101
	B-1-1	340	40	12.5	1540	28.8	99
	B-1-2	340	40	32.5	1520	29.6	100
	B-1-3	340	40	47.5	1510	30.3	100
	B-1-7	340	40	62.5	1490	31.7	102
	B-1-8	340	40	77.5	1470	32.7	102
	B-1-9	340	40	92.5	1450	33.8	103
	B-2-1	346	22.5	12.5	1540	29.1	100
	B-2-2	346	22.5	32.5	1520	29.7	99
	B-2-3	346	22.5	47.5	1510	30.5	101

Table A2-6. Continued.

Sector	Sample ID	Global angle (from main cavity) 0° – 360°	Level (from mid-height) mm	Distance (from inner ring) mm	Dry density kg/m^3	Water content %	Deg. of Saturation %
	B-2-4	346	22.5	62.5	1470	31.9	100
	B-2-5	346	22.5	77.5	1450	32.6[1]	99
	B-2-6	346	22.5	92.5	1440	33.7	100
	B-2-1	340	22.5	12.5	1540	29.1	100
	B-2-2	340	22.5	32.5	1520	29.7	99
	B-2-3	340	22.5	47.5	1510	30.5	101
	B-2-7	340	22.5	62.5	1480	31.5	100
	B-2-8	340	22.5	77.5	1460	32.6	100
	B-2-9	340	22.5	92.5	1440	33.6	100
	B-3-1	346	7.5	12.5	1540	28.9	99
	B-3-2	346	7.5	32.5	1520	29.6	99
	B-3-3	346	7.5	47.5	1500	30.7	99
	B-3-4	346	7.5	62.5	1470	31.0	97
	B-3-5	346	7.5	77.5	1460	32.0	99
	B-3-6	346	7.5	92.5	1440	32.9	98
	B-3-1	340	7.5	12.5	1540	28.9	99
	B-3-2	340	7.5	32.5	1520	29.6	99
	B-3-3	340	7.5	47.5	1500	30.7	99
	B-3-7	340	7.5	62.5	1480	31.1	99
	B-3-8	340	7.5	77.5	1470	32.1	100
	B-3-9	340	7.5	92.5	1450	33.1	100
Sector C	C-1-1	335	40	12.5	1530	29.1	99
	C-1-2	335	40	32.5	1520	29.9	100
	C-1-3	335	40	47.5	1500	30.7	100
	C-1-4	335	40	62.5	1490	31.3	101
	C-1-5	335	40	77.5	1470	32.2	101
	C-1-6	335	40	92.5	1450	33.1	101
	C-1-1	329	40	12.5	1530	29.1	99
	C-1-2	329	40	32.5	1520	29.9	100
	C-1-3	329	40	47.5	1500	30.7	100
	C-1-7	329	40	62.5	1490	31.4	101
	C-1-8	329	40	77.5	1470	32.2	101
	C-1-9	329	40	92.5	1450	33.0	101
	C-2-1	335	22.5	12.5	1530	29.3	99
	C-2-2	335	22.5	32.5	1510	30.0	100
	C-2-3	335	22.5	47.5	1500	30.6	99
	C-2-4	335	22.5	62.5	1490	31.3	100
	C-2-5	335	22.5	77.5	1460	32.3	99
	C-2-6	335	22.5	92.5	1440	33.2	100
	C-2-1	329	22.5	12.5	1530	29.3	99
	C-2-2	329	22.5	32.5	1510	30.0	100
	C-2-3	329	22.5	47.5	1500	30.6	99
	C-2-7	329	22.5	62.5	1490	30.6	99
	C-2-8	329	22.5	77.5	1470	32.1	100
	C-2-9	329	22.5	92.5	1450	32.8	100
	C-3-1	335	7.5	12.5	1530	29.2	99
	C-3-2	335	7.5	32.5	1510	29.8	99
	C-3-3	335	7.5	47.5	1500	30.4	99
	C-3-4	335	7.5	62.5	1490	31.3	101
	C-3-5	335	7.5	77.5	1460	32.3	99
	C-3-6	335	7.5	92.5	1440	33.0	99
	C-3-1	329	7.5	12.5	1530	29.2	99
	C-3-2	329	7.5	32.5	1510	29.8	99
	C-3-3	329	7.5	47.5	1500	30.4	99

Table A2-6. Continued.

Sector	Sample ID	Global angle (from main cavity) 0° – 360°	Level (from mid-height) mm	Distance (from inner ring) mm	Dry density kg/m^3	Water content %	Deg. of Saturation %
	C-3-7	329	7.5	62.5	1490	30.9	99
	C-3-8	329	7.5	77.5	1460	32.1	99
	C-3-9	329	7.5	92.5	1450	32.5	99
Sector D	D-1-1	323	40	12.5	1530	29.1	99
	D-1-2	323	40	32.5	1520	30.0	100
	D-1-3	323	40	47.5	1500	30.7	100
	D-1-4	323	40	62.5	1490	31.2	100
	D-1-5	323	40	77.5	1480	31.9	101
	D-1-6	323	40	92.5	1460	32.6	100
	D-1-1	318	40	12.5	1530	29.1	99
	D-1-2	318	40	32.5	1520	30.0	100
	D-1-3	318	40	47.5	1500	30.7	100
	D-1-7	318	40	62.5	1500	31.1	101
	D-1-8	318	40	77.5	1480	31.9	101
	D-1-9	318	40	92.5	1460	32.5	100
	D-2-1	323	22.5	12.5	1520	29.5	99
	D-2-2	323	22.5	32.5	1510	30.0	99
	D-2-3	323	22.5	47.5	1500	30.5	99
	D-2-4	323	22.5	62.5	1490	31.0	100
	D-2-5	323	22.5	77.5	1480	31.8	100
	D-2-6	323	22.5	92.5	1460	32.7	100
	D-2-1	318	22.5	12.5	1520	29.5	99
	D-2-2	318	22.5	32.5	1510	30.0	99
	D-2-3	318	22.5	47.5	1500	30.5	99
	D-2-7	318	22.5	62.5	1490	30.9	100
	D-2-8	318	22.5	77.5	1470	31.8	100
	D-2-9	318	22.5	92.5	1460	32.5	100
	D-3-1	323	7.5	12.5	1530	29.3	99
	D-3-2	323	7.5	32.5	1510	29.9	99
	D-3-3	323	7.5	47.5	1500	30.4	99
	D-3-4	323	7.5	62.5	1490	30.9	99
	D-3-5	323	7.5	77.5	1470	31.7	100
	D-3-6	323	7.5	92.5	1460	32.3	100
	D-3-1	318	7.5	12.5	1530	29.3	99
	D-3-2	318	7.5	32.5	1510	29.9	99
	D-3-3	318	7.5	47.5	1500	30.4	99
	D-3-7	318	7.5	62.5	1490	30.9	100
	D-3-8	318	7.5	77.5	1480	31.6	100
	D-3-9	318	7.5	92.5	1460	32.4	100

[1] The water content of B-2-5 is a corrected value.

Appendix 3

Results from the FLR-series

The information below is focused on specimens FLR6 and FLR7, dismantled after 4 and 6 years, respectively. In Table A3-1 initial data from all specimens FLR1–FLR10 are given. In Figure A3-1 the swelling pressure from the instrumented tests are shown where FLR2 resembles the dismantled FLR6 and FLR7. In Figure A3-2 the influence of temperature on the swelling pressure is illustrated with results from one-month measurements of FLR1.

In Table A3-2 and A3-3 the timetables, from start to end of test, for FLR6 and FLR7 are given. In Table A3-4 and Table A3-5 the resulting distributions of water content and density of FLR6 and FLR7, respectively, are tabulated.

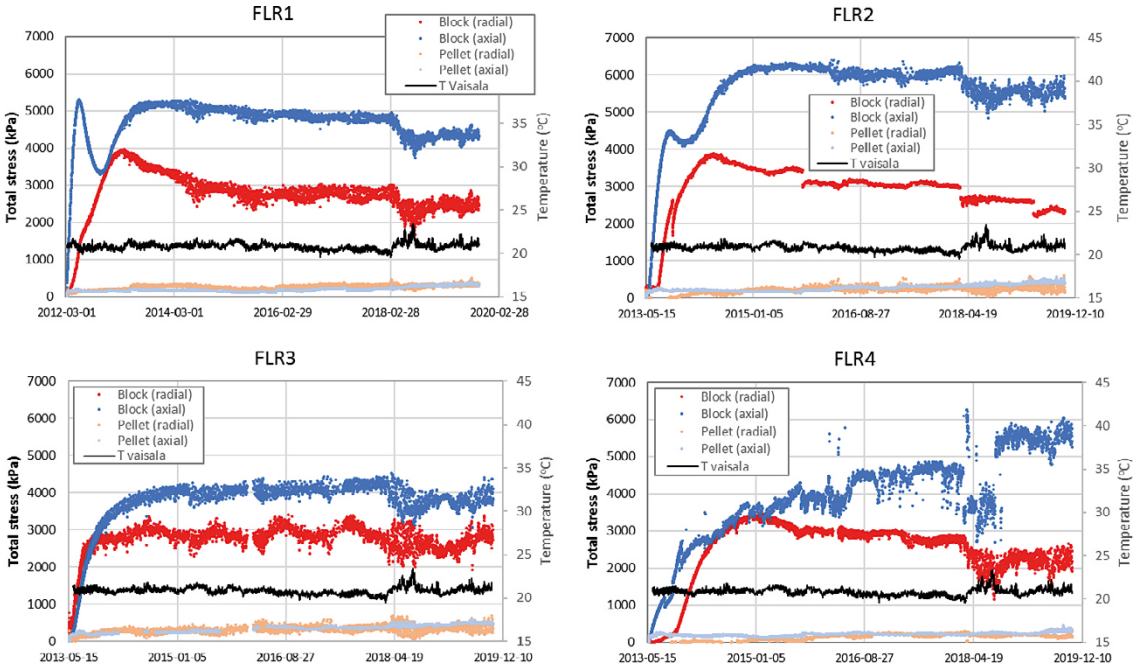

Figure A3-1. *Swelling pressure from start to 2019-10-15 from the set-ups FLR1–FLR4. All four set-ups are shown in Figure 6-2 and the set-up of FLR2 resembles that of FLR6 and FLR7.*

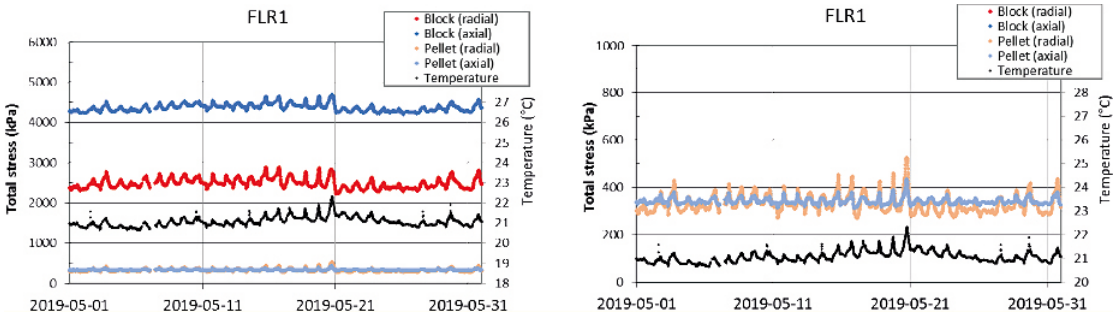

Figure A3-2. *Swelling pressure of FLR1 and measured temperature (black line) for one month. The results illustrate the influence of temperature on the measured swelling pressure.*

Table A3-1. Data from the installation of the 10 tubes in the test series, FLR1 to FLR10. The average degrees of saturation are given before (at t_1) and after (at t_2) the initial addition of water.

Test ID	LR1	FLR2	FLR3	FLR4	FLR5	FLR6	FLR7	FLR8	FLR9	FLR10
Start date	**2012-03-08**	**2013-05-14**	**2013-05-22**	**2013-05-23**	**2013-05-14**	**2013-05-16**	**2013-05-16**	**2013-05-17**	**2013-05-17**	**2013-05-20**
Pellet (upper part)										
w (%)	14.8	15.7	15.7	15.7	15.7	15.7	15.7	15.7	15.7	15.7
Actual total mass mp, tot (g)	58.8	67.7	62.6	181.7	67.7	67.7	67.7	67.7	67.7	67.7
Dry density (at installation) (kg/m^3)	835	955	882	933	955	955	955	955	955	955
Degree of saturation (at installation) (%)	18	23	20	22	23	23	23	23	23	23
Pellet (upper part) final dimensions										
D (mm)	26	26	25	36	26	26	26	26	26	26
H (mm)	125	125	125	175	125	125	125	125	125	125
Dry density (final dimensions) (kg/m^3)	772	882	881	882	882	882	882	882	882	882
Degree of saturation (final dimensions) (%)	16	20	20	20	20	20	20	20	20	20
Buffer (lower part)										
w (%)	19.2	21.6	26.9	22.7	21.6	21.6	21.6	21.6	21.6	21.6
Actual total mass mb, tot (g)	123.8	124.0	120.5	337.7	123.8	124.2	124	124.1	124.3	124.2
Dry density (at installation) (kg/m^3)	1 693	1 702	1 574	1 700	1 702	1 702	1 702	1 702	1 702	1 702
Degree of saturation (at installation) (%)	83	95	98	99	95	95	95	95	95	95
Buffer (lower part) final dimensions										
D (mm)	26	26	25	36	26	26	26	26	26	26
H (mm)	125	125	125	175	125	125	125	125	125	125
Dry density (final dimensions) (kg/m^3)	1 565	1 536	1 548	1 546	1 534	1 539	1 537	1 538	1 540	1 539
Degree of saturation (final dimensions) (%)	69	74	94	79	74	74	74	74	74	74
Pellet and Buffer										
Average degree of saturation (%) at t_1	36	42	49	43	42	42	42	42	42	42
Mass of water added (g)		39.8	39.9	103.8	42.6	41.5	44.0	42.9	42.7	46.5
Average degree of saturation (%) at t_2		95	107	95	98	97	100	99	99	104

Table A3-2. Timetable from start to end of FLR6.

Project	**Buffer homogenisation**	
	Long steel tubes	
Test ID	**FLR-6**	
Information	**No sensors**	
	Equipment	Steel cylinder with triangular grooves along the inner surface
	Sensors	No
	Material	MX-80 five compacted blocks, lower part MX-80 extruded pellet, upper part
	Water	2 mM NaCl at first but later changed to 50 mM NaCl
Date/time	Comments	
2013-05-16	**Test start**	
2013-05-10 10:00	Device assembled and specimen mounted	
2013-05-16 14:33	Water added (vacuum used)	
2013-05-16 14:40	Circulation of water Water circulation through the filter was made approximately once a week	
2013-08-07 16:25	Water circulation through the filter was made approximately once a month	
2015-10-05 14:00	Continuous water pressure of 70 kPa applied Flushing each month	
2017-05-22 14:10	Water pressure adjusted to zero	
2017-05-29	**End of test and dismantling**	

Table A3-3. Timetable from start to end of FLR7.

Project	**Buffer homogenisation**	
	Long steel tubes	
Test ID	**FLR-7**	
Information	**No sensors**	
	Equipment	Steel cylinder with triangular grooves along the inner surface
	Sensors	No
	Material	MX-80 five compacted blocks, lower part MX-80 extruded pellet, upper part
	Water	2 mM NaCl at first but later changed to 50 mM NaCl
Date/time	Comments	
2013-05-16	**Test start**	
2013-05-16 14:00	Device assembled and specimen mounted	
2013-05-16 14:33	Water added (vacuum used)	
2013-05-16 15:00	Circulation of water Water circulation through the filter was made approximately once a week	
2013-08-07 16:25	Water circulation through the filter was made approximately once a month	
2015-10-05 14:00	Continuous water pressure of 70 kPa applied Flushing each month	
2019-04-26 12:00	Water pressure adjusted to zero	
2019-05-02	**End of test and dismantling**	

Table A3-4. Distribution of water content after dismantling of FLR6. The dry density is calculated from a measured water content and a degree of saturation S_r = 100 %. At three positions the dry density is also calculated, from measured water content and measured bulk density.

Sample ID (FLR6)	Distance[1] mm	Thickness mm	Water content %	Dry density (from bulk density) kg/m^3	Dry density (assume S_r = 100 %) kg/m^3
1	247	6	69.3		950
2	240.5	7	68.7		955
3	233.5	7	66.2		979
4	227.5	5	64.1		999
5	222.5	5	62.7		1 014
6	217.5	5	62.7		1 013
7	212.5	5	63.5		1 006
8	207.5	5	61.9		1 022
9	202.5	5	61.0		1 032
10	197.5	5	61.3		1 028
11	192.5	5	60.1		1 041
12	187.5	5	59.5		1 047
13	182.5	5	59.2		1 051
14	177.5	5	58.5		1 059
15	172.5	5	58.1		1 063
16	165	10	56.3	1 095	1 083
17	157.5	5	54.8		1 102
18	152.5	5	54.5		1 105
19	147.5	5	52.7[2]		1 127
20	142.5	5	51.5		1 143
21	137.5	5	47.4		1 200
22	132.5	5	42.9		1 269
23	127.5	5	41.5		1 291
24	122.5	5	41.3		1 294
25	117.5	5	40.2		1 313
26	112.5	5	38.7		1 340
27	107.5	5	38.8		1 337
28	102.5	5	37.8		1 355
29	97.5	5	37.3		1 365
30	92.5	5	37.3		1 365
31	87.5	5	36.7		1 377
32	82.5	5	36.1		1 387
33	77.5	5	35.7		1 396
34	72.5	5	35.3		1 404
35	67.5	5	34.8		1 413
36	62.5	5	34.0		1 429
37	57.5	5	33.4		1 441
38	52.5	5	33.1		1 447
39	45	10	31.9	1 483	1 473
40	37.5	5	31.2		1 489
41	32.5	5	30.3		1 508
42	27.5	5	29.9		1 517
43	22.5	5	29.2		1 535
44	17.5	5	28.3		1 556
45	12.5	5	28.0		1 564
46	5	10	27.9	1 581	1 566

[1] Distance from the bottom to centre of the sample.
[2] Uncertain water content.

Table A3-5. Distribution of water content after dismantling of FLR7. The dry density is calculated from a measured water content and a degree of saturation S_r = 100 %. At three positions the dry density is also calculated from measured water content and measured bulk density.

Sample ID (FLR7)	Distance[1] mm	Thickness mm	Water content %	Dry density (from bulk density) kg/m^3	Dry density (assume S_r = 100 %) kg/m^3
1	250	4–7[2]	65.4		987
2	243	4–7[2]	63.9		1 001
3	239	5	63.0		1 010
4	234	5	63.1		1 009
5	229	4	63.1		1 010
6	225	4	63.2		1 008
7	221	5	63.0		1 011
8	216	5	63.4		1 007
9	211	5	64.2		998
10	206	5	63.3		1 008
11	201	5	62.6		1 015
12	196	5	61.7		1 024
13	191	5	60.9		1 032
14	186	5	60.0		1 042
15	181	5	60.3		1 039
16	173	10	57.9	1 063	1 065
17	166	5	57.0		1 076
18	161	5	56.6		1 080
19	156	5	54.7		1 103
20	152	3	54.1		1 111
21	148	5	51.0		1 149
22	143	5	49.1		1 175
23	138	5	44.7		1 240
24	133	5	43.5		1 259
25	128	5	43.0		1 266
26	123	5	42.1		1 281
27	118	5	41.4		1 293
28	113	5	40.7		1 303
29	108	5	40.1		1 315
30	103	5	39.5		1 326
31	98	5	39.1		1 331
32	93	5	38.4		1 345
33	88	5	37.8		1 356
34	83	5	37.6		1 358
35	78	5	37.1		1 369
36	73	5	35.7		1 395
37	68	5	36.1		1 388
38	63	5	35.5		1 399
39	55	9.3	35.0	1 412	1 410
40	48	5.6	32.5		1 461
41	42	5.6	32.7		1 456
42	37	5.6	31.8		1 477
43	31	5.6	31.1		1 492
44	26	5.6	30.7		1 500
45	20	5.6	29.7		1 522
46	15	5.6	28.9		1 542
47	7	11.3	28.4	1 547	1 553

[1] Distance from the bottom to centre of the sample.

[2] Uncertain thickness.

Appendix 4

Samples and reports

The following tables show all specimens presented in this report together with all specimens from TR-14-25 (Dueck et al. 2014), TR-16-04 (Dueck et al. 2016) and TR-17-04 (Dueck et al. 2018). In addition, some important specimens from the report TR-02-12 (Dueck et al. 2011) are also mentioned.

The materials used, i.e. MX-80 or Calcigel, are mentioned in the tables below and for the specimens presented in this report, in TR-16-04 and in TR-17-04 the year of the delivery is also given; MX-80#2010[b], MX-80#2012, Calcigel#2006 or Calcigel#2014. The material MX-80#2010[b] was delivered before 2010.

Table A4-1. Tests made in the basic series A0, R1 and R2.

Sample ID	Material	Report
A01-09, A01-10	MX-80	TR-02-12
A01-12, A01-13	MX-80	TR-14-25
A01-14, A01,15, A01-16	MX-80#2010[b]	TR-16-04
A04-1, A04-2	Calcigel#2006	TR-16-04
R11-10, R11-11	MX-80	TR-02-12
R11-17, R11-18, R11-19, R11-20, R11-21	MX-80	TR-14-25
R11-22, R11-23	MX-80#2010[b]	TR-16-04
R11-24	MX-80#2012	TR-16-04
R14-1, R14-2	Calcigel#2006	TR-16-04
R21-09, R21-10, R21-11, R21-12	MX-80	TR-14-25
R21-13, R21-14	MX-80#2010[b]	TR-16-04
R24-1, R24-2	Calcigel#2006	TR-16-04

Table A4-2. All tests made in the wetting series W.

Sample ID	Material	Report
W1-2, W1-3, W1-4	Calcigel#2006	TR-17-04

Table A4-3. All tests made in the series HR-A, HR-Ro, HR-Ri and HR-Iso.

Sample ID	Material	Report
HR-A1	MX-80	TR-14-25
HR-A2, HR-A3, HR-A4	MX-80#2010[b]	TR-16-04
HR-A6	Calcigel#2006	TR-16-04
HR-A7	Calcigel#2006	TR-17-04
HR-A8	Calcigel#2014	TR-17-04
HR-A9	Calcigel#2014	This report
HR-A10	Calcigel#2014	This report
HR-A11	MX-80#2012	This report
HR-Ro1	MX-80	TR-14-25
HR-Ro2	Calcigel#2006	TR-16-04
HR-Ro3	Calcigel#2014	TR-17-04
HR-Ri1	MX-80#2010[b]	TR-16-04
HR-Ri2	Calcigel#2014	TR-17-04
HR-Iso	MX-80#2010[b]	TR-16-04

Table A4-4. All tests made in the friction series, Fr.

Sample ID	Material	Report
Fr1-1 to Fr1-5, Fr1-7 to Fr1-9	MX-80	TR-14-25
Fr1-10, Fr1-12, Fr1-13	MX-80#2010[b]	TR-16-04
Fr1-11, Fr1-14	MX-80 pellet	TR-16-04
Fr1-15 to Fr1-17, Fr-19, Fr1-20	MX-80#2012	TR-16-04
Fr2-1	Calcigel#2006	TR-16-04
Fr2-2	Calcigel#2006	TR-17-04

Table A4-5. Three tests in the series with self-healing tests, SH.

Sample ID	Material	Report
SH1	MX-80#2012	TR-16-04 TR-17-04
SH2	MX-80#2012	TR-16-04
SH3	Calcigel#2014	This report
SH4	MX-80#2012	This report

Table A4-6. All tests in the series with long tubes, FLR.

Sample ID	Material lower part	Material upper part	Report
FLR1–4 on going	MX-80#2012	MX-80 pellet#2011	TR-17-04 This report
FLR5	MX-80#2012	MX-80 pellet#2011	TR-17-04
FLR6, FLR7	MX-80#2012	MX-80 pellet#2011	TR-17-04 This report
FLR8 to FRL10 on going	MX-80#2012	MX-80 pellet#2011	TR-17-04 This report

Arkitektkopia AB, Bromma, 2022

SKB is responsible for managing spent nuclear fuel and radioactive waste produced by the Swedish nuclear power plants such that man and the environment are protected in the near and distant future.

skb.se